3.5 MICRON LIGHT CURVES OF LONG PERIOD VARIABLE STARS

By

DONALD WALTER STRECKER

(NASA-CR-138078) THE 3.5 MICRON LIGHT CURVES OF LONG PERICD VARIABLE STARS Ph.D. Thesis (Minnesota Univ.) 205 p HC $13.25 CSCL 03A

N74-21427

Unclas G3/30 16072

1973

Report No. 15

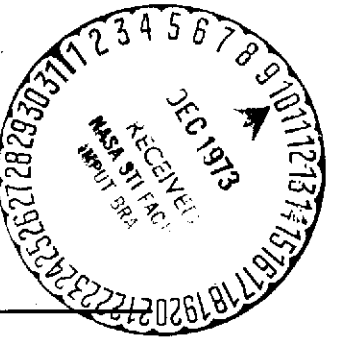

ASTROPHYSICS

School of Physics and Astronomy

UNIVERSITY OF MINNESOTA

3.5 MICRON LIGHT CURVES OF LONG PERIOD VARIABLE STARS

A THESIS

SUBMITTED TO THE FACULTY OF THE GRADUATE SCHOOL

OF THE UNIVERSITY OF MINNESOTA

By

DONALD WALTER STRECKER

IN PARTIAL FULFILLMENT OF THE REQUIREMENTS

FOR THE DEGREE OF

DOCTOR OF PHILOSOPHY

DECEMBER, 1973

I

TABLE OF CONTENTS

LIST OF FIGURES

LIST OF TABLES

LIST OF APPENDICES

Acknowledgments

This project owes its existence to the contributions of a great many people. Each individual, in his own manner, provided ideas, encouragement, criticism, assistance, materials, and time. To all, a heartfelt thank you.

My advisor, Dr. Edward P. Ney, deserves most of the accolades. He provided the telescope, detectors, and money, as well as other tangible and intangible assistance. His teaching, training, encouragement and criticism have been invaluable.

Many ideas resulted from discussions with Dr. N. J. Woolf, Dr. W. A. Stein, Dr. R. M. Humphreys, and Dr. J. G. Sparrow of the University of Minnesota.

Fellow students, who have long since graduated, Dr. D. A. Allen, Dr. T. L. Murdock, Dr. J. H. Hackwell, Dr. M. Cohen, and Dr. T. J. Pepin, aided and abetted with time and assistance at the telescope. Special acknowledgment is given to Dr. R. D. Gehrz, who acquired the lore of astronomy and astrophysics coincidentally with the author, and, who assisted in most of the observations for this project.

James W. Stoddart and the late Raymond Maas must be thanked for maintaining the telescope and for

keeping the infrared detection systems in excellent operating condition. Thanks, too, to R. Pearson who constructed the dewars and to James Stoddart who built the bolometers.

Patty Sheldon, who provided typing and incalculable moral support, deserves more than a simple acknowledgment.

To my parents, a very special thank you, and to all other relatives and friends, who assisted throughout the years, my sincere appreciation.

This work was partially supported under the National Aeronautics and Space Administration Contract No. NGL-24-005-008.

Abstract

Infrared observations at an effective wavelength of 3.5μ of a selected group of Long Period Variable (LPV) stars are presented. Mira type and semi-regular stars of M, S, and C spectral classifications are monitored throughout the full cycle of variability. Although the variable infrared radiation does not exactly repeat in intensity or time, the regularity is sufficient to produce mean 3.5μ light curves. For the M, S, and C stars as a group, the mean 3.5μ alterations are about $0^{m}.7$. The 3.5μ maximum radiation lags the visual maximum by about one-seventh of a cycle, while the minimum 3.5μ intensity occurs nearly one-half cycle after infrared maximum. In some stars, there are inflections or humps on the ascending portion of the 3.5μ light curve which may also be seen in the visual variations.

The 1.04μ narrow band photometry of Lockwood and Wing (1971) and Lockwood (1972), in conjunction with the present 3.5μ observations, is utilized to form a color index ([1.04μ]-[3.5μ]). This color index is available during most of the full variability

cycle for the stars in common between the two programs. The color index is converted into a color temperature under the assumption that α Lyra (AOV) is zero magnitude at all wavelengths and,in the infrared, radiates as a black body with a 10,000 °K color temperature.

From the deduced color temperature, via the Planck function and the 3.5μ magnitudes converted into absolute fluxes, the angular size of the source is calculated. Color temperatures, sizes, luminosities, visual magnitudes and radial velocities are computed for the cool M giant variables over the entire cycle and compared with observational results.

The color temperatures attain maximum coincidentially with visual maximum or zero phase, while the minimum is realized almost exactly one-half cycle later. Maximum compression occurs about one-tenth cycle before maximum temperature; maximum radius occurs about four-tenths of a cycle after minimum radius. Maximum luminosity happens about one-tenth cycle after maximum temperature and minimum energy output takes place nearly one-half cycle after maximum. The fractional change of temperature is about 20%; that of diameter is a little larger and the luminosity alters by a factor of two.

The calculated results are in excellent agreement

with Pettit and Nicholson (1933) and in good agreement with other observed quantities. The phase lag of maximum luminosity to minimum radius is similar to that seen in Cepheid variables and suggests that the physical mechanisms producing the variations may be similar.

..."Variability is a disease of bloated stars"...

P. W. Merrill, 1938

I

INTRODUCTION

One of the most curious facts of history is that the first variable star ever discovered is still probably one of the least well understood. A second point is that, even with the great interest in the heavens demonstrated by early civilizations, the first recording of a star altering its apparent brightness, other than supernovae, waited until 1596. On August 13, 1596, a German clergyman, David Fabricus, announced that the star designated omicron in the constellation of Cetus, the whale, did not appear constant in intensity. Again in 1638, yet fourteen years before the invention of the telescope, this same star, omicron Ceti, was rediscovered by Holwarda and its variability was confirmed. This interesting star, o Ceti, was given the name Mira - the wonderful - in honor of its unusual behavior.

Several theories were formulated to explain the underlying cause or causes of the stellar variability. One of the earliest and most obvious hypotheses was a binary or multiple star system with eclipses producing the changes in visual magnitude. This theory is able to account for many of the variable stars -- namely the extrinsic variables.

Some brightness alterations, however, were not acceptably explained by the binary star hypothesis. Shapely pointed out that the probable dimensions of some of the variable stars were on the order of ten times larger than the computed orbits of their companions. Gradually, as theoretical work on stellar structure progressed, the pulsation hypothesis, as supported by Eddington, was invoked to account for the stellar variability. At the present time, it is generally accepted that many stellar luminosity changes may be adequately described by radial oscillations or pulsations of either the entire star or its atmosphere alone. These stars are then called intrinsic variables.

One particular type of variable star called Cepheids, after the prototype of this class δ Cephei, has been quite extensively studied. From an observational standpoint, these stars are relatively bright, have well defined periods, and are quite reproducible from cycle to cycle. Due to the accuracy and availability of the observational data, many theoretical models have been proposed. Recent work has quite satisfactorily explained the static structure of F, G, and K giants from which dynamical calculations are able to proceed. At the present time, the observable

parameters of Cepheids (apparent brightness, radial velocity, and period) and the calculated quantities of Cepheids (temperature, angular diameter, and luminosity) are quite satisfactorily explained by the stellar structure dynamical models.

On the negative side, however, there exists a group of intrinsic variables which are not as well understood as the Cepheids. These are the red giant stars called Mira variables after the first one of this type discovered. Mira type stars are part of a larger group designated long period variable (LPV) stars. The Miras are characterized by cool photospheric temperatures (~2500°K), large size (~100 $R_{\odot}$), and periods approximating one year.

Long period variables have been studied since the turn of the century and have been quite extensively described and catalogued. However, the physical processes which cause and maintain the pulsations are less assured. Due to the cool effective temperature of the photosphere, the maximum energy is radiated at infrared wavelengths longer than about one micron. Also, due to the low temperatures, LPV stars possess extremely complex spectra. Absorption by atomic lines and molecular bands and line emission by hydrogen distort the energy distribution. As a result of these complex

spectra and convective energy transport, theoretical models of non-variable red giants have only recently been forthcoming, whereas dynamical models for the variability have been extremely scarce. Because of this dearth of prediction, comparison with observational quantities has been non-existent.

The original goal of this research program was to ascertain if stars do alter in intensity in the infrared at a wavelength of 3.5μ. If so, the aim was to determine the magnitude of the variation and its phase with respect to the well documented visual brightness changes. The wavelength of 3.5μ is relatively unaffected by interstellar and circumstellar extinction, at least compared to the visual region, and cool stars radiate much of their energy at this wavelength. Because the period and amplitude of Mira type stars are more reproducible than in other types of cool giants, the decision was made to monitor a selected group of Miras to ascertain answers to the previously posed problems. Also included in the observational program are a few semi-regular variables to determine some of the same quantities.

The general tone of this present investigation will be primarily the presentation of observational results. Quantities such as color temperature, angular size, luminosity, radial velocity and others, which

may be calculated from the observational data, are included in later chapters. It will not be the attempt of this essay to explain all of the phenomena which occur in the colors and spectra of variable red giants. It is hoped, however, that the quantities and relations presented herein will inspire further development of stellar models to explain the complex nature of long period variable stars.

II

CHARACTERISTICS OF LONG PERIOD VARIABLES

The ensuing paragraphs summarize a few of the more salient features of long period variable stars and are included for historical, descriptive, and informative purposes.

Periods: The frequency of occurrence of LPV's maximizes near periods of 280 days (Merrill, 1938) with the later types possessing longer periods (Cameron and Nassau, 1956). One of the outstanding differences between LPV stars and the Cepheids is that the cooler giants are not nearly as regular in period (~10%) as the shorter period, hotter stars. These single cycle alterations of period appear random and there is no systematic change. There exist two exceptions to this rule, namely R Aql and R Hya, both whose periods have decreased about 20% (Campbell and Jacchia, 1941). A period-spectrum relation does exist for LPV's with the later spectral types having longer periods (Campbell and Jacchia, 1941), but there seems to be no period-luminosity law (Glasby, 1969).

Spectral Type: Approximately 89% of the long period variables are classified as M stars, 7%

as R, N and C stars and the remaining 4% as S type stars (Merrill, 1960). The oxygen rich stars are denoted as M; the carbon rich are given the R, N or C classification, whereas the S type stars exhibit relatively high heavy metal abundances (Merrill, 1960). Eggen (1972) states that all N type stars are variable and R types are constant with a few exceptions. Wyckoff (1970) finds that the average change in spectral class from maximum to minimum is three subclasses for the M type stars.

Galactic Distribution and Age: In general, long period variables are thought to be old, evolved objects. None are found in Pop I galactic clusters but few are found in globular clusters (Payne-Gaposchkin, 1954). The shorter period Miras have higher space velocities (Eggen, 1955) and tend to form a spherical distribution throughout our galaxy, whereas those of longer period tend towards an intermediate population (Payne-Gaposchkin, 1954) with lower space velocities and somewhat higher masses (Glasby, 1969). In contrast, the non-variable M giants, as well as the R and N stars, tend toward a rather flattened galactic distribution (Payne-

Gaposchkin, 1954). The latest M type Miras of the longest periods may even be Pop I objects (Cameron and Nassau, 1956; Eggen, 1955).

Visual Light Curves: The amount of the apparent visual brightness alterations (Δm_v) increases as the period lengthens. The mean change in m_v is 4^m for variables with periods near 200 days and Δm_v increases to 5^m near 300 day periods (Merrill, 1960b) but tends to remain the same for longer periods (Merrill, 1960a). Mira type variables often have a pronounced hump either on the ascending or descending portion of the light curve which may not be present during each cycle (Glasby, 1969). S type variables generally possess wider flatter maxima and a greater visual magnitude alteration than do the M type stars (Campbell and Jacchia, 1941). R stars have broad flat maxima with sharp narrow minima; N type stars evidence smaller Δm_v, longer periods, broad maxima and narrow minima, decline faster than ascend and possess humps as a rule rather than as the exception (Campbell and Jacchia, 1941). Terrill (1969) demonstrated that the M type Mira variables show a tendency to be somewhat brighter at a given spectral type on the rising portion of the light curve than on the declining branch.

Spectra: The variables designated as Mira type are characterized by hydrogen emission lines, whereas cool variables, in which the lines are absent, are called semi-regular (SR) or irregular (Irr) (Campbell and Jacchia, 1941). These bright emission lines appear approximately one-quarter cycle before visual maximum and persist for about one-half cycle until about phase 0.25 and then are absent until the next cycle (Campbell and Jacchia, 1941). These hydrogen lines are believed to arise from shock waves in the stellar atmosphere. The shock wave is generated below the reversing layer within the hydrogen convection zone and then propagates outward through the reversing layer (Glasby, 1969).

Luminosities: Clayton and Feast (1969) have determined the absolute visual magnitude at mean maximum light for the M type Miras. They reported an absolute magnitude of -3^m for Miras of 200 day periods and decreasing to -1^m for the 400 day periods. They also report the absolute visual magnitude at mean light is about 2^m dimmer than at mean maximum. The Mira type S stars typically have M_v about -3^m, also (Takayanagi, 1960). The absolute bolometric magnitude for LPV stars as a group is about -4^m

(Campbell and Jacchia, 1941) but near -5^m for the Miras only (Smak, 1966). In M type stars, the change in visual blanketing throughout the cycle, caused by molecular bands attributed to TiO, could account for some of the differences as compared to stars of other spectral types and also could explain the differences between the visual and bolometric light curves (Campbell and Jacchia, 1941).

Masses: Mira type variables were believed to have masses on the order of ten solar masses but recent work by Fernie (1959) and Fernie and Brooker (1961) on X Oph and o Cet seems to indicate masses more on the order of one solar mass.

Mass Loss: Many of the brighter M type Mira variables exhibit excess radiation near 11μ (Gillett, Merrill and Stein, 1971; Gehrz and Woolf, 1971) which has been attributed to circumstellar shells composed of silicate grains (Woolf and Ney, 1969). Gehrz and Woolf (1971) deduce an average mass loss for Miras of about 2×10^{-6} $M_\odot$/year.

At the conclusion of this recap of characteristics of long period variable stars, a short summary of the

very early yet often cited work of Pettit and Nicholson (1933) on LPV stars is included. They measured eleven stars throughout the variability cycle and found an average radiometric magnitude change of nearly one magnitude with the maximum energy output occurring about one-seventh cycle after visual maximum. They also computed the stellar diameter to be more in phase with the luminosity or about 180° out of phase with the temperature. Their deduced mean diameters were 18% larger at minimum than at maximum light.

III

EQUIPMENT

All of the previously unpublished observations were obtained with detectors, dewars, and photometers designed and built at the University of Minnesota under the direction of Dr. E. P. Ney.

Nearly all of the observational data which forms the basis of this thesis was obtained with the 30 inch (76 cm) Cassegrain telescope of the O'Brien Observatory of the University of Minnesota located near Marine-on-St. Croix, Minnesota. A few data points were accomplished via the 60 inch (152 cm) metal mirror telescope of the University of Minnesota - University of California, San Diego Infrared Observatory on Mt. Lemmon near Tucson, Arizona.

In general, throughout the time span of June, 1968 through June, 1972, when the data were obtained, all equipment was altered and, hopefully, improved. Assortments of detectors, dewars, beam switching techniques, electronics, interference filters, and observers were utilized. One of the prime concerns during the system alterations was to maintain, as nearly as possible, the same effective 3.5μ wavelength of all photometric systems, so that meaningful inter-comparisons among all the data could be accomplished.

Figure 1 is a block diagram of the early (1968) single wavelength photometric system.

From 1968 through June, 1971, the beam switching system consisted of a four section, two level mirror which, when rotated at 5 Hz, produced a 10 Hz signal on the detector. Two sections of the mirror were movable, allowing the separation of beam centers to be varied from 1 mm. through 1 cm. corresponding to 25 $\widehat{11}$ through 250 $\widehat{11}$, respectively, with the scale of the O'Brien telescope.

Most of the observations made in Minnesota utilized a detector system employing a 3 mm. focal plane limiting aperture which resulted in a 1-1/4 arc min beam diameter. The rotating two level mirror was generally used with a 2 mm separation implying that the two beams overlapped in area on the sky. This overlap introduced no problems on stellar point sources and needed no correction factors.

In June of 1972, the rotating mirror was replaced by a linearly translating mirror. The cam driving mechanism produced a 10 Hz square wave signal on the detector. This translator had a fixed beam separation of 1-1/4 mm and only systems with focal plane diaphragms less than or equal to 1 mm were used.

The first infrared (3.5μ) observations obtained with the Minnesota equipment were made in January,

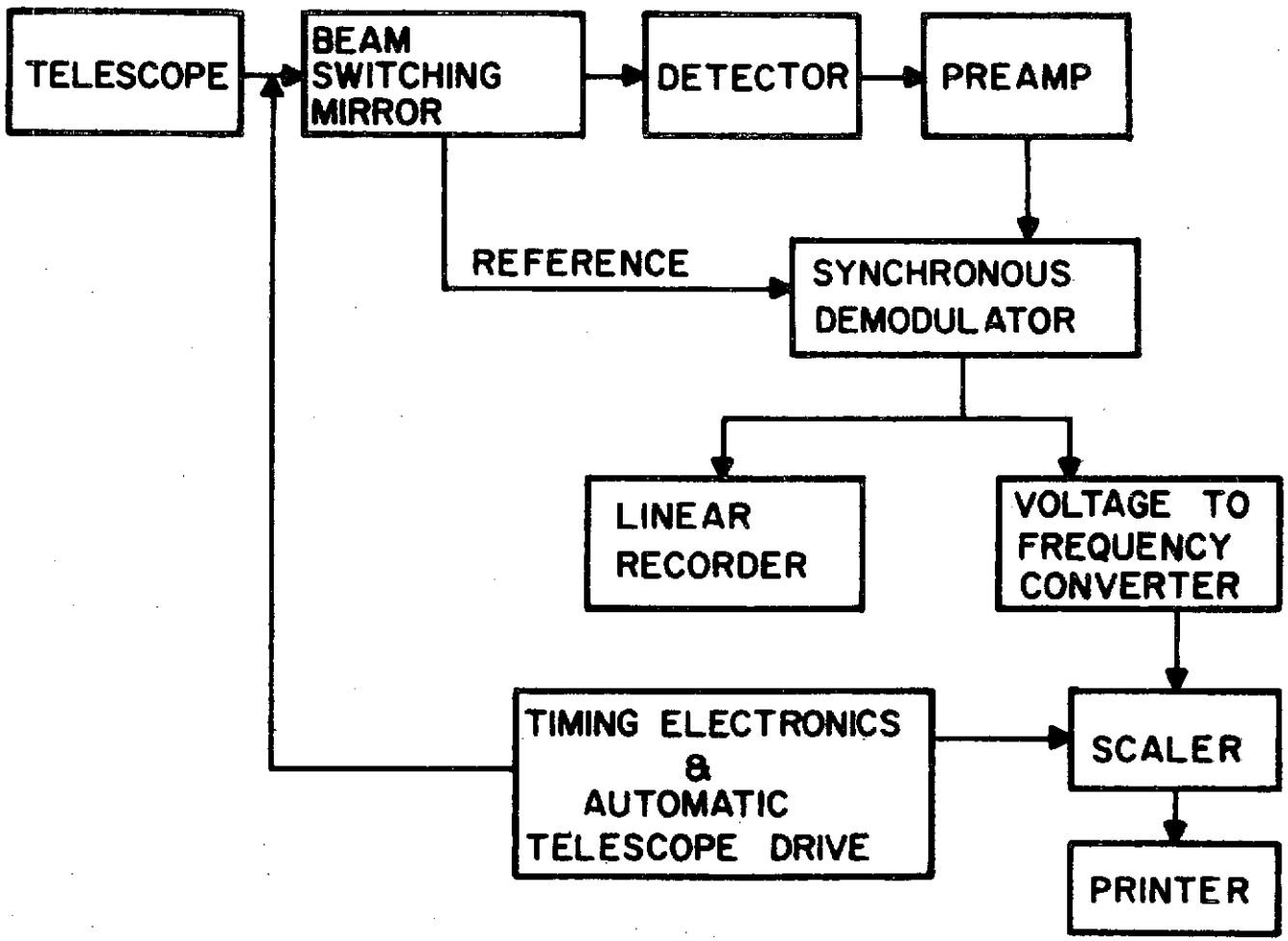

Figure 1. Block diagram of the equipment.

1968. These earliest detectors possessed a Noise Equivalent Power (NEP) of about 10^{-13} watts in a 1 Hz bandpass. This sensitivity and resulting signal-to-noise ratio imposed some restrictions on the possible choices of program stars, more of which will be mentioned later. As systems improved after 1968, the NEP was reduced by about a factor of 10. Thus, the accuracy and rate of observations improved, allowing more and dimmer stars to be included in the observing program.

The infrared detectors used in this study were gallium doped germanium bolometers operating at liquid helium temperatures. The earlier (1968) systems were pumped to just below the lambda point of liquid helium (2.2 °K), whereas later improved dewar systems facilitated operation near 1.2 °K.

The photometric systems of the 1968 vintage had only a single wavelength available. The effective wavelength was determined by an interference filter at liquid helium temperature. In these same dewars, the heat shield was cooled to approximately 150 °K by the escaping helium blow off gas.

In addition to the 3.5μ single wavelength systems, since 1970, it became possible to make observations at many wavelengths on the same night with the development of a multi-filter photometric system. The dewar utilized a ten position filter wheel in thermal contact with the

heat shield which was kept at about 80 °K by a liquid nitrogen container inside the dewar. In these systems, the basic set of standard filters available had effective wavelengths of 2.3, 3.5, 4.8, 8.6, 10.7, 12.2μ, and when atmospheric water vapor content allowed, 18μ.

As previously stated, as systems changed and improved, every effort was made to keep the interference filters nearly identical, especially at 3.5μ. Of course, this effort was not totally successful. The interference filters were purchased from Optical Coating Laboratories, Inc. (OCLI) and were originally intended to closely conform to Johnson's (1965) photometric systems.

Equation 1 describes the method for determining the effective wavelength (λe) of the photometric system.

$$\lambda e = \frac{\int_0^\infty \lambda T_F(\lambda)\ T_A(\lambda)\ D(\lambda)\ B(\lambda)\ d\lambda}{\int_0^\infty T_F(\lambda)\ T_A(\lambda)\ D(\lambda)\ B(\lambda)\ d\lambda} \qquad (1)$$

$T_F(\lambda)$ is the transmission of the interference filter obtained from a dual beam spectrophotometer. $T_A(\lambda)$ is the atmospheric transmission, $D(\lambda)$ is the detector response and $B(\lambda)$ is the energy distribution of the source.

In practice, the detector response $D(\lambda)$ is assumed constant and independent of wavelength due to the nature of a bolometer. Also, $B(\lambda)$ is approximately proportional to λ^{-4} particularly longward of about 3μ because the source energy distribution may be approximated by the Rayleigh-Jeans tail of a black body. The temperatures of most stellar energy sources exceed 2000 °K and their peak energy output would then be shortward of about 1.5μ.

Figure 2 is a dual beam spectrophotometer tracing of the transmission (T_F) of the interference filter used for most of the 3.5μ measurements. This transmission curve was obtained with the filter at room temperature. When the interference filter is cooled to liquid nitrogen or liquid helium temperature, the bandpass has a tendency to shift toward shorter wavelengths. This shift may be as much as 0.1μ.

The atmospheric infrared transmission (T_A) has been studied by Taylor and Jates (1957). The transmission is a variable which depends on the amount of precipitable water vapor in the earth's atmosphere. In Minnesota, during the cold, dry winters, the water vapor content is typically less than 1 mm for which the infrared transmission is approximately constant between 3 and 4μ. During the warm, humid summers, this H_2O content may exceed 10 mm for which the

the transmission is greatly reduced shortward of about 3.3μ.

With allowances for these two aforementioned effects, the effective wavelength of the photometric system used for most of the observations was determined to be 3.5μ ± 0.07 .

A few observations at other wavelengths were obtained on some of the stars of this research program. Many different dewars, filters and photometric systems were employed but the systems had some common or equivalent filters such that the results should not be system dependent.

The absolute calibration of the 3.5μ filters and other wavelengths is based primarily on the work of Murdock (1972), Johnson (1966), Gehrz and Woolf (1971), Gillett, Merrill and Stein (1971) and Gehrz (1972). The absolute calibrations of Gehrz and Woolf (1971) and Gillett et al., (1971) have been used for the 3.5μ effective wavelength in which zero magnitude corresponds to 7.1×10^{-15} watts/cm^2/μ. Table I lists the effective wavelengths, λe, and bandpass, $\Delta\lambda$, and the flux for zero magnitude for all of the filters used as a part of this research.

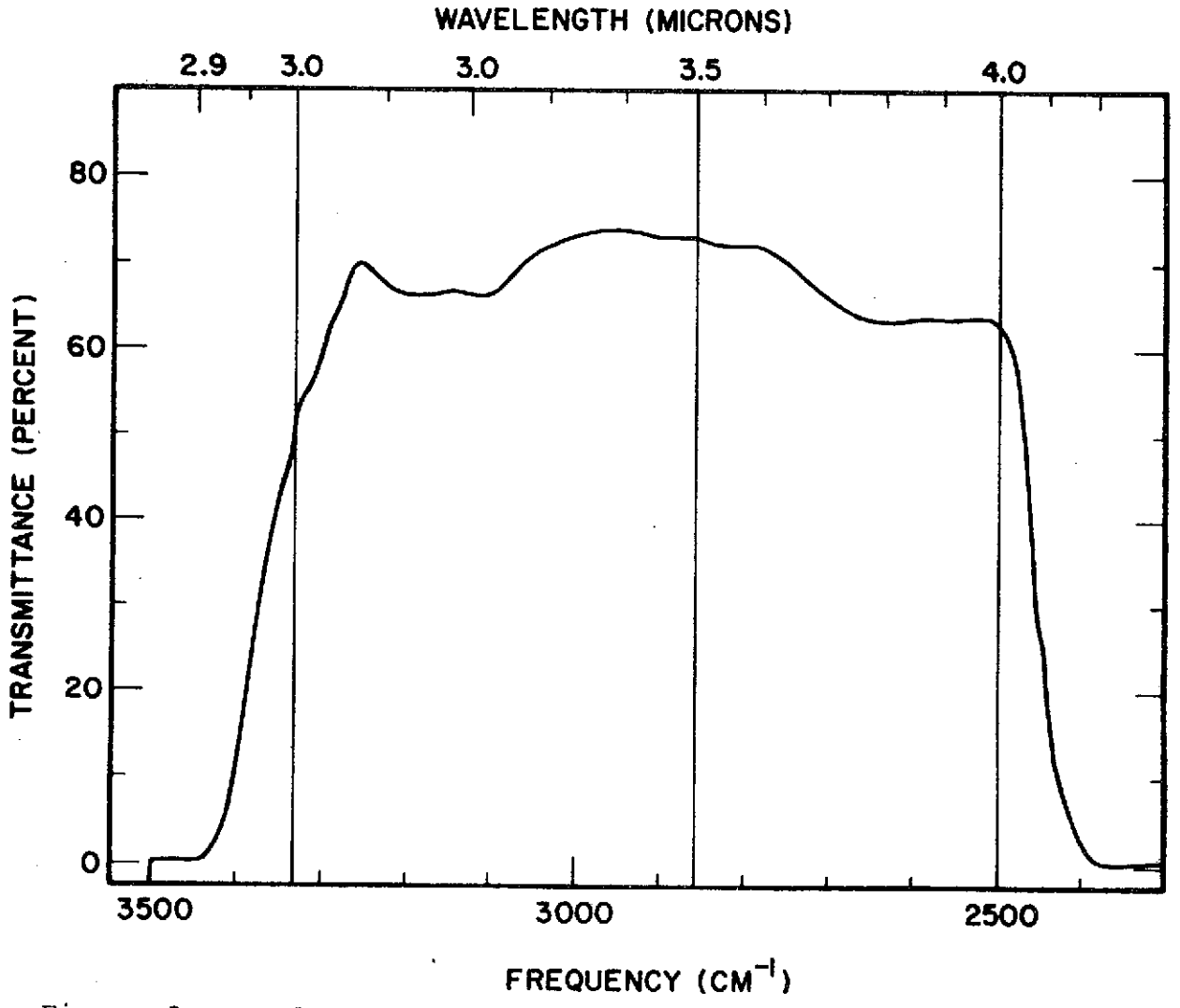

Figure 2. Dual beam spectrophotometer tracing of the 3.5μ filter.

Table I

Effective wavelength, bandpass, and absolute calibration of the Minnesota photometric system

$\lambda_e(\mu)$	$\Delta\lambda\mu$	Flux for zero magnitude $F(\lambda)$ in watts/cm^2/μ
2.3	0.5	3.3×10^{-14}
3.5	1.1	7.1×10^{-15}
4.8	0.9	2.2×10^{-15}
8.6	0.9	2.3×10^{-16}
10.7	1.1	9.8×10^{-17}
11.3	2.0	8.0×10^{-17}
12.2	1.1	6.0×10^{-17}
18	4	1.3×10^{-17}

IV

SELECTION OF OBJECTS AND OBSERVATIONAL PROCEDURE

From various sources, a list of the visually brightest semi-regular and Mira type variable stars was compiled. Preliminary measurements at 3.5μ on some of these stars indicated that the proposed research project was indeed feasible, particularly for the cooler stars of later spectral type. From these survey observations and the sensitivity of the Minnesota infrared equipment available in 1968, the decision was made to observe only the brighter (at 3.5μ) variables. A semi-final list of program stars was then compiled which numbered about 35 stars distributed throughout the sky north of the celestial equator. The judgment to observe chiefly objects north of zero degrees declination was made to minimize the effects of atmospheric extinction. The program stars selected in this manner were mainly stars of spectral type M2 through M6 at maximum as well as several carbon stars and a few S stars.

During the compilation of the program stars, it was not known by what magnitude, if any, nor on what time scale, other than the visual period, these red giants vary at infrared wavelengths. For this reason, it was decided to measure the selected objects as often as clear weather and available telescope time

permitted, hopefully every 5 to 10 days, Because Mira type variables have periods approximating one year, observations would be needed throughout the entire year, not just during the portion of the year when the star crosses the meridian between sunset and sunrise. In other words, daylight data were necessary although it had not been confirmed that accurate infrared observations could be obtained during daylight hours, especially when neither the object nor any field stars nearby could be visually identified. There was hope, however.

Within the framework of the limitations previously described, the program stars were selected. The brighter infrared sources were chosen with aspirations of daytime observing but with the realization of the limitations imposed by the equipment. An effort was made to keep at least some representation of earlier (MO-M2) stars, and to maintain a somewhat uniform distribution of objects throughout the sky. However, stars near spectral type M6 at maximum tend to dominate the source list.

The earliest observational data employing the inherently noisier detector systems was particularly difficult to obtain, because the observers were learning both infrared techniques and astronomy simultaneously.

The original method of data acquisition consisted

of measuring a calibration star, a variable, the same calibration object, the same variable, etc. An evening's data were composed of observations of a few (~5) calibration stars each measured 3 separate times and about five variable stars each observed at three distinct times. A typical integration time was 10 minutes for each observation of each star while about 10 minutes elapsed acquiring the next object. This procedure filled the entire observing run which lasted as long as clear skies allowed or until the dewar exhausted its helium supply after about 8 hours at the telescope.

The actual observing schedule and procedure evolved throughout the time span of data collection. By 1971, the procedure consisted of measuring each calibration star available once per session and each variable once per night; the implicit assumption being if the calibrations were correct to a few percent then the variables were accurate to that same value. When doubts existed, the specific stars were re-observed during the same session. The observational log consisted approximately of calibration, variable, new calibration star, new variable..... This method was employed so that any alterations in system sensitivity, atmospheric transmission, undetected clouds and other factors could hopefully be noted and, consequently, corrections

applied.

About one year into the observing program, it was noted that Mira type stars do vary at 3.5μ on a time scale compatible with the visual variations, although the amount of the change was considerably less, being about 1 magnitude at 3.5μ compared to an average visual range of about 5 magnitudes. The original observing schedule of one data point per star every 5-10 days was revised to one point every 10-20 days or, hopefully, about 30 points per cycle.

The optimistic outlook was to follow the planned schedule for one or two cycles of each variable star. Such was not the case. The largest obstacle in the path of the proposed program was the lack of clear photometric quality weather in Minnesota. The second pitfall was the amount of available telescope time. The planned regular observations were purely at the mercy of the elements and nothing even approximating the planned data collection rate was achieved. Gaps in the observations would hopefully be filled by measurements during the next cycle. This latter assumption rested upon yet another hypothesis that the infrared magnitudes were reproducible from cycle to cycle.

In an attempt to amass more complete data, daylight observations were attempted in the summer of 1969. By

this date, the O'Brien telescope had been debugged and tuned up to the extent that it could be accurately pointed to ± 1 arc min on the sky. These first daytime measurements were obtained with the 1-1/4 arc min beam diameter 3.5μ system. After calibration, the telescope was set to the position of the variable to be measured. More often than not, the chart recorder indicated the star was within one of the two beams. If not, the telescope was driven in a raster pattern nearby until the signal was acquired from the star. The signal was maximized and the variable star measured. The chances of measuring a wrong star with the correct magnitude and position of the variable by this method were negligibly small.

With this observational procedure, it was noted that daylight observations were only slightly more difficult than during the night. Drifts and variable offsets caused by solar heating of the telescope walls, defocusing of the mirror, and gradients in the sky background were minimal, at least at 3.5μ with 1-1/4 arc min diameter beams. In general, these daytime observations were limited to greater than about 20 degrees from the sun.

Even with the improvements in detectors and systems since early 1968, some of the program stars were too dim at 3.5μ to acquire during the sunlit

hours and gaps are obvious in the data. However, by 1971, systems had progressed so that almost any of the program stars could be measured night or day by scanning the correct position and maximizing the 3.5μ signal. In fact, even with beams reduced to 25 arc sec diameter, acquisition of an object was often faster using this scanning method than to visually identify the correct star field and then the proper variable. Although, when possible, visual verification was often attempted.

Additional observations of some of the program stars were obtained at wavelengths other than 3.5μ with some of the multi-filter systems. The basic procedure was the same as previously described for 3.5μ except that, due to the increased sky noise and the declining intensity of the source, the integration time necessary to achieve statistical significance was increased at the longer wavelengths.

The multi-filter photometric system had an improved signal-to-noise ratio at 3.5μ compared to the single wavelength dewar. However, because it employed a smaller beam diameter than the single 3.5μ system (25 arc sec vs. 75 arc sec), the increased gain was partially offset by the poorer response profile and difficulties in accurate guiding. Daytime measurements were still feasible although the time needed to acquire

the stellar signal by scanning was increased.

Data reduction was a relatively uncomplicated procedure. The digital output of the accumulator was recorded automatically. The object name, hour angle, universal time, and amplifier gain were recorded manually. The accumulator output was then returned to the laboratory where means and standard deviations of the mean could be computed. The total integration time on a specific star was quite subjective and depended on the signal-to-noise ratio, quality of the night, photometric system in use, infrared and visual seeing and transmission, as well as the philosophical bias of the observer. Generally, about 3 minutes of true integration time were deemed sufficient to reduce the statistical errors well below other uncertainties.

The measured stellar fluxes were converted to magnitudes at unit air mass by equation 2.

$$m_1 = m_s + \varepsilon(AM_1 - AM_s) - 2.5 \log (F_1/F_s) \qquad (2)$$

Where m_1 and m_s are the stellar magnitudes at 1.00 air masses of the unknown and standard objects respectively, ε is the extinction coefficient in magnitudes per air mass ($\varepsilon<0$), AM_1 and AM_s are the air masses through which the unknown and standard are

observed while F_1 and F_s are the measured fluxes from the unknown and the standard.

The air mass through which a star was observed was calculated from the standard formula 3

$$AM = \sec Z \qquad (3)$$

where Z is the zenith angle. Because the program stars were always at zenith angles less than 60° and generally less than 45° equation (3) is an adequate approximation.

The atmospheric extinction in the 3 to 4μ window was measured during each observing session whenever possible. The mean value during the four years of data collection was 0.2 magnitudes per air mass at the 3.5μ effective wavelength. After the first two years of observation, this value was checked less frequently but was found to be the same within observational errors.

This value of 0.2 magnitudes per air mass for the atmospheric extinction at 3.5μ was adopted and used for all of the extinction corrections on all of the data. Due to the fact that the program stars generally had positive declinations and were measured as near the meridian as possible, for the 45° latitude of the Minnesota telescope, the air masses were always less than 1.5 and the extinction correction was less than 0.10 mag. The 30% variations of ε, as measured from

night to night and season to season, therefore, are able to produce only a $\pm$ 0.03 mag.uncertainty in the final results.

From the preliminary and first year's measurements, it was pleasantly discovered that observations of brighter stars on a given night were reproducible to about 2%. These errors are assumed to be caused by inaccurate guiding, beam positioning, telescope tracking, fluctuations in atmospheric transmission, poor seeing, non-linearity of the photometric system, statistical fluctuations, and other assorted gremlins. For sources whose 3.5μ magnitude was dimmer than about $+1^{m}.5$, the chief uncertainty was statistical, due to the poorer signal-to-noise ratio and limited integration time. For stars below about 1.5 air masses, the extinction must be more accurately determined for each night than was attempted.

A separate discrepancy in the absolute flux calculated for the variables may result if the assumed flux for zero magnitude is not correct.

The zero point of the Minnesota photometric system was defined by the assumption that α Lyra (AOV) was zero magnitude at all wavelengths. The magnitudes of the calibration stars for the preliminary observations were adopted as published by Johnson (1964). At that time, it was discovered that the magnitudes

calculated for some of the calibration stars did not agree to within ± 10% of the quoted values. In general, stars of later spectral type were brighter than as measured by the Arizona equipment, possibly indicating the difference in effective wavelength as defined by the two groups. Due to this possible systematic difference and, in order to define more calibration stars, a new list of standards was compiled. This new list was comprised of stars of later spectral type, bright at 3.5μ, and whose positions on the celestial sphere were more compatible to the distribution of variables in the observational program. This new calibration list was based on α Lyra still defined as zero magnitude, and the standards were measured directly with respect to Vega if possible.

Table II lists the primary standard stars by their HR number, name, spectral type and 3.5μ magnitude defined by the Minnesota system. Table III compiles the same quantities for the secondary calibration stars. All of the magnitudes listed include corrections for atmospheric extinction and are referenced to unit air masses.

When the results of Minnesota photometry can be compared with magnitudes published by other groups (Lee, 1970; Gillett, Merrill and Stein, 1971; for example) there exists surprisingly good agreement,

Table II

3.5μ Magnitudes of Primary Standard Stars

HR	Name	Spectral Type *	3.5μ Magnitude
337	β And	MO III	-2.05
1457	α Tau	K5III	-3.02
1708	α Aur	G8III?+F	-1.92
2943	α CMi	F5IV	-0.76
2990	β Gem	KO III	-1.23
4058	γ^2 Leo	G7III	-0.79
4301	α UMa	KO II-III	-0.77
5340	α Boo	K2IIIp	-3.12
6705	γ Dra	K5III	-1.44
7001	α Lyra	AOV	0.00
8775	β Peg	M2II-III	-2.45

* Hoffleit, 1964.

Table III

3.5μ Magnitudes of Secondary Standard Stars

HR	Name	Spectral Type*	3.5μ Magnitude
168	α Cas	KO II-III	-0.40
603	γ' And	K3 II	-1.00
617	α Ari	K2 III	-0.77
911	α Cet	M2 III	-1.90
921	ρ Per	M4 II-III	-2.20
1577	ι Aur	K3 II	-0.85
2061	α Ori	M2 Iab	-4.54
2091	π Aur	M3 II	-1.07
2216	η Gem	M3 III	-1.64
2286	μ Gem	M3 III	-2.10
3705	α Lyn	MO III	-0.76
4069	μ UMa	MO III	-1.00
4434	λ Dra	MO III	-0.28
4910	δ Vir	M3 III	-1.40
5506	ε Boo	KO II-III	-0.07
6406	α' Her	M5 II	-3.70
7139	δ^2 Lyra	M4 II	-1.41
7157	R Lyra	M5 III	-2.28
7417	β Cyg	K5II?+B?	0.05
7525	γ Aql	K3 II	-0.75
7536	δ Sge	M2II?+B?	-0.96
7949	ε Cyg	KO III	0.03
8308	ε Peg	K2 Ib	-0.98
8316	μ Cep	M2 Ia	-2.23
9064	ψ Peg	M3 III	-0.17

* Hoffleit, 1964.

generally to within 2-3%, even though effective wavelengths may differ somewhat.

V

OBSERVATIONAL RESULTS AT 3.5μ

Table 4 summarizes the characteristics of the variable stars of this research project for which more than a few (~5) reliable observations have been secured. Column 1 lists the star name by constellation, while columns 2 and 3 tabulate the galactic coordinates of longitude and latitude, respectively (Kukarkin, et al., 1958). Column 4 quotes the type of variation as Mira type (M) or semi-regular (SR) (Kukarkin, et al., 1958). Columns 5 and 6 list the average periods cited by Kukarkin, et al., (1958) and Campbell (1955), whereas column 7 lists the adopted period used for the phase calculations. Column 8 lists the mean spectral types at maximum (Keenan, 1966) or the spectral type (Kukarkin, et al., 1958) and column 9 tabulates the minimum spectral types of Lockwood and Wing (1971) or Kukarkin, et al., (1958). Columns 10, 11 and 12 quote the maximum and minimum mean visual magnitude and range determined by Campbell (1955). Last, but not least, columns 13, 14 and 15 tabulate the observed 3.5μ magnitude extrema and range as determined by this present project. The extrema of the last columns represent the brightest and dimmest reliable measurements at 3.5μ and probably are not a true measure of the mean behavior of the stellar fluctuations. When the

Table IV

Characteristics of the Program Stars

Name	l *	b *	Type of Variation *	Period Days *	Period Days +	Adopted Period Days	Spectral Type at Maximum	Spectral Type at Minimum	Mean Visual + Magnitude Max	Mean Visual + Magnitude Min	Mean Visual + Magnitude Range	3.5μ Magnitude Max	3.5μ Magnitude Min	3.5μ Magnitude Range
R And	085°	-24°	M≡Mira	409.4	409.0	410	S4,7e +	-	$6^m.9$	$14^m.3$	$7^m.4$	$-1^m.3$	$-0^m.1$	$1^m.2$
W And	107	-15	M	397.0	397.0	392	S8,2e +	M8e *	7.4	13.7	6.3	-0.6	0.0	0.6
R Aql	010	-01	M	300.3	306.2	283	M6.5e +	M8.5 :	6.1	11.5	5.4	-1.5	-1.1	0.4
R Aqr	037	-71	M	386.9	386.4	387	M7e+pec *	-	6.5	10.3	3.8	-2.3	(-1.9)	-
P Aur	124	+10	M	458.9	461.8	454	M6.5e +	M9.0 :	7.7	13.5	5.8	(-1.6)	-1.1	-
R Boo	005	65	M	223.3	223.4	224	M4.5e +	M8.0 :	7.2	12.3	5.1	1.0	1.7	0.7
R Cnc	180	26	M	362.1	362.2	360	M6.5e +	M8e *	6.8	11.2	4.4	-1.3	(-1.0)	-
T Cnc	175	38	SRa	482.4	-	-	N3($C4_5$) *	-	7.6	10.5	*	0.2	0.4	(0.2)
R Cas	083	-10	M	431.2	429.6	422	M7e +	M10 :	7.0	12.6	5.6	(-2.6)	-2.1	-
T Cas	087	-07	M	445.0	445.0	445	M7.5e +	M8.5 :	7.9	11.9	4.0	(-1.8)	-1.4	-
WZ Cas	084	-02	SRa	186.0	-	-	Np($C9_1$)*	-	9.4p	11.1p	*	-0.1	0.4	0.5
S Cep	081	19	M	487.5	484.8	482	N8e($C7_4$e) *	-	8.3	11.0	2.7	-1.8	-1.2	0.6
T Cep	072	14	M	389.7	392.9	382	M6.5e +	M8.5 :	6.0	10.3	4.3	-2.4	-2.2	(0.2)
O Cet	137	-57	M	331.6	331.4	332	M5.5e +	M9.0 :	3.5	9.2	5.7	-3.7	-2.9	0.8
S CrB	016	56	M	360.7	359.5	359	M6.5e +	M8e *	7.3	12.9	5.6	-0.8	-0.3	0.5
V CrB	030	50	M	357.8	357.6	358	N2($C6_2$e) *	-	7.5	11.0	3.5	0.3	1.1	0.8
R Cyg	050	13	M	426.3	426.3	427	S3,9e +	S6,8e *	7.5	13.9	6.4	0.2	1.4	1.2

Table IV(continued)

Name	ℓ *	b *	Type of Variation *	Period Days *		Adopted Period Days	Spectral Type at Maximum	Spectral Type of Minimum	Mean Visual + Magnitude Max	Min	Range	3.5μ Magnitude Max	Min	Range
U Cyg	052	06	M	464.7	462.9	455	Npe($C7_2$e) *	$C9_2$ *	7.2	10.7	3.5	-0.1	1.0	1.1
RS Cyg	044	02	SRa	417.8	419.0	418	NOpe($C8_2$e)*	-	7.2	9.0	1.8	0.8	1.0	(0.2)
RT Cyg	049	11	M	190.4	190.7	190	M2.5e +	M8.2 :	7.3	11.8	4.5	2.5	3.0	(0.5)
χ Cyg	036	02	M	406.9	409.0	411	S7,2e +	M9.0 :	5.2	13.4	8.2	-3.1	-2.4	0.7
RY Dra	088	51	SRb	172.5	-	-	N4p($C3_4$) *	-	9.4p	11.4p	*	-0.6	-0.4	(0.2)
U Her	003	39	M	406.0	405.3	413	M6.5e +	M9.0 :	7.5	12.5	5.0	(-1.1)	-0.6	-
R Leo	192	46	M	312.6	312.8	310	M7e +	M9.0 :	5.9	10.1	4.2	(-3.4)	-2.9	-
R LMi	158	51	M	372.3	372.2	372	M7e +	M8.8 :	7.1	12.7	5.6	-1.4	(-1.0)	-
R Lep	182	-30	M	432.5	-	-	N6e($C7_2$e) *	-	5.9	10.5	4.6	-	-	-
X Oph	007	06	M	334.2	334.3	332	M6.5e +	M8.5 :	6.8	8.8	2.0	-1.6	-1.2	0.4
U Ori	156	-01	M	372.3	373.2	372	M6.5e +	M9.0 :	6.3	12.0	5.7	-1.7	-1.0	0.7
W Ori	167	-21	SRb	212	-	-	N5($C5_3$) *	-	5.9	7.7	*	-1.0	-0.8	(0.2)
R Ser	354	45	M	356.8	356.6	352	M6.5e +	M8e *	6.9	13.4	6.5	(-0.4)	0.0	-
R Tri	115	-23	M	266.4	266.0	267	M4e +	M8.2 :	6.2	11.7	5.5	0.1	0.6	0.5
R UMa	105	45	M	301.7	301.0	302	M4.5e +	M6e *	7.5	13.0	5.5	(0.5)	1.0	-
R Vir	265	69	M	145.6	145.4	146	M4.5e +	M8e *	6.9	11.5	4.6	1.4	(1.6)	-
SS Vir	259	63	M	354.7	355.9	355	Ne($C6_3$e) *	-	6.8	8.9	2.1	0.0	(0.3)	-

*Kukarkin et al., 1958. +Keenan, 1966. :Lockwood and Wing, 1971. + Campbell (1955).

maxima or minima are enclosed in parentheses, it indicates that the observed extrema are caused by limitations in the available data and therefore do not depict the true stellar range of brightness. When the 3.5μ range is on the order of the uncertainties of measurement ($\sim 0^{m}.2$), it is also enclosed in parentheses and indicates that the implied alterations may not be real.

The adopted periods of column 7, as used in the phase calculations, may differ somewhat from the average periods of Campbell (1955) in column 6. The adopted periods were calculated from visual data kindly supplied by Mayall (1972) from Julian dates 2439000 through 2441500. These periods represent an average period of the star over the inclusive dates and are intended to depict the present, rather than the past, average behavior. Only in one notable exception do the adopted periods differ from Campbell's averages by more than 11 days or more than about 3%. Generally, the difference in the two periods is less than about 5 days and therefore represents an error of less than 2%. Differences of 0.01 in the phase calculations are much less than the cycle to cycle variations in the period. The notable exception is R Aql, which is known to have a decreasing period as previously stated.

Appendix I summarizes all of the program stars' measurements as observed with the Minnesota photometric system's 3.5μ effective wavelength. The headings for each star include the star name and the average period used to determine the phase. Column 1 lists the Julian date (rounded to the nearest whole day) of the observation, column 2 represents the phase with respect to the visual maximum, column 3 tabulates the magnitude at 3.5μ and column 4 contains an estimate of the quality of the data.

Appendix II tabulates the 3.5μ observations for sources other than the final program stars which have been measured more than one time. It is included only as a summary. Column 1 lists the star name (alphabetically by constellation); column 2, the Julian date of observation; columns 3 and 4, the 3.5μ magnitude and quality estimate, similar to appendix I; columns 5, 6, 7, 8 list the type of variability, period, spectral type and visual range, respectively. The period, spectral type and visual magnitudes are from Campbell (1955), if available, and from Kukarkin, et al. (1958), when noted.

The phase of the star at the time of the infrared observation is measured with respect to the time of visual maximum. As a general rule, the phase is measured from zero at one visual maximum through

phase + 1.00 at the ensuing maximum, thus making the phase always positive and ranging between 0.00 and +1.00. However, cycle to cycle differences exist in both the visual and infrared observed magnitudes. A visual maximum may be brighter than average, and, if so, there exists a tendency for this particular extremum to be earlier than average (Harrington, 1965) implying a shorter observed period for that cycle. Phase calculations from 0 through +1 tend to split this brighter maximum into two different cycles. In order to reduce this apparent discontinuity at zero phase, it was decided to measure phases on either side of the visual maximum, from phase -0.50 to 0.00 to +0.50 and then recycle. This method of computation stresses the time of visual maximum and confines the unusual brightness to only one cycle and not over two cycles.

The 3.5μ magnitudes tabulated in column 3 include the effects of atmospheric extinction and refer to unit air mass.

The numbers listed in column 4 (Quality) are a measure of the performance of the photometric system's noise, beam size, and stability throughout the observing session. These numbers also represent constancy of the atmospheric transmission, cloud cover, if any, visual and infrared seeing, as well as assorted

other objective and subjective decisions. The major factor in determining the quality of the observations was the accuracy to which the calibrations stars were measurable and reproducible during the observing run.

On an excellent photometric night, the atmospheric extinction, as measured, was found to agree within about 20% of the adopted 0.2 magnitudes per air mass. Also, there were few or no clouds present, and the detector system was stable to within a few (~2) percent throughout the observing session. On these excellent nights, the calibration stars were reproducible to about 2 or 3 percent, and the night was rated as quality 5.

Quality 4 implies a good photometric night. Some of the aforementioned criteria may have influenced the results. For example, the calibration stars were accurate to 2 or 3 percent after corrections were applied for changing sensitivity or transmission. Quality 3 implies fair reproducibility, while 2 represents a poor night. Quality 1 data are not included because, for a multitude of reasons, the results are not reliable to within an estimated 50%.

It is appealing to assign overly optimistic errors to the excellent nights. During these observing sessions, as previously stated, the calibration stars

were accurate to about 2%. It is tempting to assume that the variable stars are accurate to the same 2%. Even though this may be often a reality, a conservative estimate would be doubling this 2%; therefore, nights of quality 5 were given 4% uncertainties.

Along a similar vein, quality estimate 4 nights were most likely accurate to better than 5% on the calibration stars after the various correction factors were applied to the data. However, the errors are conservatively estimated to be between 5 and 10%. An arbitrary error of 10-20% is assigned to quality 3 nights due to the presence of clouds, equipment problems, and more or larger applied correction factors. Last, but not least, quality estimate 2 represents basically poor data reliability of 20 to 50% errors.

At this point, a brief discussion of the sources of errors and uncertainties involved in limiting the accuracy of the 3.5μ magnitudes is in order. The chief difficulty in obtaining observational data, at least in Minnesota, is the lack of clear or partly clear weather -- especially during the daylight hours. One major producer of poor data quality is unseen, thin cirrus cloud cover. At the 3.5μ wavelength, these clouds do not introduce additional noise; they simply reduce the signal. In fact, thin uniform

overcast cirrus may reduce the observed signal level by 20 to 30% and this reduction may go unnoticed for some time. If this reduction did occur during an observing session, it was usually noticeable upon final analysis of the data and this correspondingly poor data was omitted. Clouds, fog, and haze are classified as major sources of observational uncertainty.

Many possible causes of minor errors do also exist. Minor errors are the 1 or 2 percent variety which may go undetected for some time, quite possibly forever. One gremlin is the changing sensitivity of the bolometer. This changing sensitivity is due to oscillations in the vacuum system and/or a long time constant for the dewar to reach equilibrium. Additional uncertainties may be caused by non-linearity in the electronics, fogging over of a dewar window in humid weather, or cracking of the window in very cold conditions. More sources of minor error include positioning of the telescope to obtain maximum source signal strength, non-uniformity of response over the area of the detector, and non-linearity of the detector for very bright sources. As previously mentioned, the changing atmospheric transmission and the associated extinction do also affect the accuracy of the results. Last, but not least, are the Minnesota winters where the temperature does occasionally dip to -40 F. This

may cause severe observational problems; however, the cold weather observing technique is an entirely separate tale to be told to one's grandchildren.

Many of the possible sources of error can be eliminated or at least minimized. The ones which cannot be eliminated or minimized may hopefully be accounted for and corrections applied. As also stated previously, the final errors were estimated from the quality and degree of reproducibility of the data and not from the possible problems.

Statistical errors are the major producer of uncertainty for objects with a low signal-to-noise ratio and a limited integration time. For the earlier (1968-1970) observations, the minimum detectable signal, in about twenty minutes of real integration time, was a 3.5μ magnitude of about $+4^m$ at the three standard deviation limit. Since 1971, this limit has improved to about $+7^m$ in the same integration time. Most of the program stars are brighter than $+1^m$ and the statistical errors are not the prime source of uncertainty. But for objects near 2^m, the statistics start to become important, particularly for the daylight observations; therefore, for objects with a 3.5μ magnitude near $+2^m$, the assigned errors are almost always greater than 20%.

Figure 3 plots the visual variation and the 3.5μ

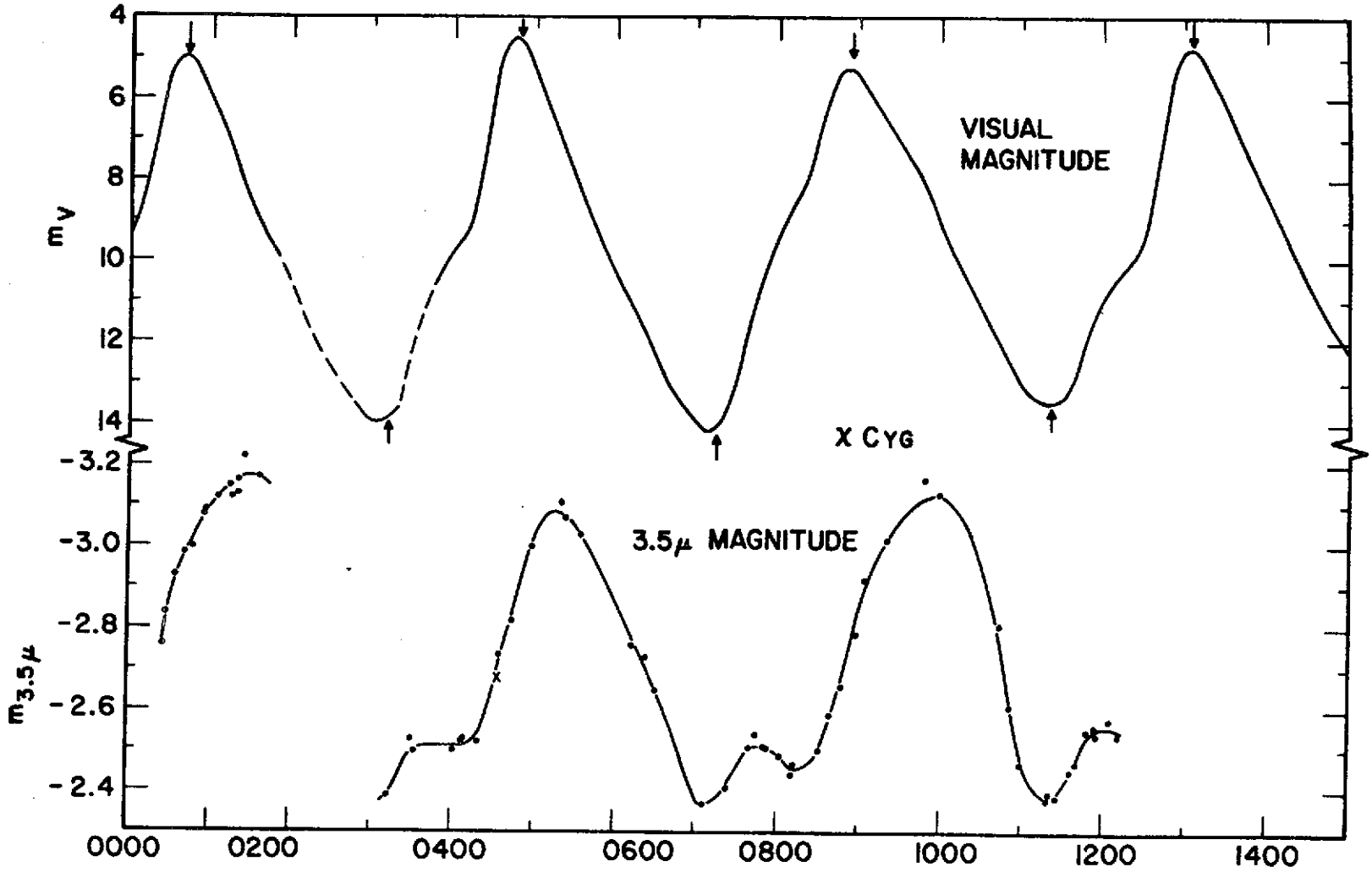

Figure 3a. Continuous visual and 3.5μ light curves for the mild S star χ Cyg(S7,2e). Typical errors are ±5% for the 3.5μ points. The arrows denote the times of visual extrema.

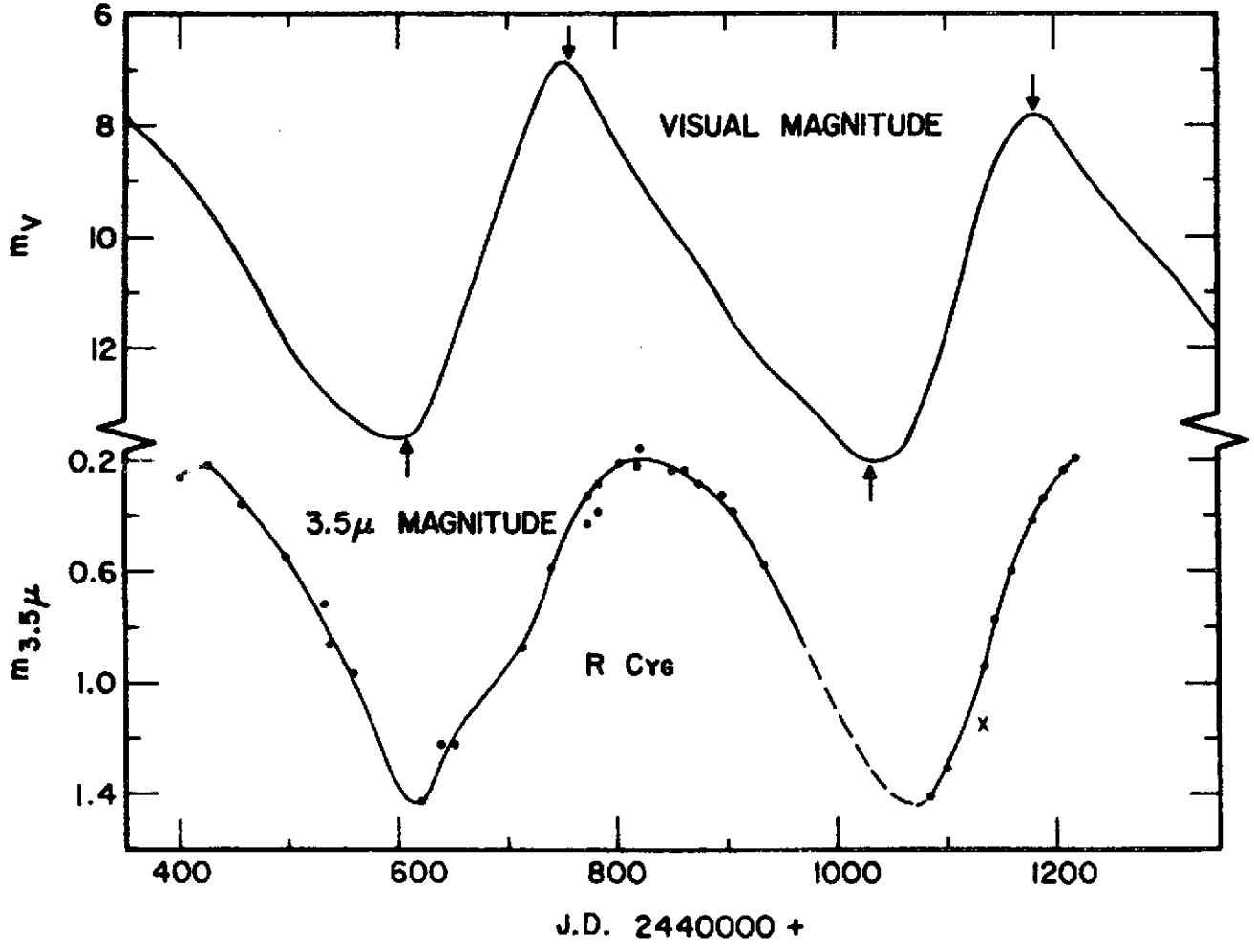

Figure 3b. Smilar to figure 3a but for R Cyg (S3,9e).

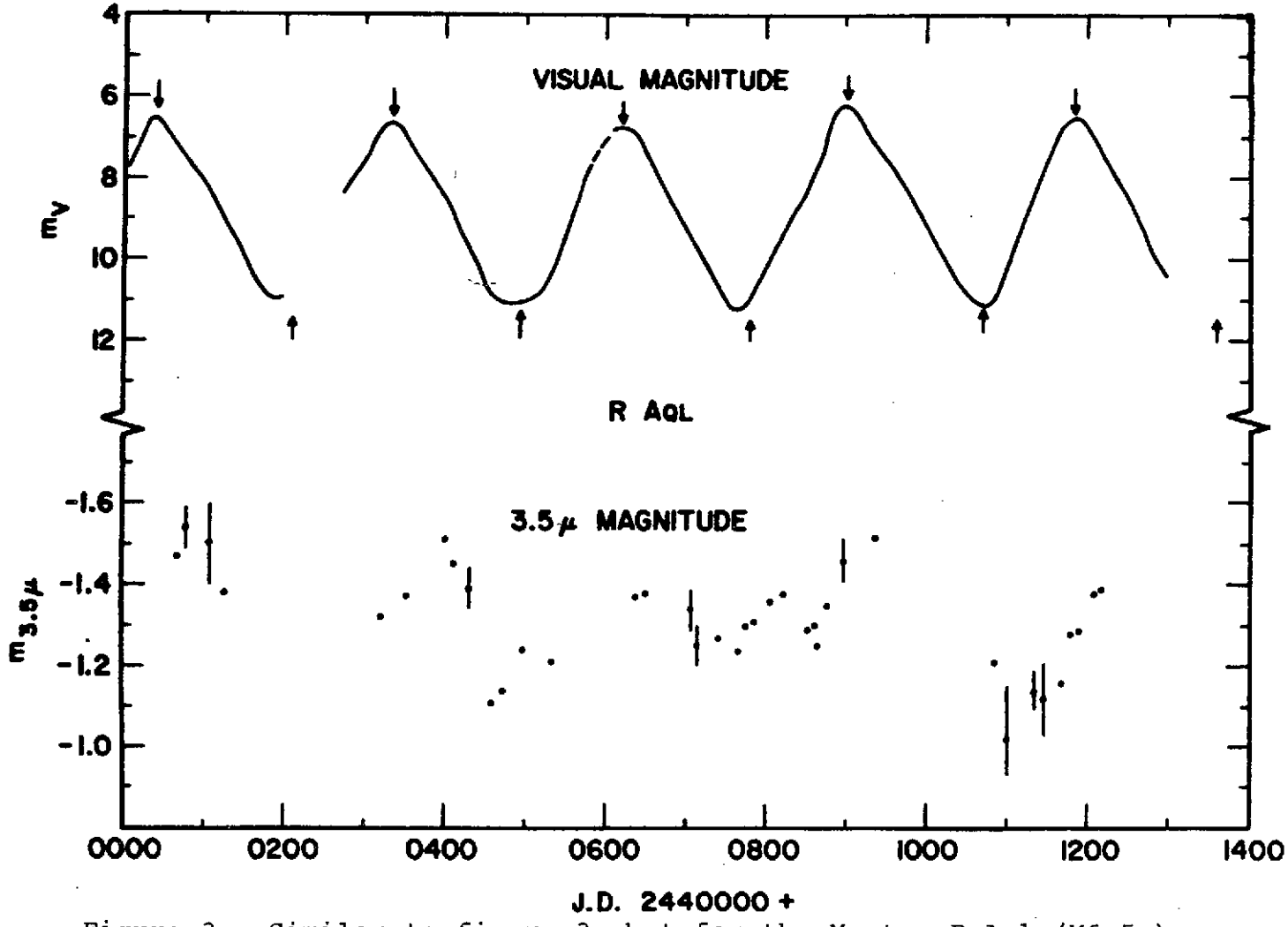

Figure 3c. Similar to figure 3a but for the M star R Aql (M6.5e).

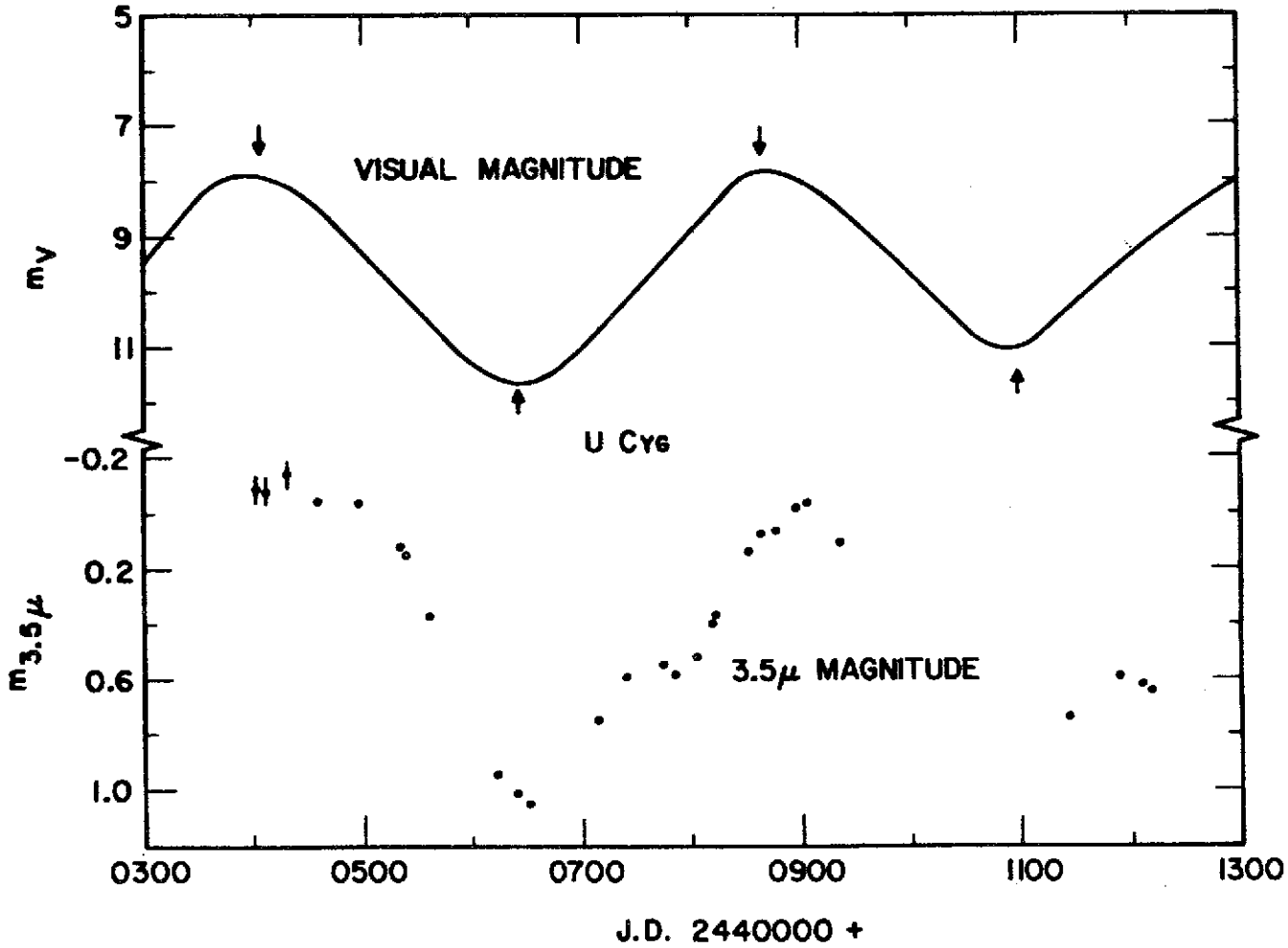

Figure 3d. Similar to figure 3a but for the carbon star U Cyg($C7_2e$).

variability as functions of Julian date for χ Cyg, R Cyg, R Aql, and U Cyg. These stars were selected because their data are among the most complete and continuous. The visual curves represent an eye estimate of the raw observational data supplied by the AAVSO. Representative error bars for the 3.5μ observations are typically about $\pm\ 0^{m}.05$, unless otherwise noted. The times of visual maximum (AAVSO) and minimum are noted by arrows on the graphs.

Figure 4 graphs the 3.5μ magnitude as a function of phase for all of the M stars in the program for which phases could be computed. The distinct light cycles are coded as follows: + = cycle 1, o = 2, ● = 3, x = 4, Δ = 5, □ = 6. Figure 4a plots those stars with periods less than 300 days, figure 4b does the same for stars whose periods lie between 301 and 350 days; figure 4c is the same except for periods between 351 and 400 days and figure 4d includes stars whose periods exceed 400 days. Figure 5 is similar to figure 4 but includes only S type stars and figure 6 graphs the data for carbon stars.

It is obvious that some stars in the original program listed in table IV are not plotted in figures 4, 5 or 6. These omissions of T Cnc, WZ Cas, RT Cyg, RY Dra, and W Ori merit further comment:

T Cnc[N3($C4_5$),482^{d},IRC+20207]is a semi-regular variable

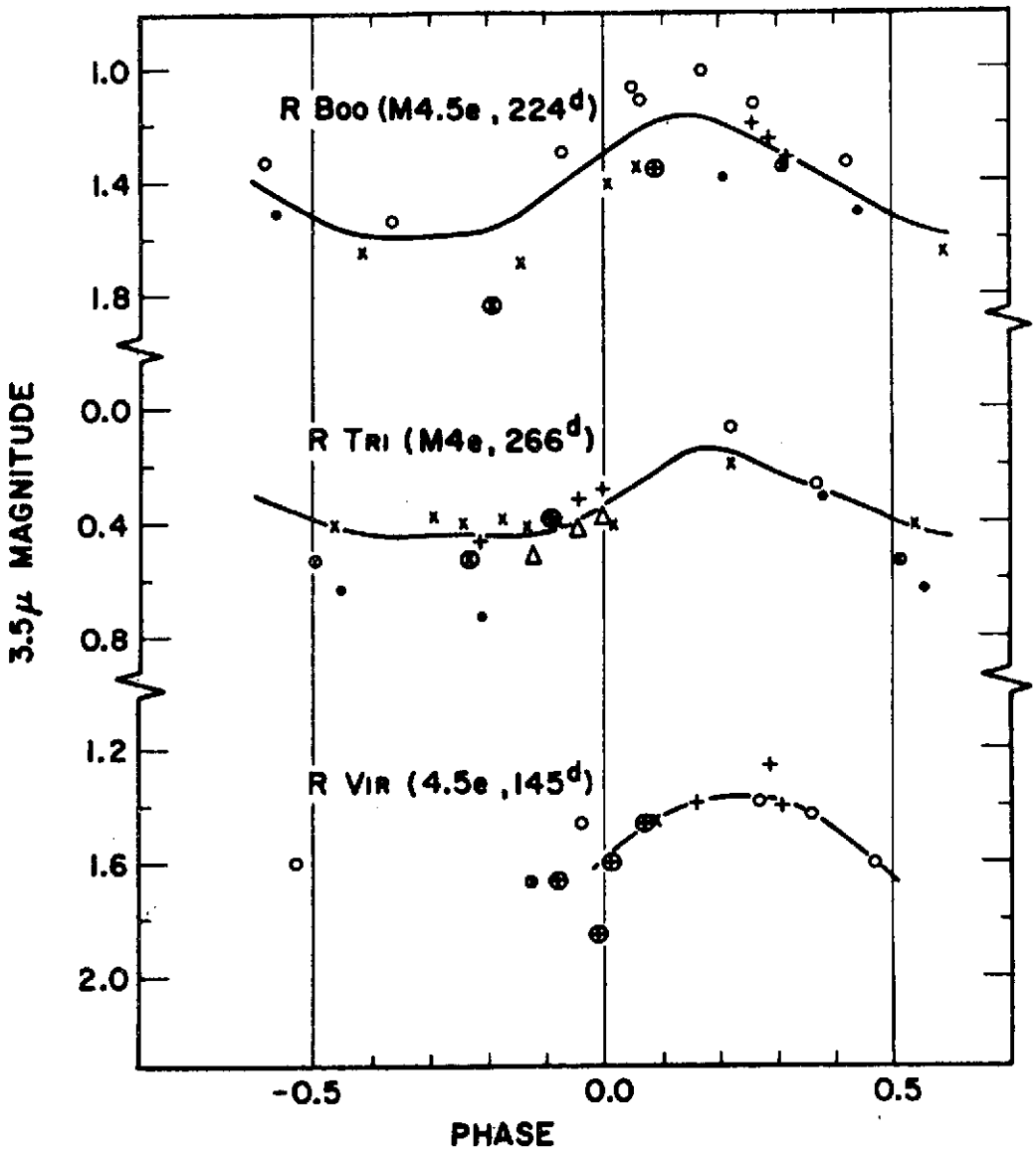

Figure 4a. 3.5μ light curves as a function of visual phase for the M stars with periods less than 300 days. The distinct cycles are coded as follows: +=cycle 1, 0=2, ●=3, x=4, Δ=5, □=6. The errors in the measurements are estimated to be between 5 and 10%. The magnitudes enclosed in circles are of poorer quality. The curve drawn through the measurements represents a best "eye" estimate as to the shape and mean value of the 3.5μ variations.

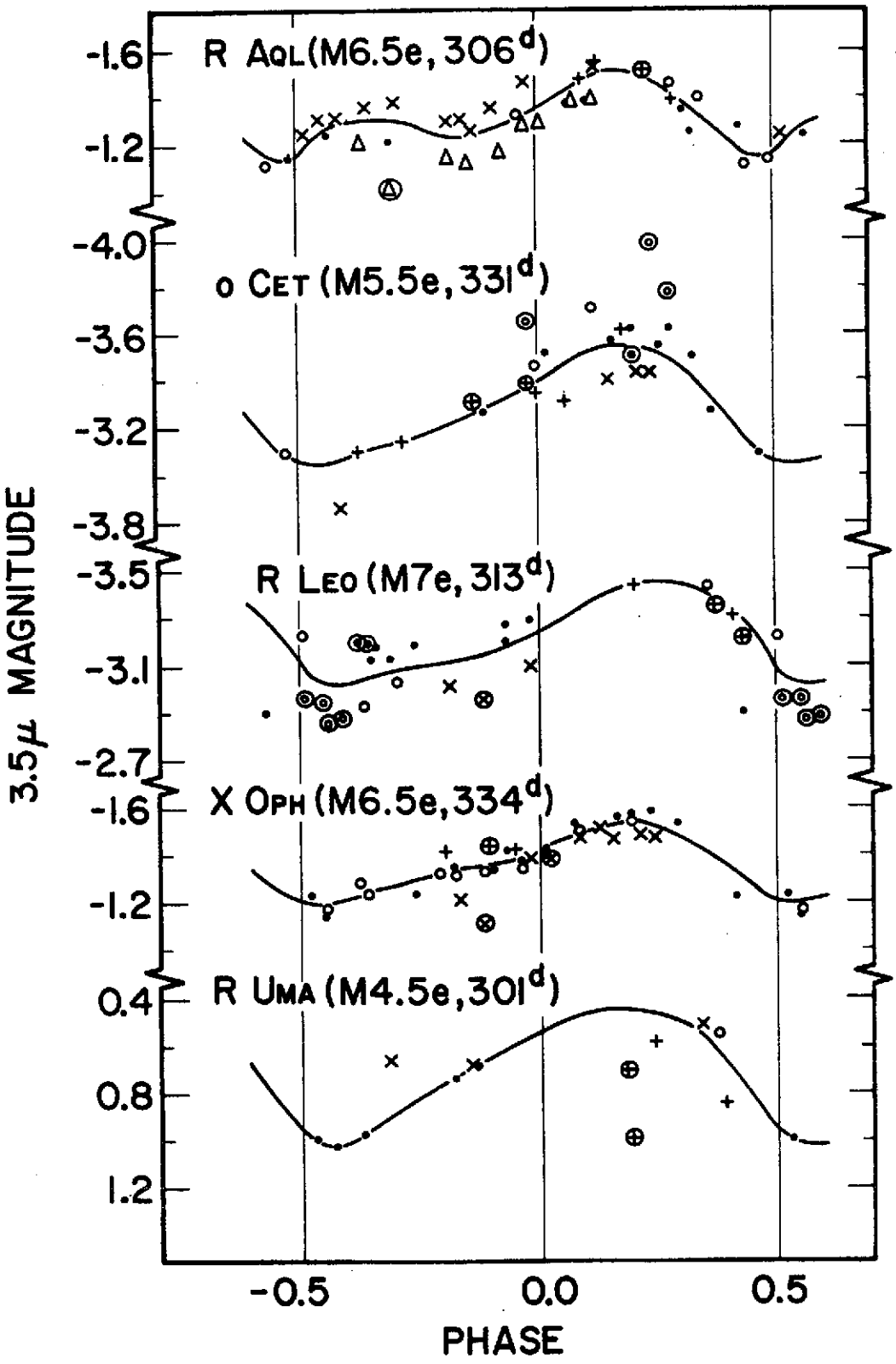

Figure 4b. Similar to figure 4a but for M stars with periods between 301 and 350 days.

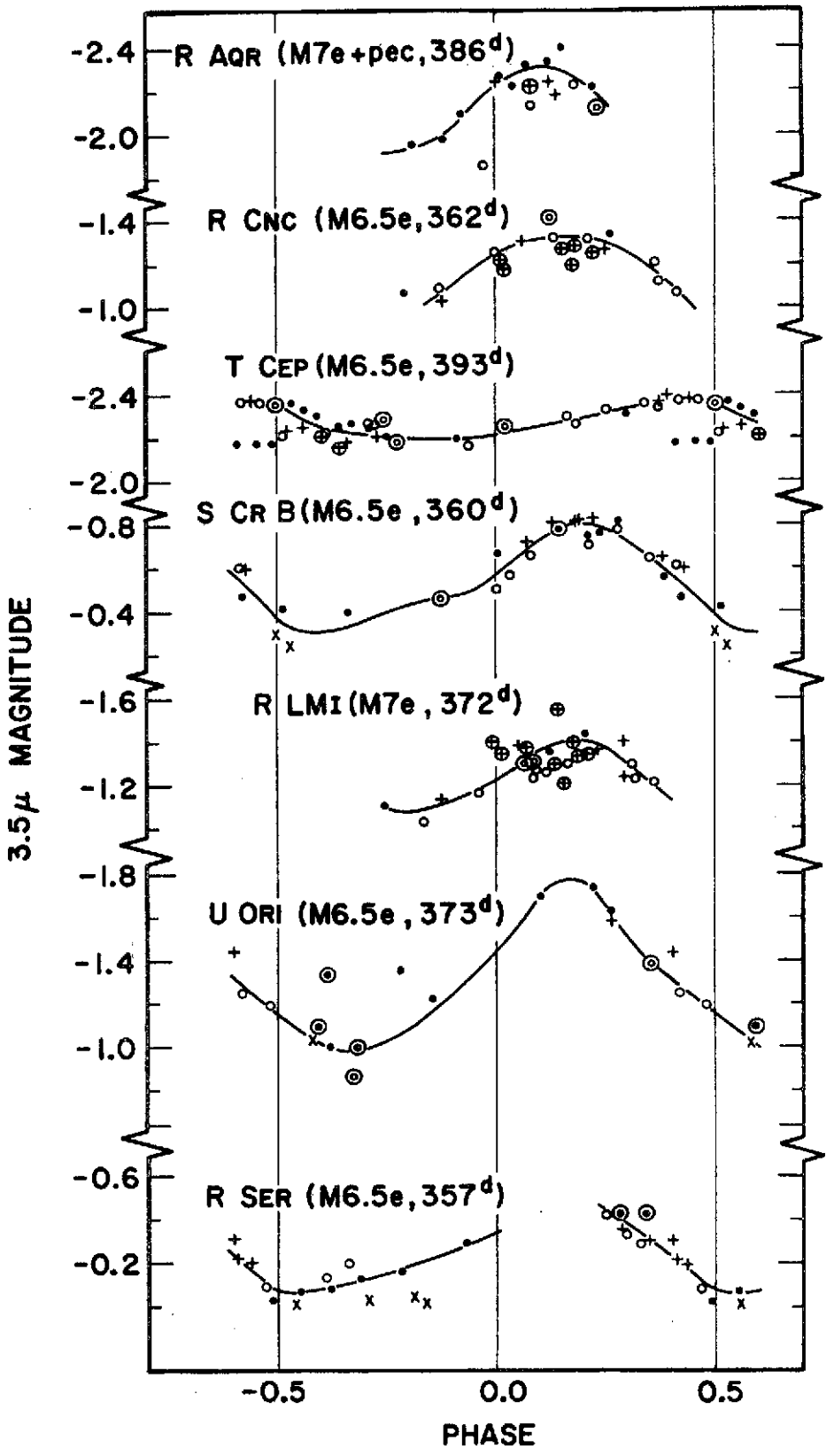

Figure 4c. Similar to figure 4a but for M stars with periods between 351 and 400 days.

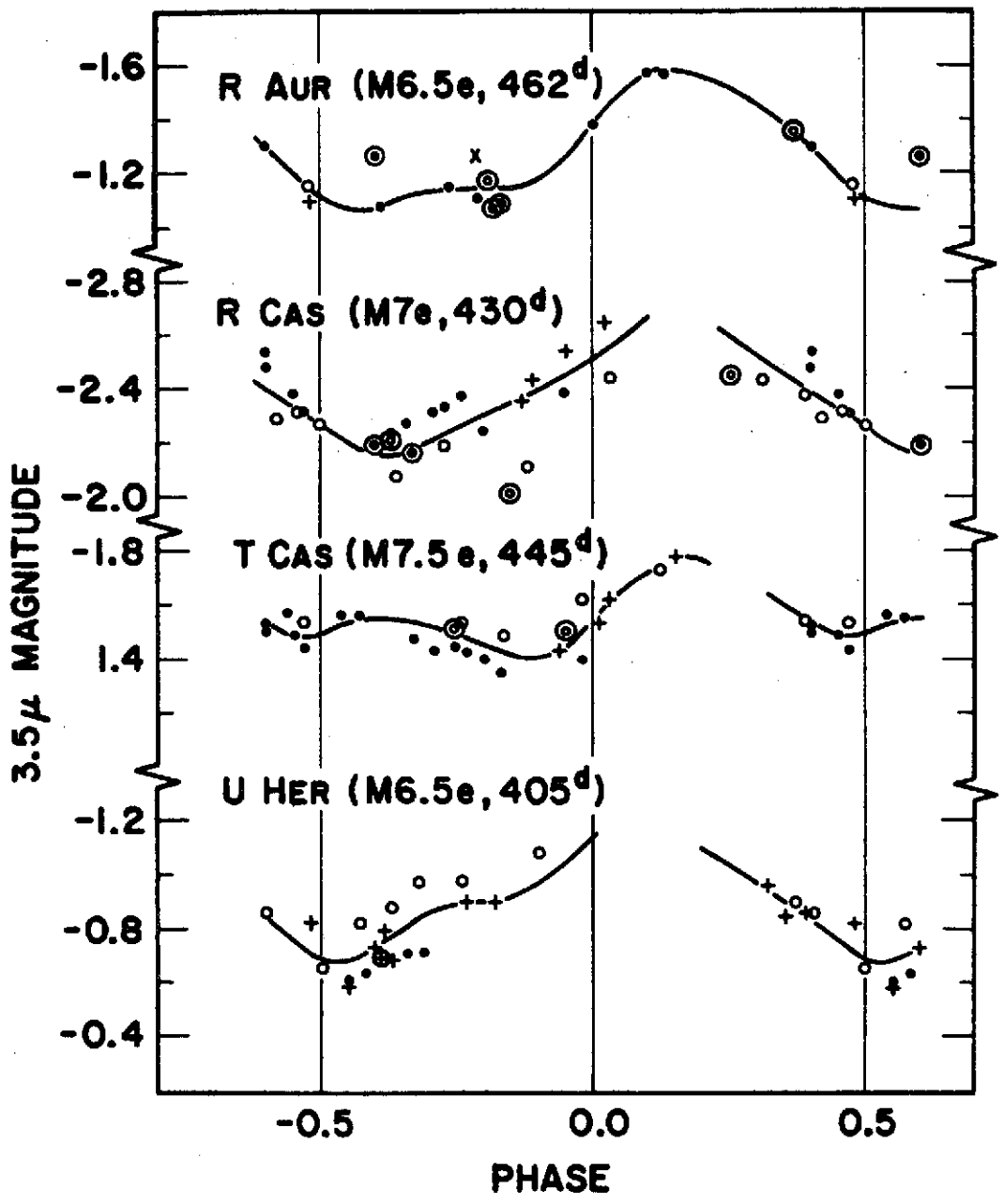

Figure 4d. Similar to figure 4a but for M stars with periods greater than 400 days.

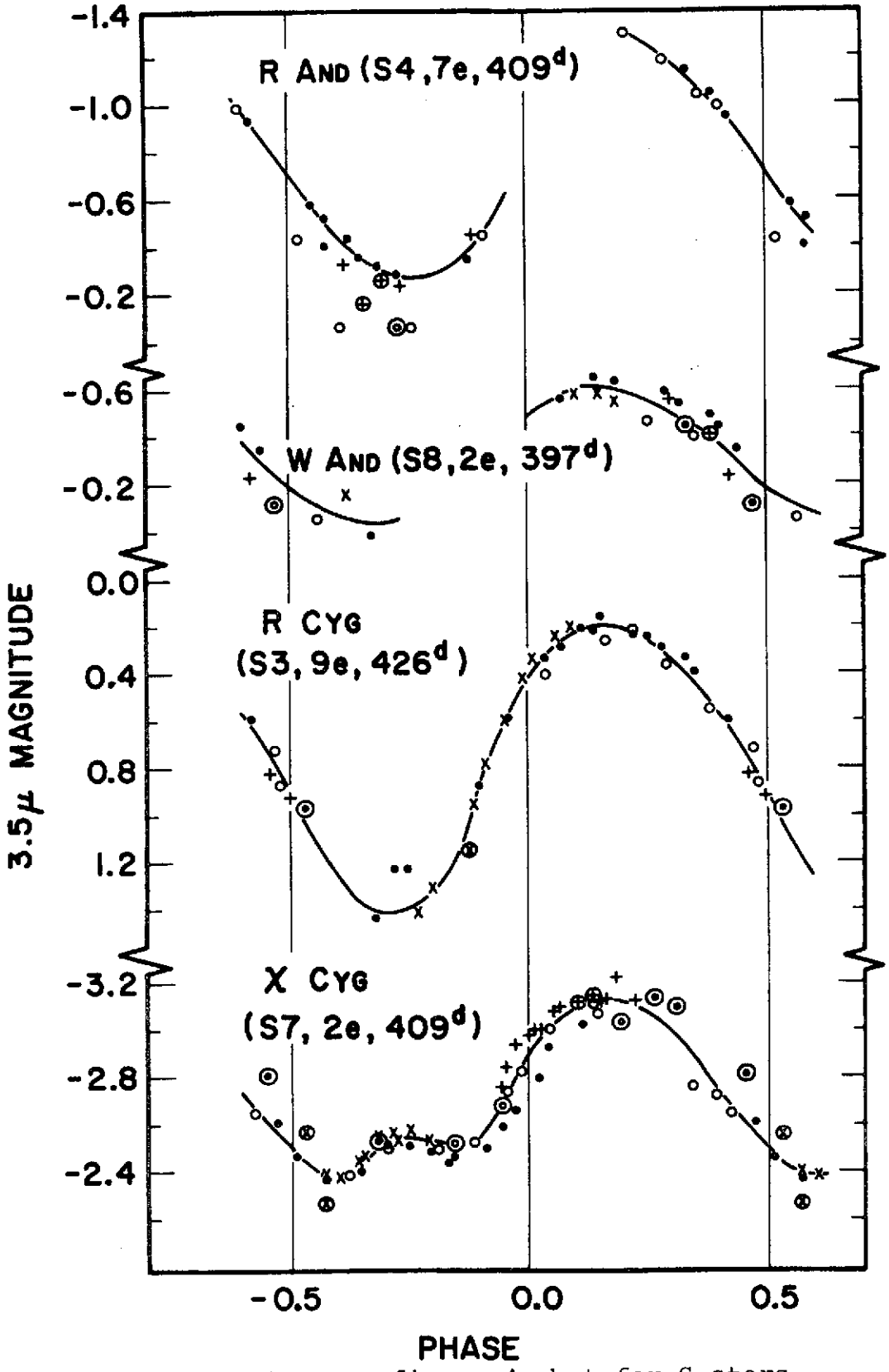

Figure 5. Similar to figure 4a but for S stars.

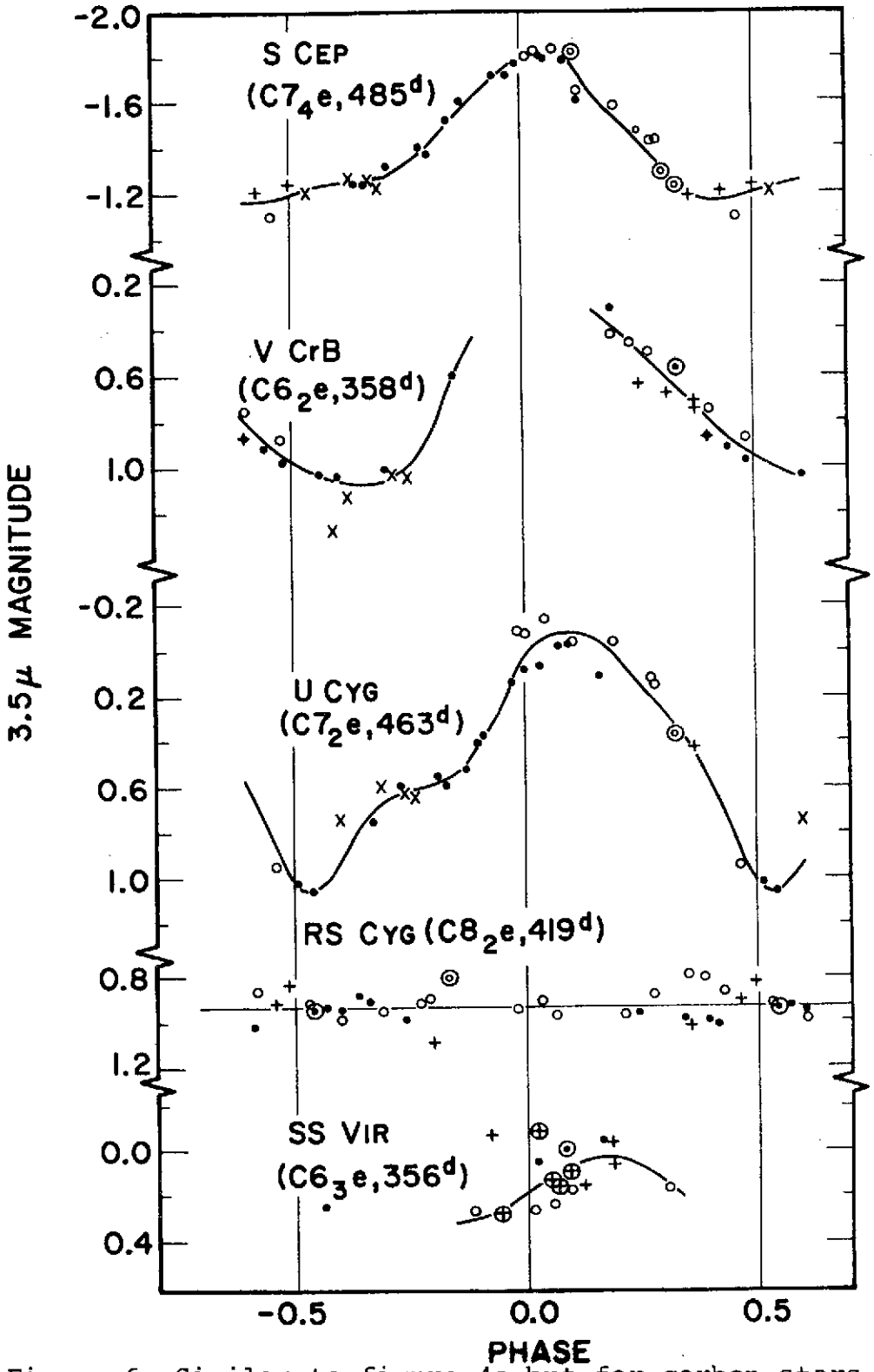

Figure 6. Similar to figure 4a but for carbon stars.

whose visual data from the AAVSO were deemed insufficient to produce Julian dates of visual maxima. The scarcity of reliable 3.5μ data points, which seem to exhibit little if any variation other than observational errors, allows little to be stated about variability and phase. The adopted 3.5μ magnitude is $+ 0^{m}.26 \pm 0^{m}.02$ (1 standard deviation of the mean) from 12 data points.

WZ Cas [Np ($C9_1$), 186^{d}, IRC+60433] is another SRa variable. Again, the AAVSO visual data were considered insufficient for determining dates of visual maxima. However, in contrast to other omitted stars, WZ Cas does seem to exhibit a real variation at the 3.5μ wavelength.

RT Cyg [M2.5e, 191^{d}, IRC+50306], in contrast to the previous stars, is a Mira type variable. The AAVSO data well demonstrated the visual variations, but at 3.5μ this star was too dim for reliable data. The adopted 3.5μ magnitude is $+2^{m}.74 \pm 0^{m}.07$ from 9 observations.

RY Dra [N4p ($C3_4$), $172^{d}.5$, IRC+70116, SRb]: No visual observations from the AAVSO were available. The 3.5μ magnitudes are scarce and range between $-0^{m}.40$ to $-0^{m}.59$ for good quality observations. The adopted mean 3.5μ magnitude is $-0^{m}.52 \pm 0^{m}.02$.

W Ori [N5 ($C5_3$), 212^{d}, IRC+00066, SRb]: The AAVSO

visual data were again inadequate for days of visual maxima. The reliable 3.5μ data were sparse and ranged between $-0^m.82$ to $-1^m.01$. The adopted mean magnitude was determined to be $-0^m.94 \pm 0^m.02$.

Figure 7 is a plot of the 3.5μ observational magnitudes as a function of visual phase for χ Cyg, the star with the most complete and continuous data. This is the same data as in figure 5 but on an expanded magnitude and phase scale. From this curve, the reproducibility and quality of the data and the cycle to cycle changes in magnitude and shape are more easily seen.

The solid lines drawn on the preceding figures represent a best eye estimate to the data. The attempt was made to determine the shape of the 3.5μ light curve from observations on the same cycle. This general shape for each stellar curve was then adjusted (again, by eye) to represent a mean magnitude averaged over the separate cycles. Of course, data of poor quality were given less weight. The solid curves thus depict the best eye estimate to the available data, and represent shape and mean magnitude as functions of phase. It was felt that a more sophisticated analysis of the data, such as a least squares method, would not produce more meaningful curves because of the apparent cycle to cycle changes in magnitude

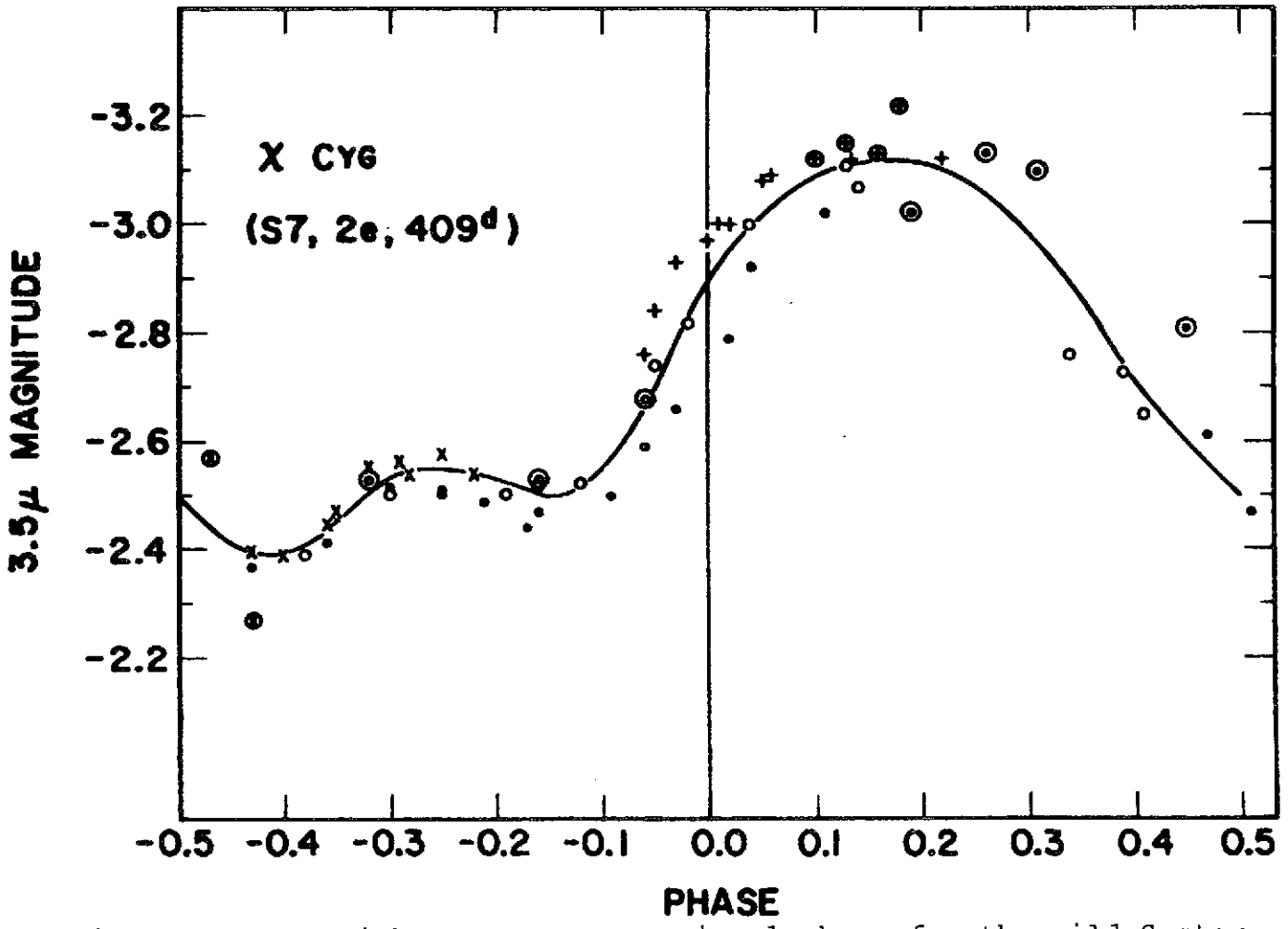

Figure 7. 3.5μ light curve versus visual phase for the mild S star χ Cyg(S7,2e) on an expanded magnitude and phase scale.

Table V

Adopted 3.5μ Magnitudes as a Function of Phase

Phase	R And	W And	R Aql	R Aqr	R Aur	R Boo	R Cnc	R Cas	T Cas
-0.50	-0.72	-0.18	-1.16	-	-1.11	1.52	-	-2.27	-1.50
.45	-0.58	-0.12	-1.25	-	-1.07	1.57	-	-2.19	-1.54
.40	-0.46	-0.08	-1.29	-	-1.07	1.59	-	-2.15	-1.55
.35	-0.36	-0.04	-1.30	-	-1.11	1.60	-	-2.16	-1.54
.30	-0.29	-0.03	-1.30	-	-1.13	1.60	-	-2.20	-1.53
.25	-0.27	-	-1.28	-	-1.13	1.59	-	-2.25	-1.50
.20	-0.28	-	-1.24	-1.94	-1.13	1.58	-	-2.30	-1.46
.15	-0.32	-	-1.22	-1.97	-1.14	1.53	-1.03	-2.35	-1.41
.10	-0.41	-	-1.25	-2.03	-1.17	1.46	-1.10	-2.39	-1.41
-0.05	-0.60	-	-1.29	-2.13	-1.25	1.39	-1.18	-2.44	-1.45
0.00	-	-0.49	-1.34	-2.22	-1.38	1.31	-1.25	-2.51	-1.54
+0.05	-	-0.55	-1.40	-2.28	-1.49	1.24	-1.29	-2.59	-1.65
.10	-	-0.60	-1.46	-2.30	-1.56	1.19	-1.32	-2.66	-1.72
.15	-	-0.61	-1.50	-2.29	-1.58	1.17	-1.33	-	-1.78
.20	-1.30	-0.59	-1.50	-2.23	-1.56	1.19	-1.32	-	-1.77
.25	-1.25	-0.55	-1.46	-2.15	-1.51	1.24	-1.31	-2.60	-

Table V (continued)

Phase	R And	W And	R Aql	R Aqr	R Aur	R Boo	R Cnc	R Cas	T Cas
.30	-1.17	-0.50	-1.40	-	-1.45	1.29	-1.26	-2.53	-
.35	-1.08	-0.45	-1.32	-	-1.38	1.35	-1.20	-2.46	-1.61
.40	-0.99	-0.37	-1.23	-	-1.30	1.40	-1.11	-2.40	-1.55
.45	-0.86	-0.27	-1.15	-	-1.20	1.46	-1.00	-2.33	-1.49
+0.50	-0.72	-0.18	-1.16	-	-1.11	1.52	-	-2.27	-1.50

Phase	S Cep	T Cep	O Cet	S CrB	V CrB	R Cyg	U Cyg
-0.50	-1.20	-2.35	-3.06	-0.38	0.96	0.90	1.01
.45	-1.23	-2.30	-3.05	-0.32	1.01	1.10	1.04
.40	-1.25	-2.26	-3.07	-0.31	1.05	1.25	0.92
.35	-1.25	-2.24	-3.11	-0.33	1.07	1.37	0.74
.30	-1.27	-2.22	-3.13	-0.36	1.05	1.41	0.65
.25	-1.33	-2.21	-3.16	-0.40	1.00	1.40	0.61
.20	-1.41	-2.20	-3.20	-0.43	0.85	1.34	0.58
.15	-1.51	-2.20	-3.24	-0.45	0.60	1.20	0.54
.10	-1.62	-2.20	-3.29	-0.47	0.43	0.86	0.41
-0.05	-1.71	-2.20	-3.33	-0.50	-	0.62	0.22
0.00	-1.79	-2.21	-3.39	-0.58	-	0.44	0.02

Table V (continued)

Phase	S Cep	T Cep	O Cet	S CrB	V CrB	R Cyg	U Cyg
+0.05	-1.81	-2.23	-3.46	-0.65	-	0.30	-0.06
.10	-1.79	-2.25	-3.51	-0.73	-	0.23	-0.08
.15	-1.63	-2.27	-3.54	-0.79	0.33	0.20	-0.05
.20	-1.53	-2.29	-3.54	-0.80	0.41	0.21	0.04
.25	-1.44	-2.31	-3.52	-0.78	0.51	0.26	0.16
.30	-1.33	-2.33	-3.47	-0.73	0.60	0.34	0.26
.35	-1.21	-2.35	-3.38	-0.66	0.70	0.43	0.39
.40	-1.17	-2.37	-3.25	-0.58	0.79	0.57	0.58
.45	-1.17	-2.37	-3.13	-0.48	0.88	0.71	0.80
+0.50	-1.20	-2.35	-3.06	-0.38	0.96	0.90	1.01

Phase	χ Cyg	U Her	R Leo	R LMi	X Oph	U Ori	R Ser	R Tri
-0.50	-2.50	-0.69	-3.09	-	-1.20	-1.16	-0.08	0.38
.45	-2.41	-0.69	-3.03	-	-1.20	-1.08	-0.07	0.42
.40	-2.39	-0.73	-3.03	-	-1.22	-1.00	-0.08	0.45
.35	-2.45	-0.80	-3.06	-	-1.25	-0.98	-0.10	0.45
.30	-2.53	-0.86	-3.08	-	-1.27	-0.99	-0.13	0.44

Table V (continued)

Phase	χ Cyg	U Her	R Leo	R LMi	X Oph	U Ori	R Ser	R Tri
.25	-2.55	-0.89	-3.10	-1.08	-1.30	-1.02	-0.15	0.44
.20	-2.53	-0.90	-3.11	-1.07	-1.33	-1.07	-0.19	0.44
.15	-2.50	-0.92	-3.13	-1.09	-1.35	-1.15	-0.22	0.45
.10	-2.55	-0.97	-3.16	-1.12	-1.36	-1.24	-0.26	0.44
-0.05	-2.70	-1.04	-3.19	-1.17	-1.38	-1.33	-0.30	0.41
0.00	-2.90	-1.13	-3.24	-1.22	-1.42	-1.44	-0.34	0.34
+0.05	-3.01	-	-3.29	-1.29	-1.46	-1.55	-	0.28
.10	-3.09	-	-3.35	-1.37	-1.50	-1.70	-	0.21
.15	-3.11	-	-3.41	-1.40	-1.52	-1.77	-	0.15
.20	-3.11	-1.09	-3.44	-1.40	-1.54	-1.76	-	0.14
.25	-3.07	-1.03	-3.45	-1.38	-1.51	-1.65	-0.44	0.18
.30	-2.98	-0.97	-3.44	-1.30	-1.46	-1.51	-0.38	0.23
.35	-2.87	-0.90	-3.41	-1.22	-1.41	-1.40	-0.31	0.27
.40	-2.73	-0.84	-3.35	-1.13	-1.34	-1.32	-0.24	0.31
.45	-2.61	-0.76	-3.26	-	-1.26	-1.24	-0.16	0.35
+0.50	-2.50	-0.69	-3.09	-	-1.20	-1.16	-0.08	0.38

Table V (continued)

Phase	R UMa	R Vir	SS Vir
-0.50	0.95	1.65	-
.45	1.01	-	-
.40	1.01	-	-
.35	0.94	-	-
.30	0.88	-	-
.25	0.82	-	-
.20	0.76	-	-
.15	0.71	-	-
.10	0.65	-	0.30
-0.05	0.60	-	0.26
0.00	0.55	1.58	0.20
+0.05	0.50	1.50	0.13
.10	0.47	1.43	0.08
.15	0.45	1.39	0.05
.20	0.46	1.37	0.06

Table V (continued)

Phase	R UMa	R Vir	SS Vir
.25	0.48	1.37	0.10
.30	0.51	1.38	0.17
.35	0.57	1.42	-
.40	0.69	1.48	-
.45	0.81	1.57	-
+0.50	0.95	1.65	-

and phase.

After these eyeball curves were drawn, the average 3.5μ magnitude as a function of phase was recorded in table V for phases -0.5 to +0.5 in steps of 0.05. It must be emphasized that table V is a mean curve; individual cycles may deviate 10 to 20% from the magnitude but, hopefully, will retain the general shape of the curve.

There are some general remarks to be made concerning the 3.5μ light curves as plotted in figures 4-7. One comment is that there are cycle to cycle variations- the 3.5μ magnitudes are not identical at similar phase points in differing cycles. Part of this alteration may be masked within the observational errors, and part may be due to slightly changed periods among different cycles causing errors in the phase calculations. However, where the data are most complete, as in χ Cyg for example, the cycle to cycle changes appear to be real and can vary as much as 10-20% from the adopted mean curve. Inspection of the figures does not allow any statement about the relation of cycle to cycle variations to period or to spectral type.

A second feature evidenced by the figures concerns the shape of the 3.5μ light curve. Again, for stars with the most complete data, the general shape of the 3.5μ curve may be retained, but its magnitude is

altered. The shape of the light curve is not a simple trigonometric function and certainly is not a reproduction of the visual curve reduced in amplitude.

One of the most significant aspects of the figures is the phase lag between the 3.5μ and visual light curves. This lag is the rule rather than the exception. Maximum brightness at 3.5μ usually occurs between phase 0.1 and 0.2, whereas minimum brightness occurs (about one-half cycle later) near phase -0.4 to -0.3. There are some exceptions to this minimum phase, however, notably T Cep and T Cas which will be discussed later.

Probably the second most interesting aspect of the 3.5μ light curves is the existence of humps in the rising branch near phase -0.3 to -0.2. The most obvious examples are R Aql, T Cas, U Her, χ Cyg and U Cyg. This hump may be on the order of the estimated errors in measurement but appears to be real as it is evident over more than one cycle (e.g. χ Cyg). This feature then tends to move the primary minimum 3.5μ brightness to earlier phases near -0.4 and may then produce a secondary maximum near phase -0.25 and a secondary minimum near phase -0.15.

Unfortunately, for some of the stars much of the data is not complete enough to ascertain the presence of humps. For the objects with good data coverage, these secondary extrema do not seem to occur

in all cases. Some light curves merely possess an inflection point or shape alterations on the rising portion of the 3.5μ light curve near phase -0.25. True humps seem to be the rarity while inflections are more common.

Each Mira type variable star seems to have a personality all its own and its behavior cannot be sufficiently described by a few parameters such as mean spectral type at maximum, mean period and mean amplitude at distinct wavelengths. Comments pertaining to some of the individual stars in figures 4, 5 and 6 are included in the following section to provide additional information.

R Boo {M 4.5e, 224^d, IRC + 30260}: Cycle 2 which had its visual maximum near J. D. 2440730 was brighter than normal and appears to be reflected in the 3.5μ data also.

R Tri {M 4e, 266^d, IRC + 30044}: This star demonstrates reasonably good reproducibility at visual and 3.5μ wavelengths. It was measured radiometrically by Pettit and Nicholson (1933).

R Vir {M 4.5e, 145^d, IRC + 10256}.

R Aql {M 6.5e, 306^d, IRC + 10406}: The period of this star has been decreasing from near 350^d, at the turn of the century, to 293^d since 1954 (Ahnert,

1964, 1965; Schnellar, 1965). Campbell (1955) cites a 306^d period, whereas a 283^d period was used in the phase calculations. This object has a hump on the ascending portion of the 3.5μ light curve. It is also a known OH (Wilson and Barrett, 1970) and H_2O microwave emitter (Schwartz and Barrett, 1970).

o Cet {M 5.5e, 331^d, IRC + 00030}: This object had an unusually bright visual maximum near J. D. 2440460, or 3.5μ cycle 2, which also may be reflected in the 3.5μ data. o Cet is a known binary, but its companion should not affect the 3.5μ observations at all. Unfortunately, the 3.5μ data quality and coverage could be improved for this prototype. It was also monitored by Pettit and Nicholson(1933).

R Leo {M 7e, 313^d, IRC + 10215}: Another Pettit and Nicholson (1933) object.

X Oph {M 6.5e, 334^d, IRC + 10366}: Another Pettit and Nicholson (1933) source. It is another known binary but the 3.5μ measurements should not be influenced by the K type companion.

R UMa {M 4.5e, 301^d, IRC + 70099}.

R Aqr {M 7e + pec, 386^d, IRC - 20642}: This star, with its peculiar spectrum,is extremely low in the Minnesota sky such that extinction uncertainties may seriously affect the data quality (which is limited to near zero phase). Pettit and Nicholson (1933)

also measured this star radiometrically.

R Cnc {M 6.5e, 362^d, IRC + 10185}: Another Pettit and Nicholson (1933) source.

T Cep {M 6.5e, 393^d, IRC + 70168}: This star is the exception to the rule at 3.5μ. It possesses a very small amplitude, but even with the observational errors, it seems unique in its phase with respect to the visual. This source seems to minimize near zero phase and maximize near phase 0.50, in direct contrast to the other variables. Lockwood and Wing (1971) support this small amplitude and the unusual shape at 1.04μ. They also comment that the period may be decreasing. Campbell (1955) quotes a mean period of 393^d, while Keenan (1966) mentions a reduction of the period since 1951 to $375^d.5$. A 382^d period seemed to fit the recent visual behavior and was used in the phase calculations. This object has been classified as an S star by Spinrad and Newburn (1965).

S CrB {M 6.5e, 360^d, IRC + 30272}: The 3.5μ observations repeat themselves quite well. This object has been reported as an H_2O microwave emitter (Schwartz and Barrett, 1970).

R LMi {M 7e, 372^d, IRC + 30215}: The 3.5μ data coverage is limited for this star also monitored by Pettit and Nicholson (1933).

U Ori {M 6.5e, 373^d, IRC + 20217}: This is an OH (Wilson and Barrett, 1970) and an H_2O source (Schwartz and Barrett, 1970).

R Ser {M 6.5e, 357^d, IRC + 20285}: Classified as a possible S star by Spinrad and Newburn (1965).

R Aur {M 6.5e, 462^d, IRC + 50141}.

R Cas {M 7.5e, 430^d, IRC + 50484}: This object seems to show true cycle to cycle alterations in agreement with Lockwood and Wing (1971). The visual maximum near J. D. 2441020 was brighter than normal and corresponds to 3.5μ cycle 3, which also supports this fact.

T Cas {M 7.5e, 445^d, IRC + 60009}: This source has one of the most pronounced humps on the rising branch of the 3.5μ light curve. This extreme hump is also seen in the mean visual curve (Campbell, 1955) and in the 1.04μ light curve (Lockwood and Wing, 1971). This object has also been classified as an S type star (Spinrad and Newburn, 1965).

U Her {M 6.5e, 405^d, IRC + 20298}: This H_2O microwave emitter (Schwartz and Barrett, 1970) seems to have an inflection point on the rising portion of the 3.5 light curve.

R And {S4, 7e, 409^d, IRC + 40009}: Cycle 3, which had its visual maximum near J. D. 2441050, was visually brighter than normal but this brightness

is not evidenced by the 3.5μ measurements.

W And {S8, 2e, 397^{d}, IRC + 40037}.

R Cyg {S3, 9e, 426^{d}, IRC + 50301}: Another object measured by Pettit and Nicholson (1933). The 3.5μ data reproduction is much better than could be expected for the magnitude range of this source. It has one of the largest ($\sim 1^{m}.2$) 3.5μ variations of any of the stars of this program.

χ Cyg {S7, 2e, 409^{d}, IRC + 30395}: This star has the most complete and continuous 3.5μ data coverage. The visual maximum near J.D. 2440480 was a little brighter than average, but does not seem so at 3.5μ in cycle 2. Cycle 3 at 3.5μ appears dimmer than average and may be supported by the visual observations. This object has the most well documented hump at 3.5μ in the ascending branch of the light curve. This hump is only slightly reflected in the visual curves (Campbell, 1955) but seems present at 8500 Å (Hetzler, 1936). This anomaly may or may not be present in every cycle at 1.04μ (Lockwood and Wing, 1971). This star has the largest visual range ($\sim 8^{m}.2$) of any well observed Mira variable. In the infrared, the 3.5μ range is definitely not the largest.

S Cep {$C7_{4}e$, 485^{d}, IRC + 80048}.

V CrB {$C6_2e$, 358^d, IRC + 40273}.

U Cyg {$C7_2e$, 463^d, IRC + 50324}: This carbon star has an inflection point near phase -0.25.

RS Cyg {$C8_2e$, 419^d, IRC + 40397}: This star is unusual because it demonstrated no detectable variation at 3.5μ. This limited alteration is in reasonable agreement with the AAVSO visual data.

SS Vir {$C6_3e$, 356^d, IRC + 00217}.

In order to describe the 3.5μ variations of Mira type stars, a limited Fourier analysis method was employed. The mean magnitudes from Table V for each star were converted to relative intensities and then fitted by a seven term Fourier series. Equation 4 is the series which was used in the curve fitting.

$$I_{3.5\mu}(\theta) = K + A \sin\theta + B \cos\theta + C \sin 2\theta + D \cos 2\theta + E \sin 3\theta + F \cos 3\theta \qquad (4)$$

$I_{3.5\mu}(\theta)$ is the 3.5μ intensity expressed in relative units; $\theta = 2\pi\alpha$, where α is the visual phase; K-F are constants to be determined from the analysis.

The 7 unknowns were calculated by solving 7 simultaneous equations for intensity as a function of phase where the data were most complete (hopefully,

over the entire cycle). Seven phases were chosen from phases 0, .16, .25, .33, .50, -.33, -.25, -.16. If the data were limited to about one-half cycle, the last two terms of equation 4 were omitted.

The point must be stressed that this analysis was not accomplished with the aid of a computer but represents a simple attempt to determine the relative contributions of the various terms of the series. As seen from figures 4-7, the 3.5μ variations are typically described by a sine curve which lags the visual light curves. Table VI lists the program stars and the constants determined from this crude method. The amplitude in the second column is the ratio of the maximum to minimum observed intensity. Figure 8 plots the observed and computed relative fluxes as functions of phase for three representative stars: χ Cyg, T Cas and S Cep. This figure is included to demonstrate what shapes of curves may be described by this simple method.

It must be strongly emphasized, at this time, that the previous curve fitting, Fourier method is purely descriptive and does not imply that the overtones of the fundamental frequency are present. Mira variables are most surely non-linear oscillators and the overtones are not simple multiples of the fundamental frequency.

Table VI

Fourier Analysis Parameters

Star	Spectral Type at Maximum	Amplitude	K	A	B	C	D	E	F
R And	S4,7e	2.59	1.62	.72	.08	.10	-.07		
W And	S8,2e	1.70	1.40	.30	.195	.005	-.025		
R Aql	M6.5e	1.39	1.11	.105	.09	.055	-.06	-.005	0
R Aqr	M7e+pec	1.43	1.05	.115	.15	.08	.015		
R Aur	M6.5e	1.60	1.21	.255	.135	.06	-.06	.015	.005
R Boo	M4.5e	1.49	1.20	.20	.12	.04	0	.015	0
R Cnc	M6.5e	1.36	1.08	.25	.19	-.04	-.005		
R Cas	M7e	1.61	1.23	.22	.155	.045	-.025	.02	-.025
T Cas	M7.5e	1.41	1.18	.14	.025	.08	-.06	0	-.005
S Cep	$C7_4e$	1.81	1.28	.06	.36	.11	.085		
T Cep	M6.5e	1.17	1.07	.05	-.06	-.015	.01	0	-.01
o Cet	M5.5e	1.57	1.32	.22	.15	.03	-.06	-.01	.02
S CrB	M6.5e	1.57	1.26	.24	.11	.01	-.07	.01	-.01
V CrB	$C6_2e$	1.99	1.42	.25	.48	-.01	.14	-.04	.04
R Cyg	S3,9e	3.04	2.16	1.04	.42	.12	.04	.015	.045

Table VI (continued)

Star	Spectral Type at Maximum	Amplitude	K	A	B	C	D	E	F
U Cyg	$C7_2e$	2.82	1.78	.45	.64	.15	-.035	.08	.10
χ Cyg	S7,2e	1.89	1.27	.34	.21	.08	-.04	.05	.015
U Her	M6.5e	1.50	1.26	.12	.23	.05	-.02	.03	.02
R Leo	M7e	1.47	1.24	.215	.05	-.03	-.07	.01	.03
R LMi	M7e	1.36	1.08	.155	.10	.04	-.055		
X Oph	M6.5e	1.37	1.16	.10	.115	.02	-.05	-.01	-.005
U Ori	M6.5e	2.06	1.38	.415	.215	.11	-.045	.015	-.045
R Ser	M6.5e	1.40	1.18	.15	.12	0	-.045	-.01	.015
R Tri	M4e	1.33	1.07	.14	.035	.03	-.025	.01	-.01
R UMa	M4.5e	1.64	1.34	.22	.20	-.035	-.06	.005	.03
R Vir	M4.5e	1.31	.98	.28	.04	-.005	.01		

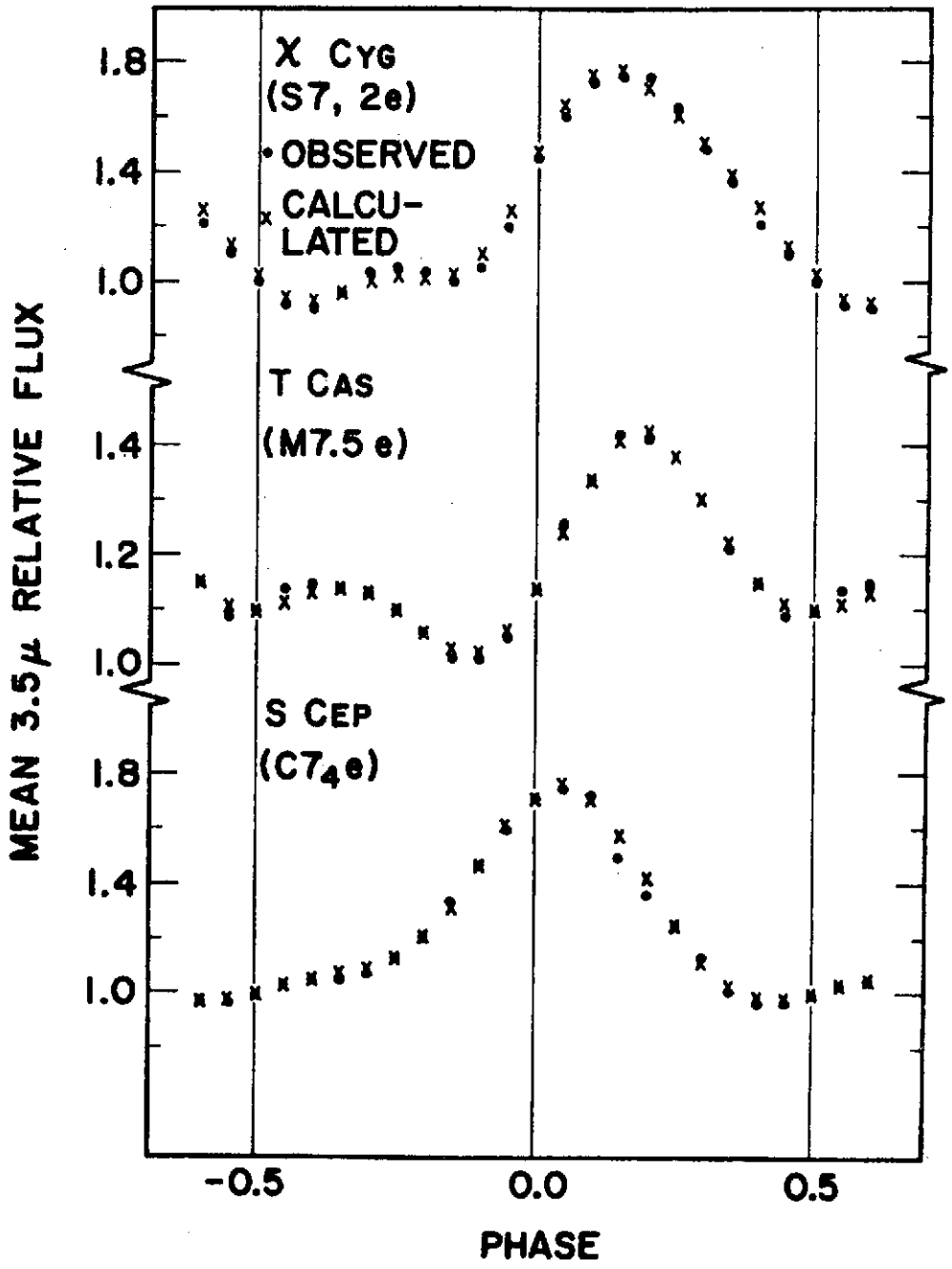

Figure 8. A comparison of the mean 3.5μ relative flux versus visual phase and the calculated flux from the limited Fourier curve fitting analysis.

VI

OTHER WAVELENGTH OBSERVATIONS

In addition to the 3.5μ observations, measurements at other wavelengths were obtained on a limited number of the same program stars. These data were collected with the Minnesota photometric systems used on the O'Brien telescope in Minnesota and on the Mt. Lemmon infrared telescope in Arizona. The details of the photometer and the absolute calibration for the various wavelengths have been previously described. The method of data acquisition and analysis was similar to that prescribed for the 3.5μ observations in preceding sections.

Table VII lists some of the calibration stars by their HR number, name, spectral type, visual magnitude, and magnitudes at other effective wavelengths. Most of the listed magnitudes are quoted to an accuracy $\pm$ 10%.

Appendix 3 tabulates the observational data for the program stars at wavelengths in addition to 3.5μ. The results are again quoted to an accuracy of $\pm$ 10%. The data are by no means complete over entire cycles because another observer (Forrest, 1973) is monitoring many of these same program stars, primarily at effective

Table VII

Magnitudes of Calibration Stars

HR	Name	Spectral* Type	m_V*	Magnitudes at Effective Wavelength (microns) 2.3	3.5	4.8	8.6	10.7	12.2	18
337	β And	MO III	2.03	-1.8	-2.05	-1.7	-2.0	-2.1	-2.1	-
1457	α Tau	K5 III	0.86	-2.9	-3.02	-2.9	-3.0	-3.1	-3.1	-3.1
2061	α Ori	M2 Iab	0.80	-4.20	-4.54	-4.20	-4.75	-5.55	-5.50	-5.65
2990	β Gem	KO III	1.15	-1.1	-1.23	-1.1	-1.2	-1.2	-1.2	-1.3
4069	μ UMa	MO III	3.04	-0.8	-1.00	-0.8	-1.0	-1.1	-1.1	-
5340	α Boo	K2 IIIp	0.06	-3.02	-3.12	-2.95	-3.16	-3.20	-3.20	-3.2
6406-7	α Her	M5 II	3.1	-3.44	-3.70	-3.48	-3.79	-4.05	-4.00	-4.1
7001	α Lyra	AO V	0.04	0.00	0.00	0.00	0.00	0.00	0.00	0.00
8316	μ Cep	M2 Ia	3.99	-1.8	-2.23	-2.2	-3.1	-4.3	-4.1	-4.7
8775	β Peg	M2 II-III	2.56	-2.24	-2.45	-2.27	-2.45	-2.55	-2.52	-2.6

* Hoffleit (1964).

wavelengths of 3.5, 4.9, 8.4 and 11.0 microns.

Many of the stars of this research project have been measured at other wavelengths of 3.5, 4.9, 8.4, and 11.0μ by Gillett, Merrill and Stein (1971), Gehrz and Woolf (1971), and Dyck, Forrest, Gillett, Stein,Gehrz, Woolf and Shawl (1971). These measurements have been summarized in table VIII in order to provide a more complete description of the energy distribution of long period variables. It must be stressed that the magnitudes quoted in table VIII have no phases listed. The date of the observation is not available nor published in the articles cited. Therefore, also included in columns 6 and 7 of the table are the observed magnitude ranges at 3.5μ as taken from table IV and appendix I. Column 8 which lists the observed [3.5μ]-[11μ] color index is included to provide an estimate of the excess radiation at 11μ arising from the circumstellar shells.

A multitude of authors have published observational data at wavelengths shorter than 3.5μ for many of these same stars (Mendoza and Johnson, 1964; Johnson, Mitchell, Iriarte and Wisniewski, 1966). From these shorter wavelength magnitudes and, in conjunction with the longer wavelength data, typical spectral energy distributions may be constructed for some of the representative LPV stars. Two examples are the carbon

Table VIII

Summary of 3.5, 4.9, 8.4 and 11.0μ Magnitudes of the Program Stars

	Magnitude at effective wavelength (microns)				3.5μ		
Star	3.5	4.9	8.4	11.0	max	min	[3.5μ]-[11μ]
R Aql	-1.19	-1.24	-1.76	-2.87 +	-1.5	-1.1	1.7
R Boo	1.18			0.42 +	1.1	1.7	0.8
	1.26	1.10	0.71	0.26 :			1.0
	1.34	1.03	0.64	0.10 *			1.2
R Cnc	-1.33	-0.88	-1.49	-2.55 +	-1.3	-1.0	1.2
	-1.16	-1.51	-1.94	-2.56 *			1.4
T Cnc	0.42	0.59	-0.56	-0.65 *	0.2	0.4	1.1
R Cas	-2.06	-2.18		-4.08 +	-2.6	-2.1	2.0
	-2.00	-2.43	-3.06	-4.10 *			2.1
T Cas	-1.52			-2.61 +	-1.8	-1.4	1.1
	-1.58	-1.67	-2.22	-2.94 *			1.4
WZ Cas	0.46	0.54	0.23	-0.04 *	-0.1	0.4	0.5
S Cep	-1.64	-2.02		-2.91 +	-1.8	-1.1	1.3
	-1.47	-1.73	-2.63	-3.11 *			1.6
T Cep	-2.22	-2.12	-2.72	-3.15 *	-2.4	-2.2	0.9
o Cet	-3.49			-5.45 +	-3.7	-2.9	2.0
	-3.49	-3.81	-4.59	-5.63 :			2.1
V CrB	1.29	0.69	-0.11	-0.85 *	0.3	1.3	2.1

Table VIII (continued)

Star	Magnitude at effective wavelength (microns) 3.5	4.9	8.4	11.0	3.5μ max	3.5μ min	[3.5μ]-[11μ]
S CrB	-0.60	-0.98	-1.98	-2.83 +	-0.8	-0.3	2.2
	-0.74	-1.19	-2.18	-3.12 *			2.4
R Cyg	0.20	0.19	-0.68	-1.27 *	0.2	1.4	1.5
U Cyg	0.65	0.24	-0.57	-1.40 +	-0.1	1.0	2.1
	0.00	-0.28	-1.00	-1.61 *			1.6
RS Cyg	1.19	1.31	0.66	0.52 *	0.8	1.1	0.7
χ Cyg	-2.25	-2.57	-3.21	-4.00 +	-3.2	-2.4	1.7
	-2.95	-3.06	-3.35	-4.16 *			1.2
RY Dra	-0.37	0.03	-1.10	-1.20 *	-0.4	-0.4	0.8
U Her	-0.78	-1.11	-1.67	-2.59 +	-1.0	-0.6	1.8
R Leo	-3.25	-3.59	-4.02	-4.93 +	-3.4	-2.9	1.7
	-3.17	-3.39	-3.92	-4.65 :			1.5
	-3.21	-3.41	-3.90	-4.56 *			1.3
R LMi	-1.15	-0.96	-2.15	-2.83 +	-1.4	-1.0	1.7
	-1.14	-1.60	-2.11	-2.82 *			1.7
X Oph	-1.45	-1.49		-2.76 +	-1.6	-1.0	1.3

Table VIII (continued)

Star	Magnitude at effective wavelength (microns) 3.5	4.9	8.4	11.0		3.5μ max	3.5μ min	[3.5μ]-[11μ]
U Ori	-1.20	-0.93	-1.80	-2.82	+	-1.7	-1.0	1.6
	-1.37	-1.66	-2.11	-3.00	*			1.6
W Ori	-0.72	-0.33	-1.24	-1.74	*	-1.1	-0.8	1.0
R Ser	0.18	-0.03	-0.58	-1.26	*	-0.4	0.0	1.4
R Vir	1.49	1.08	0.78	0.64	*	1.3	1.6	0.8
SS Vir	0.17	0.46	-0.56	-0.99	*	0.0	0.3	1.2

: Dyck et al. (1971).

+ Gehrz and Woolf (1971).

* Gillett, Merrill and Stein (1971).

star U Cyg near infrared maximum and the mild S star χ Cyg near infrared (3.5μ) minimum, as plotted in figure 9. The figures depict λF_λ in watts/cm^2 versus wavelength. U Cyg has been brightened by 4 magnitudes in the graph. The short wavelength U - L points are from Mendoza and Johnson (1965). The longer wavelengths are from Gehrz and Woolf (1971), and Gillett, Merrill and Stein (1971). These two figures are included to emphasize the differences in spectral shape among the carbon rich and the oxygen rich stars. These differences will also be discussed in a later section.

In addition to these multi-wavelength measurements, brightness changes of long period variable stars at single selected wavelengths have been monitored by individuals and groups. In the visual region, the American Association of Variable Star Observers (AAVSO) monitors many LPV stars. Near 8500 Å, Hetzler (1936) catalogued the variations. Landolt measures UBV of many Mira variables. Pettit and Nicholson (1933) were the first to measure the radiometric changes. More recently, Lockwood and Wing (1971) and Lockwood (1972) have measured changes at wavelengths near one micron.

Lockwood and Wing (1971) produced narrow band photometry on a group of M type Miras at wavelengths

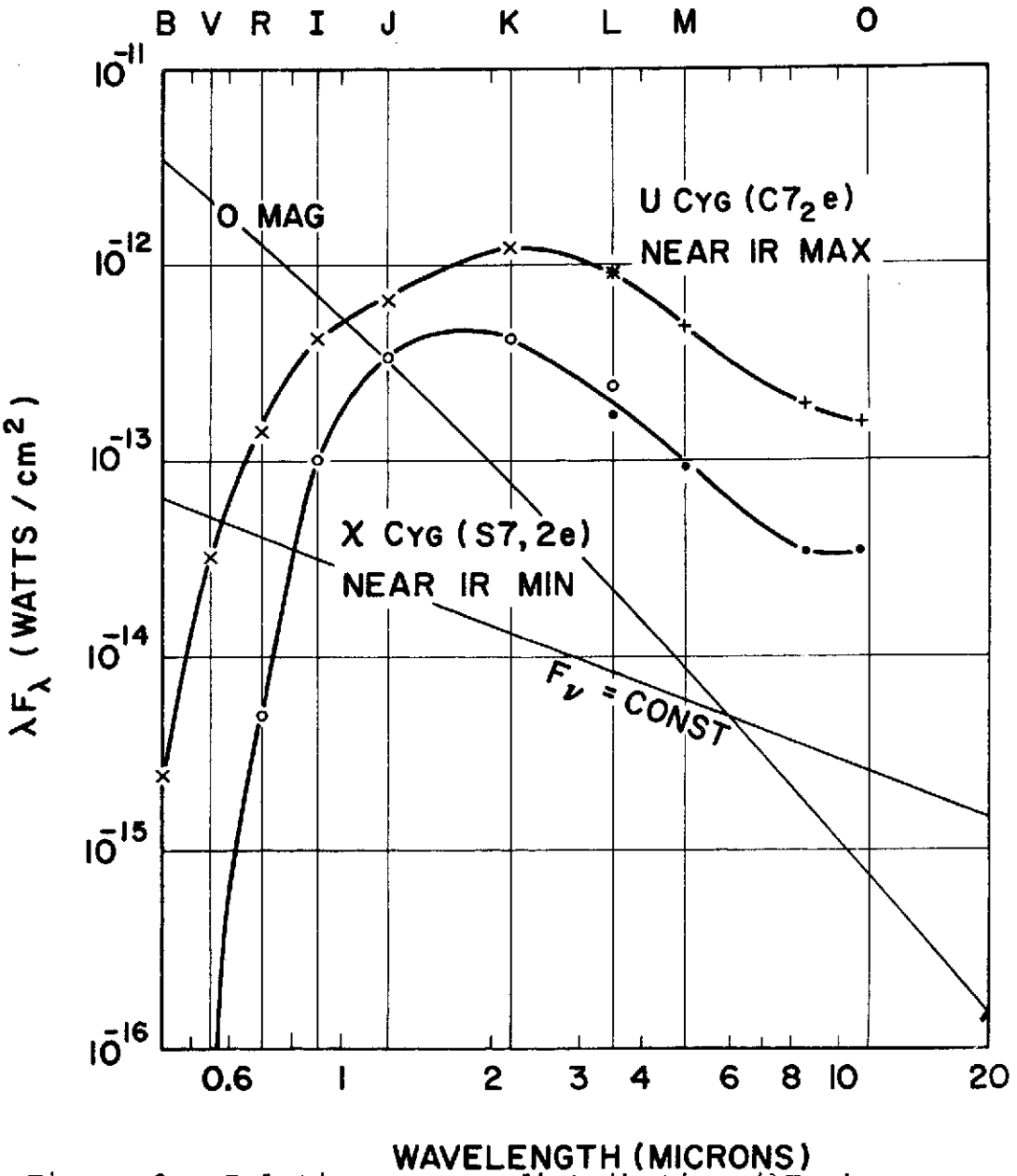

Figure 9. Relative energy distribution (λF_λ in watts/cm^2 versus wavelength) for the mild S star (χ Cyg) and a carbon star (U Cyg). U Cyg has been brightened by 4 magnitudes.

of .78, .87, .88, 1.04 and 1.05 microns. In the oxygen rich stars, they believe that the 1.04μ magnitudes are uncontaminated by absorption, and, therefore, represent the true continuum point of the photospheric temperature. They have measured light curves in 5 colors for two stars (o Cet and T Cas). For many other variables they produced light curves at 1.04μ only.

By pure chance, but also because of apparent brightness, Lockwood and Wing (1971) measured many of the same M stars which comprise this project (or vice versa). Table IX lists the LPV stars common on the two projects, their spectral type as determined by Lockwood and Wing (1971) and Lockwood (1972), the mean visual range (Campbell, 1955), the range in magnitude at 8500 Å (Hetzler, 1936), and the 1.04μ and 3.5μ magnitude variations. It merits attention that the observed extrema may not be indicative of the true range of stellar variability because of the limited 3.5μ data coverage.

The 1.04μ data of Lockwood and Wing (1971) and Lockwood (1972)were graphed as a function of visual phase in the same manner as was done for the 3.5μ observations of this project. A curve was then drawn through the individual points "by eye". The shape of the curve was determined from the magnitudes on

Table IX

Range of Mean Magnitudes at Selected Wavelengths

Star	Spectral Type		Visual*	8500Å+	1.04μ	3.5μ
R And	S4,7e	a	$7^m.4$	$3^m.6$	-	$1^m.2$
W And	S8,2e	a	6.3	-	-	0.6
R Aql	M6.0-M8.5	:	5.4	2.6	0.9 :	0.4
R Aur	M6.0-M9.5	:	5.8	-	1.2 :	≥0.5
R Boo	M2-M8.2	:	5.1	-	0.75:	0.7
R Cnc	M6.5e	a	4.4	-	-	-
R Cas	M6.0-M10	:	5.6	2.9	1.65:	≥0.5
T Cas	M6.0-M9.0	:	4.0	-	0.7 :	≥0.4
T Cep	M5.5-M8.8	:	4.3	2.2	0.55:	0.2
o Cet	M4.5-M9.2	:	5.7	2.8	1.1 :	0.8
S CrB	M6.5e	a	5.6	-	-	0.5
R Cyg	S3,9e	a	6.4	-	1.55:	1.2
χ Cyg	M2-M9.0	:	8.2	4.0	2.0 :	0.7
U Her	M7.5-M9.5	:	5.0	-	1.35:	≥0.5
R Leo	M6.0-M9.2	:	4.2	2.4	1.1 :	≥0.5
R LMi	M6.5-M9.0	:	5.6	-	0.95:	≥0.4
X Oph	M7.0-M8.5	:	2.0	-	0.55:	0.4
U Ori	M7.5-M9.0	:	5.7	-	1.2 :	0.7
R Ser	M6.5e	a	6.5	-	-	≥0.4
R Tri	M3-M8.5	:	5.5	2.5	0.85:	0.5
R Vir	M4.5e	a	4.6	1.6	-	0.2
Mean			5.4	2.7	1.1	0.7

---

* Campbell (1955).

\+ Hetzler (1936).

: Lockwood and Wing (1971).

a Keenan (1966).

individual cycles; the mean value was deduced from the constraints imposed by the different cycles. From these averaged curves, a mean 1.04μ magnitude as a function of phase was determined and is listed in table X. Figure 10 is a plot of the mean magnitudes as functions of phase for the visual, 1.04μ and 3.5μ wavelengths of the representative stars χ Cyg, R Cyg, and T Cas. This figure is included to depict the relative shapes and amount of variation at the different wavelengths. The mean visual curves are from Campbell (1955).

Because the 1.04μ and 3.5μ magnitudes are supposedly free of absorptions and represent a true continuum level of the stellar radiation, a color index of these two magnitudes should provide a good temperature indicator of the photosphere. Armed with this color index as a function of phase, the parameters of temperature, angular diameter, luminosity and assorted others seem to be the next quantities which should be computed.

Table X

Adopted 1.04μ Magnitudes as a Function of Phase

Phase	R And	W And	R Aql	R Aur	R Boo	R Cnc	R Cas
0.00	2.95	-	0.81	1.25	3.54	1.06	0.00
.05	2.48	-	.80	1.22	3.44	1.06	-0.02
.10	2.00	-	.85	1.23	3.36	1.10	0.02
.15	-	-	.95	1.29	3.35	1.20	0.12
.20	-	-	1.07	1.41	3.39	1.30	.31
.25	-	-	1.21	1.61	3.47	1.39	.50
.30	-	2.40	1.35	1.79	3.56	-	.68
.35	-	2.62	1.51	2.02	3.67	-	.85
.40	-	2.84	1.63	2.31	3.79	-	1.04
+0.45	-	3.09	1.70	2.37	3.96	-	1.26
±0.50	-	3.26	1.74	2.36	4.03	-	1.50
-0.45	4.40	3.38	1.66	2.19	4.12	-	1.69
.40	4.72	3.39	1.50	1.97	4.15	-	1.71
.35	4.72	3.20	1.35	1.79	4.07	-	1.56
.30	4.64	2.69	1.23	1.67	3.96	-	1.32
.25	4.54	-	1.17	1.57	3.87	-	1.04

Table X (continued)

Phase	R And	W And	R Aql	R Aur	R Boo	R Cnc	R Cas
.20	4.40	-	1.15	1.52	3.80	+1.34	0.74
.15	4.24	-	1.12	1.46	3.75	1.29	0.42
.10	3.94	-	1.03	1.39	3.70	1.21	0.18
-0.05	3.43	-	0.91	1.32	3.63	1.12	0.04
0.00	2.95	-	0.81	1.25	3.54	1.06	0.00

Phase	T Cas	T Cep	o Cet	S CrB	R Cyg	χ Cyg
0.00	0.85	0.09	-1.26	-	3.03	-0.02
.05	.81	.11	-1.34	1.57	2.97	-0.06
.10	.86	.16	-1.36	1.64	2.97	-0.03
.15	.98	.22	-1.34	1.72	3.02	0.08
.20	1.10	.28	-1.28	1.83	3.14	.24
.25	1.24	.31	-1.21	1.94	3.28	.46
.30	1.39	.33	-1.12	2.05	3.47	.71
.35	1.53	.37	-1.00	-	3.66	.95
.40	1.60	.44	-0.86	-	3.87	1.21
+0.45	1.58	.52	-0.71	-	4.08	1.55

Table X (continued)

Phase	T Cas	T Cep	o Cet	S CrB	R Cyg	χ Cyg
±0.50	1.50	.60	-0.52	-	4.27	1.75
-0.45	1.37	.44	-0.36	-	4.44	1.77
.40	1.26	.29	-0.28	-	4.58	1.61
.35	1.14	.21	-0.26	-	4.66	1.30
.30	1.05	.20	-0.29	-	4.54	1.04
.25	1.01	.22	-0.39	-	4.25	0.79
.20	1.08	.23	-0.49	-	4.02	0.59
.15	1.14	.22	-0.57	-	3.78	0.44
.10	1.12	.17	-0.84	-	3.54	0.31
-0.05	1.01	.11	-1.10	-	3.28	0.10
0.00	0.85	0.09	-1.26	-	3.03	-0.02

Phase	U Her	R Leo	R LMi	X Oph	U Ori	R Ser	R Tri	R Vir
0.00	1.38	-0.92	1.18	0.84	1.07	-	2.40	3.64
0.05	1.32	-0.91	1.16	0.84	0.99	-	2.33	3.53
.10	1.35	-0.84	1.19	0.87	0.92	-	2.30	3.42

Table X (continued)

Phase	U Her	R Leo	R LMi	X Oph	U Ori	R Ser	R Tri	R Vir
.15	1.50	-0.73	1.26	0.93	0.92	-	2.30	3.35
.20	1.64	-0.61	1.37	1.00	0.94	-	2.33	3.34
.25	1.77	-0.48	1.50	1.08	1.05	2.07	2.41	3.38
.30	1.90	-0.36	1.68	1.16	1.19	2.19	2.54	3.44
.35	2.05	-0.24	1.85	1.22	1.36	2.35	2.68	3.53
.40	2.20	-0.11	2.02	1.29	1.54	2.56	2.82	3.65
0.45	2.33	0.02	2.13	1.35	1.73	2.75	2.96	3.79
±0.50	2.56	0.13	2.14	1.41	1.90	2.90	3.09	3.88
-0.45	2.71	0.18	2.11	1.38	2.03	2.96	3.14	-
.40	2.74	0.12	2.04	1.30	2.14	2.92	3.13	-
.35	2.69	0.00	1.96	1.21	2.12	2.76	3.06	-
.30	2.57	-0.14	1.87	1.14	1.94	-	2.97	-
.25	2.42	-0.27	1.74	1.08	1.80	-	2.90	-
.20	2.32	-0.45	1.60	1.03	1.65	-	2.83	-
.15	2.21	-0.61	1.47	1.01	1.50	-	2.73	-
.10	1.99	-0.73	1.36	0.95	1.34	-	2.62	-
-0.05	1.58	-0.84	1.26	0.89	1.20	-	2.50	-
0.00	1.38	-0.92	1.18	0.84	1.07	-	2.40	3.64

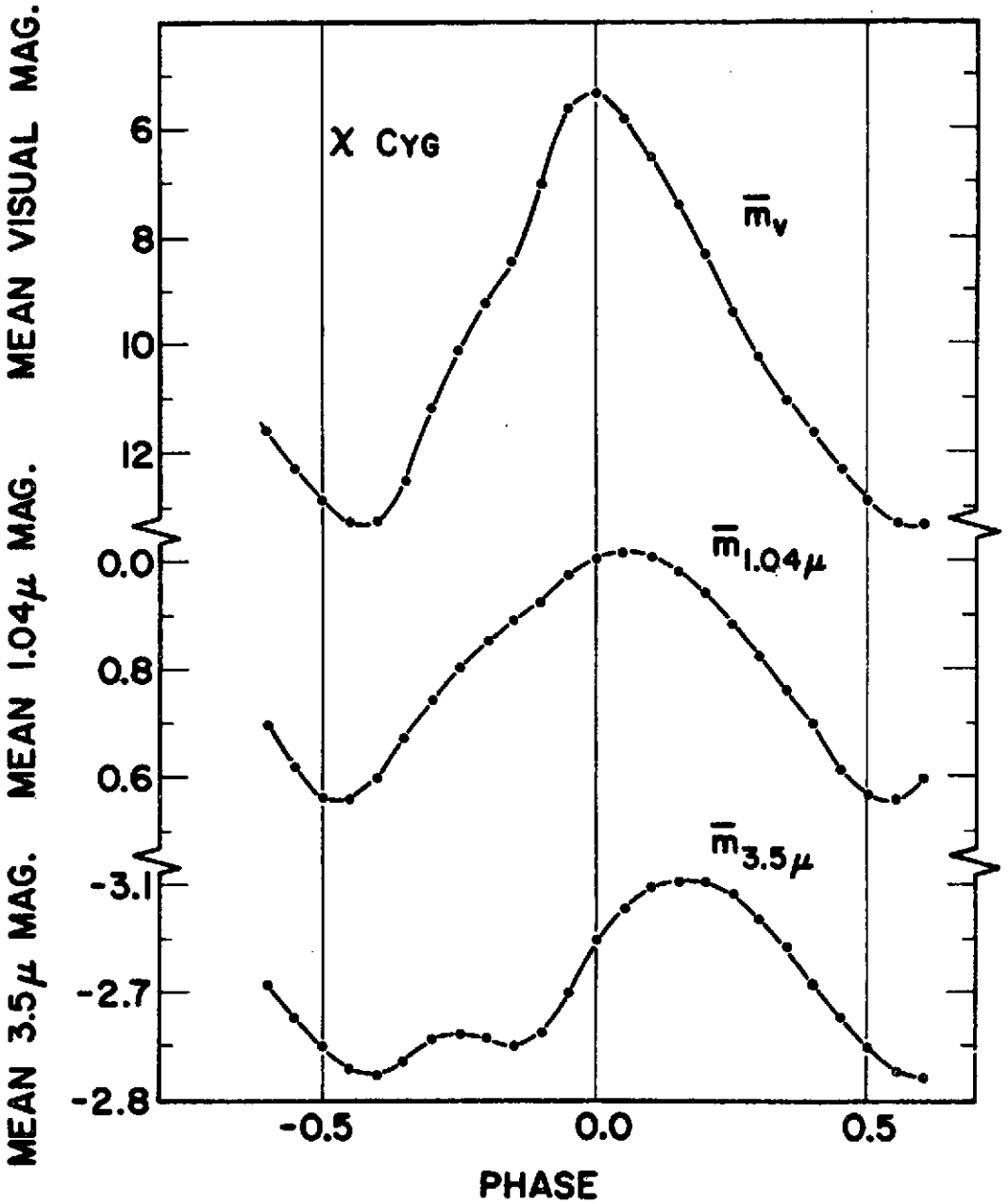

Figure 10a. Mean visual, 1.04μ and 3.5μ magnitudes versus visual phase for the mild S star χ Cyg. Of interest is the "hump" in the 3.5μ curve which may or may not be present at other wavelengths.

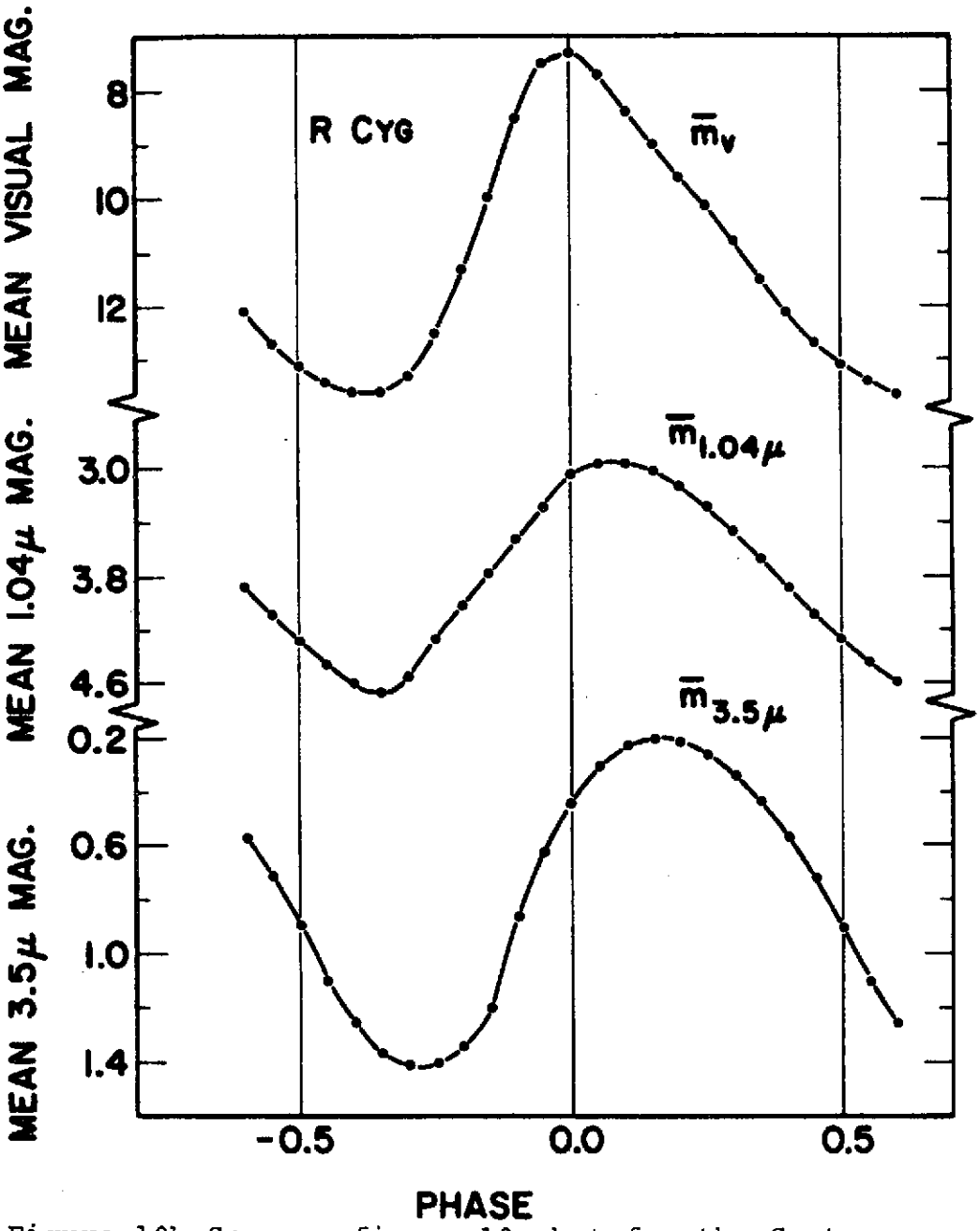

Figure 10b. Same as figure 10a but for the S star R Cyg. Note the absence of the hump at all wavelengths on the ascending portion of the light curve.

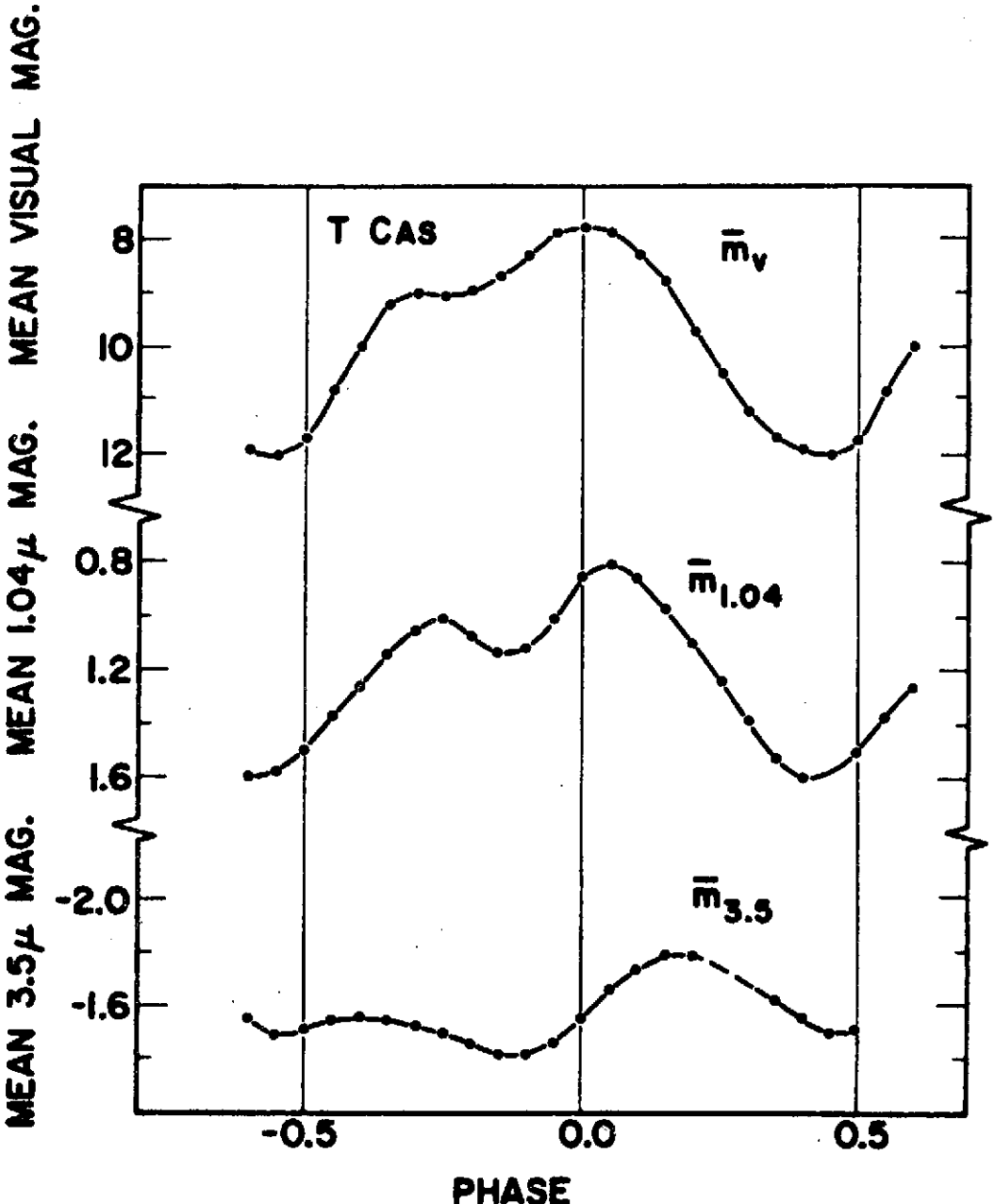

Figure 10c. Similar to figure 10a but for the M star T Cas. Note the presence of a hump at all wavelengths on the ascending branch of the light curve.

VII

TEMPERATURES, ANGULAR SIZES AND LUMINOSITIES

A multitude of attempts have been made to calculate the effective or color temperatures of the photospheres of M giant stars. One of the earliest attacks on this problem was by Pettit and Nicholson (1933) who used thermocouples to measure the radiometric magnitude and then derive temperatures for a few long period variable stars. Smak (1964) used spectroscopic and photometric UBV data to derive assorted parameters for red giants. Johnson (1966) used UBVRIJKLMN photometry to calculate effective temperatures for main sequence stars and cool giants. Lee (1970) employed much the same procedure as Johnson and calculated the effective temperatures as functions of spectral type for both M giant and supergiant stars. Smak (1964) covered the spectral range MO III - M8 III, Johnson (1966) did the same for G5III-M6III and Lee did so for MOIII-M6III.

Near minimum light, some of the stars of this present study reach spectral types later than M8 for which no effective temperatures are available. An extension of the spectral type-temperature scale was needed.

Two alternative methods of color temperature determinations are both based on the observational data. Both methods require the formation of a color index (C.I.), which is defined as the difference between the 1.04μ and 3.5μ magnitudes and is given by equation 5.

$$\text{COLOR INDEX} = \text{C.I.} = [1.04\mu]-[3.5\mu] \qquad (5)$$

The calculation of a color temperature from a color index involves the major assumption that the star radiates like a black body at the two respective wavelengths. In other words, the fluxes at each wavelength represent radiation emanating from the same temperature or optical depth. This determination of temperature also assumes that the opacities at each wavelength alter in the same manner throughout the stellar cycle.

As a first attempt to calculate temperatures, a color index-spectral type relation must be determined. This method utilizes the 1.04μ observations of representative late type giant stars by Lockwood (1972) in conjunction with the 3.4μ and 3.5μ data on the same stars as gleaned from the literature and the present study. The ensuing problem of conversion of spectral types into temperatures and the extension of the color index to later spectral types are not

simple tasks.

Table XI lists the name, spectral type, 1.04μ magnitude of Lockwood (1972), the 3.4μ or 3.5μ magnitudes from various sources, the 3.5μ mean magnitude and the [1.04μ]-[3.5μ] color index for late type giant stars.

It deserves to be mentioned at this point that Johnson's and Lee's effective wavelengths were 3.4μ and not 3.5μ as in the other observations listed. Outside of observational uncertainties, there appears to be no systematic difference in magnitude dependent on effective wavelength for these standard stars. As a result, all available magnitudes were used to determine the weighted mean magnitude for the individual stars of table XI.

The next step in the temperature determination is to assume or derive a temperature-spectral type relation. Table XII lists the effective temperatures for red giant spectral types as determined by various authors. Also included in the last column, as summarized from table XI, are the mean color index and, in parentheses, the number of stars used to determine this index.

There are two major problems inherent in the color index-effective temperature method as described above. First, the non-variable red giants of later

Table XI

Observational Summary of M Giants

Star	Spectral Type	1.04μ[a] Mag	3.5μ[b] Mag	3.4μ[c] Mag	3.4μ[d] Mag	3.5μ[e] Mag	3.5μ[f] Mag	Mean 3.5μ Mag	Color Index [1.04μ]-[3.5μ]
β And	MO III	-0.40	-2.05	-2.07	-1.97	-2.05	-	$-2^m.04$	$1^m.64$
μ UMa	MO III	0.60	-1.00	-	-1.04	-0.95	-	-1.00	1.60
75 Leo	MO IIIb	2.79	-	-	-	1.19	-	1.19	1.60
α Vul	MO III	2.00	0.42	-	-	-	-	0.42	1.58
γ Eri	M1 III	0.53	-	-0.97	-1.00	-	-	-0.98	1.51
χ Peg	M2 III	2.10	-	0.46	0.61	-	-	0.53	1.57
α Cet	M2 III	-0.19	-1.91	-1.76	-1.74	-1.89	-1.81	-1.82	1.63
π Leo	M2 III	1.99	-	-	-	0.21	-	0.21	1.78
83 UMa	M2 IIIab	1.91	0.25	-	-	-	-	0.25	1.66
β Peg	M2+IIb-IIa	-0.64	-2.45	-2.43	-2.41	-2.45	-2.22	-2.44	1.80
55 Peg	M2 III	2.05	0.46	-	-	-	-	0.46	1.59
μ Gem	M3 IIIa	-0.29	-2.10	-2.03	-	-2.01	-	-2.05	1.76
ρ Per	M4 IIIa	-0.31	-2.20	-	-	-2.14	-2.12	-2.15	1.84
ω Vir	M4-M4.5 III	1.46	-	-	-	-0.33	-	-0.33	1.79
HR 5299	M4-M4.5 III	1.34	-	-0.53	-	-	-	-0.53	1.87

Table XI (continued)

Star	Spectral Type	1.04μ[a] Mag	3.5μ[b] Mag	3.4μ[c] Mag	3.4μ[d] Mag	3.5μ[e] Mag	3.5μ[f] Mag	Mean 3.5μ Mag	Color Index [1.04μ]-[3.5μ]
VY Leo	M5 III	0.98	-	-0.99	-	-0.96	-	-0.98	1.96
RR UMi	M5 III	0.73	-	-1.12	-	-	-0.93	-1.03	1.76
τ^4 Ser	M5 IIb-IIIa	0.98	-	-	-	-1.25	-	-1.25	2.23
OP Her	M5 IIb-IIIa	1.87	-	-0.15	-	0.03	-	-0.06	1.93
R Lyr	M5 III	-0.32	-2.28	-	-	-2.32	-2.23	-2.28	1.96
W Cyg	M4e-M6	0.47	-1.70	-	-	-	-	-1.70	2.17
RZ Ari	M6 III	0.78	-	-1.24	-	-	-	-1.24	2.02
RS Cnc	M6 IIIa	0.20	-1.94	-2.00	-	-2.07	-1.82	-1.96	2.16
X Her	M6 e	0.42	-	-	-	-1.65	-1.64	-1.65	2.07
g Her	M6 III	-0.21	-2.27	-2.22	-	-2.18	-2.40	-2.28	2.07
CH Cyg	M6	1.20	-1.31	-	-	-	-1.25	-1.28	2.48
SW Vir	M7 III	0.23	-	-	-	-	-2.00	-2.00	2.23
RX Boo	M8:	0.35	-2.30	-	-	-2.25	-2.33	-2.29	2.64

a Lockwood (1972).
b This study.
c Lee (1970).
d Johnson (1964).
e Gehrz & Woolf(1971).
f Gillett,Merrill & Stein (1971).

Table XII

Comparison of Effective Temperatures
and Color Indices as Functions of Spectral Type

Spectral Type	Effective Temperature °K			
	Johnson (1966)	Lee (1970)	Smak (1964)	Mean Color Index
MO III	3660	3700	3340	$1^{m}.61(4)$
M1 III	3600	3650	3200	1.51(1)
M2 III	3500	3550	3090	1.67(6)
M3 III	3300	3350	2980	1.76(1)
M4 III	3100	3150	2850	1.83(3)
M5 III	2950	2950	2710	1.97(5)
M6 III	2800	2750	2500	2.08(4)
M7 III			2250	2.23(1)
M8 III			2000	2.64(1)

spectral types (M7 and M8) are scarce and ones of even later type (M9 and M10) are totally absent in the data. Therefore, an extension of the spectral type-color index relation to the M9 and M10 spectral types needed for the Miras near minimum cannot be directly made. Secondly, the color index method directly determines a color temperature and not an effective temperature. The conversion of color temperature into effective temperature involves many assumptions implicit in the calculations. An effective temperature is defined as the temperature obtained on the hypothesis that the total energy output of the star may be represented by one temperature. In other words, the luminosity, size and distance of the star must be known. A color temperature rests on the assumption that the stellar photosphere radiates like a black body of one temperature at two or more wavelengths. The color and effective temperatures may not be coincidental because of emission, absorption, limb darkening and wavelength dependent opacity.

The alternative path to the determination of a temperature scale avoids the difficulties previously mentioned and directly computes a color temperature from the measured color index. The 1.04μ measurements of Lockwood and Wing (1971) and Lockwood (1972), as

well as the 3.5μ observations of this program, are quoted with respect to Vega. This AOV star is defined to be zero magnitude at both wavelengths and its resulting color index is therefore zero. The remaining obstacle was to choose a color temperature for this star. α Lyra was defined to have a 10,000 °K color temperature.

Table XIII lists the black body color index in magnitudes as a function of temperature. When the temperature is on the order of one-third the reference temperature or less, the color index varies linearly with 1/T. Figure 11 graphs the color index in magnitudes as a function of 1/T for the temperatures and color indices of red giant stars. For these stars, the color index is greater than about $2^{m}.0$. In a color index range of 2 to 5, the linear approximation between color index and 1/T can be used to an accuracy better than about 1%.

Equation 6 describes the linear fit in the color index and 1/T. The constants a and b are determined from the graph.

$$C.I. = a\ (1/T_c) + b \qquad (6)$$

For color indices between 2 and 5 magnitudes, the linear approximation requires a=9850 °K and

Table XIII

[1.04μ]-[3.5μ] Color Index
as a Function of Temperature

Temperature	Color Index Magnitudes
20,000 °K	$-0^{m}.32$
15,000	-0.22
10,000	0.00
9,000	0.08
8,000	0.18
7,000	0.30
6,000	0.48
5,000	0.74
4,000	1.16
3,000	1.91
2,800	2.12
2,600	2.38
2,400	2.68
2,200	3.06
2,000	3.50
1,900	3.76
1,800	4.05
1,700	4.39
1,600	4.76
1,500	5.18

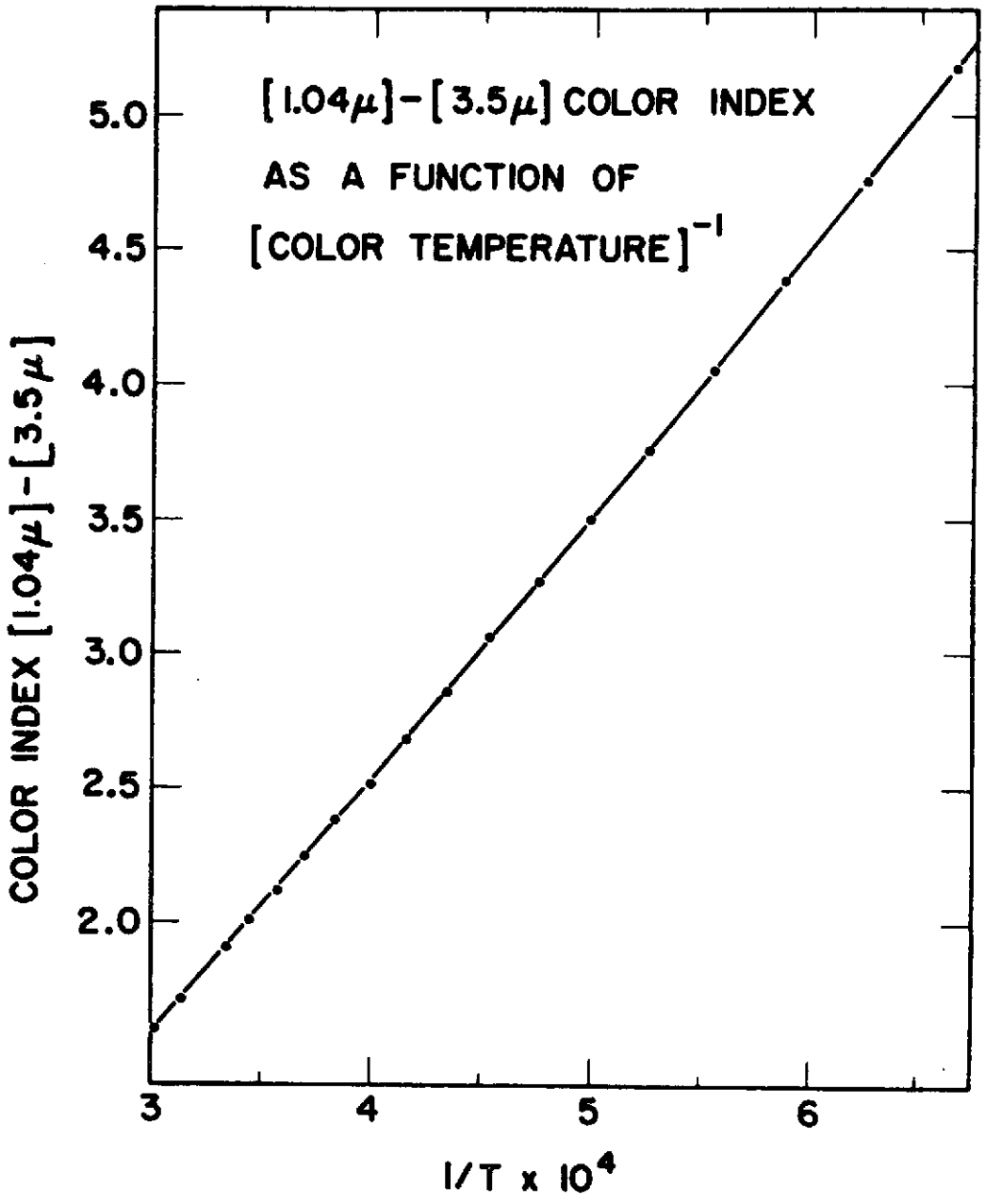

Figure 11. [1.04μ]-[3.5μ] color index as a function of (color temperature)$^{-1}$.

$b = -1^{m}.41$. Solution of equation 6 for the temperature results in equation 7 for $5^{m} > C.I. > 2^{m}$.

$$T_c = \frac{9850\ °K}{C.I. + 1.41} \tag{7}$$

Due to the difficulties of transformation of color to effective temperature, and because the color indices for the latest spectral types of variable red giants are not available, the decision was made to employ this second method of color temperature determination.

One point must be stressed: interstellar extinction will influence the color temperatures deduced from the color index. If this reddening follows an approximate λ^{-1} law, the 1.04μ magnitudes will be affected only about half as much as the visual magnitudes, while the 3.5μ extinction will be less than 20% of the visual extinction. The intrinsic colors of the Miras are not well determined and corrections to the observed colors stand on an unfirm footing. On the basis of available data, interstellar extinction has been totally ignored.

Fortunately, most of the Mira variables in this project are the brighter ones, both visually and at 3.5μ, and, therefore, are likely to be nearby stars. Also, many are at intermediate or high

galactic latitudes and probably suffer little extinction. As for the standard stars of table XI, they are, again, the brighter ones. The scatter of the color indices for these standards, to some extent, may reflect the ignorance of the interstellar extinction.

Other factors which may influence the color temperature determinations are the unknown weak bands which affect the 1.04μ magnitudes of S stars (Lockwood and Wing, 1971; Lockwood, 1972). For this reason, the S stars possess more unreliable temperatures and they must be referred to as equivalent temperatures. Unfortunately, temperatures for carbon stars may not be inferred. The present data lack a second wavelength representing a true continuum point such that color-indices may be calculated.

Armed with the assumed color index versus temperature relation as determined by equation 7, the color temperatures as function of phase throughout the stellar cycle may be computed. Once the temperature has been determined, other quantities such as angular diameter, apparent bolometric magnitude, apparent visual magnitude, and titanium oxide blanketing may be calculated.

As a prelude to the actual equations, a brief

outline of the procedure employed to determine the temperature, angular size, luminosity and visual magnitude will be listed. Given the 1.04μ and 3.5μ measurements, a color index is formed and thence the temperature. The 3.5μ magnitude and absolute calibration give the measured flux, whereas the temperature and Planck function result in the intensity at 3.5μ. From these two quantities the solid angle of the source may be deduced. The temperature and solid angle are then utilized to form the bolometric and visual magnitudes.

The color index (C.I.) (equation 5) as a function of phase was computed from the mean 1.04μ and 3.5μ curves of tables X and V, respectively. The color temperatures were then calculated via equation 7. The observed flux ($F_{OBS}(\lambda)$) at a given wavelength is determined from equation 8,

$$F_{OBS}(\lambda) = F_O(\lambda)\ 10^{-0.4\ [m_{OBS}(\lambda) - m_o(\lambda)]} \qquad (8)$$

where $F_O(\lambda)$ is the zero magnitude flux for a specific wavelength, $m_{OBS}(\lambda)$ is the observed magnitude at the same wavelength, and $m_o(\lambda)$ is the zero magnitude reference. For 3.5μ, $m_o(\lambda) = 0$ and $F_O(\lambda=3.5\mu) = 7.1 \times 10^{-15}$ watts/cm^2/μ in accordance with the authors previously cited. Thus, equation 8 becomes

equation 9.

$$F_{OBS}(3.5\mu)=7.1 \times 10^{-15} \frac{\text{watts}}{\text{cm}^2}\ 10^{-0.4\ m_{OBS}(3.5\mu)} \qquad (9)$$

From the temperature and wavelength, the intensity $B(\lambda,T)$ of a black body radiator in units of power per unit area per steradian per unit wavelength interval may be calculated from the Planck function (equation 10),

$$B(\lambda,T) = \frac{C_1}{\pi\ \lambda^5\ (e^{\frac{C_2}{\lambda T}} -1)} \qquad (10)$$

where C_1 and C_2 are constants, λ is the wavelength and T is the temperature. $C_1=3.7412 \times 10^{-12}$ watts/cm^2 and C_2 = 1.43879 cm deg (Allen, 1963).

For the 3.5μ wavelength, equation 10 becomes equation 11.

$$B(3.5\mu,T) = \frac{22.67}{(e^{\frac{4111}{T}} -1)}\ \frac{\text{watts}}{\text{cm}^2\ \mu\ \text{ster.}} \qquad (11)$$

From $F_{OBS}(3.5\mu)$ and $B(3.5\mu,T)$, the solid angle subtended by the source in steradians(Ω) may be computed by equation 12.

$$\Omega = F_{OBS}(3.5\mu)/B(3.5\mu,T) \qquad (12)$$

The angular diameter of the source(θ) in milli-

seconds of arc may then be deduced via equation 13.

$$\theta_{ms} = [\Omega/1.846x10^{-17}]^{1/2} \tag{13}$$

From the temperature and solid angle of the source, the apparent bolometric and visual magnitudes are next on the list of parameters to be found. The apparent bolometric magnitude (m_{bol}) is found through equation 14,

$$m_{bol} = -2.5 \log (F_{bol}/F_{o\ bol}) \tag{14}$$

where $F_{o\ bol}$ is the flux for zero apparent bolometric magnitude, $F_{o\ bol} = 2.52 \times 10^{-12}$ watts/cm^2 (Allen, 1963) and F_{bol} is the computed total flux found from equation 15,

$$F_{bol} = \frac{\sigma}{\pi} T_c^{\ 4}\ \Omega \tag{15}$$

where σ is the Stefan-Boltzmann constant, {$\sigma=5.70x10^{-12}$ watts/cm^2/deg^4 (Allen, 1963)} , T_c is the color temperature in degrees Kelvin from equation 7 and Ω is the solid angle from equation 12.

The calculation of bolometric magnitude or luminosity from the derived color temperature assumes that the star radiates as a uniform disk, and limb darkening is ignored. The absolute value of the bolometric

magnitude may then be in error. However, the desire in the computations was to ascertain the shape of the luminosity curve as a function of phase and its relative range.

The apparent visual magnitude, m_v, can also be determined from equations 14 and 10. The visual magnitudes were computed for an effective wavelength of 0.55μ and the zero magnitude flux was taken to be F_o (λ=0.55μ) = 3.92×10^{-12} watts/cm^2/μ (Johnson, 1965).

Appendix IV lists the stars for which 1.04μ and 3.5μ color indices exist as a function of visual phase. The first column tabulates the phase, the second column gives the color index, the third and fourth columns list the color temperature and angular diameter, columns 5 and 6 list the computed apparent bolometric and visual magnitudes, whereas column 7 tabulates the mean observed visual magnitude. The data for column 7 were taken from the mean visual curves of Campbell (1955).

Figure 12 graphs the color temperature (T_c), angular diameter (θ) in milliseconds of arc, and apparent bolometric magnitude (m_{bol}) as functions of phase. The data were obtained from appendix IV. R And, W And, R Cnc, S CrB, R Ser are omitted from the plot because the observational data were not complete over more than about one-half a cycle. Of

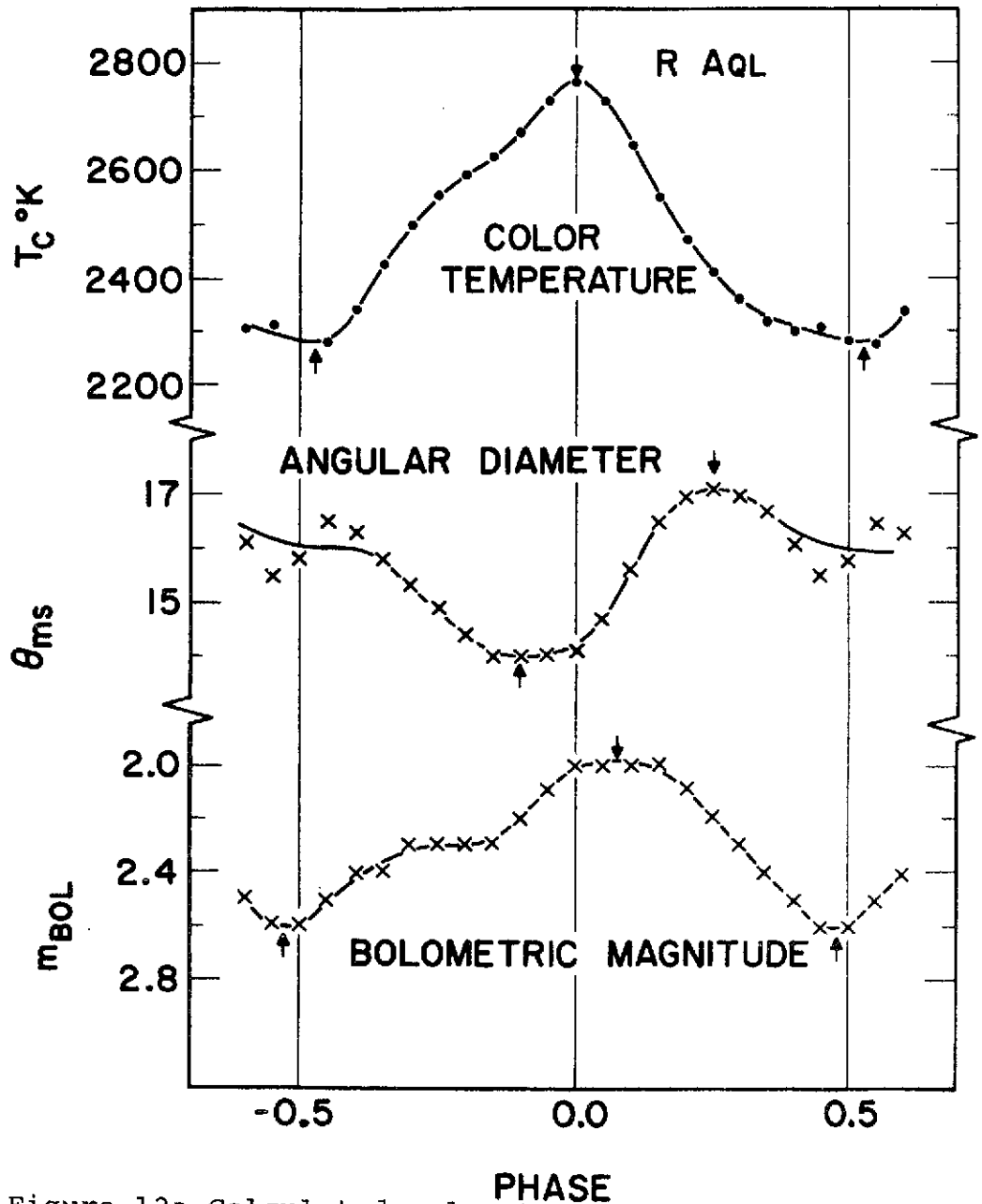

Figure 12a. Calculated color temperature, angular diameter, and apparent bolometric magnitude as functions of visual phase for the M star, R Aql. The arrows on each curve denote the phases of calculated extrema.

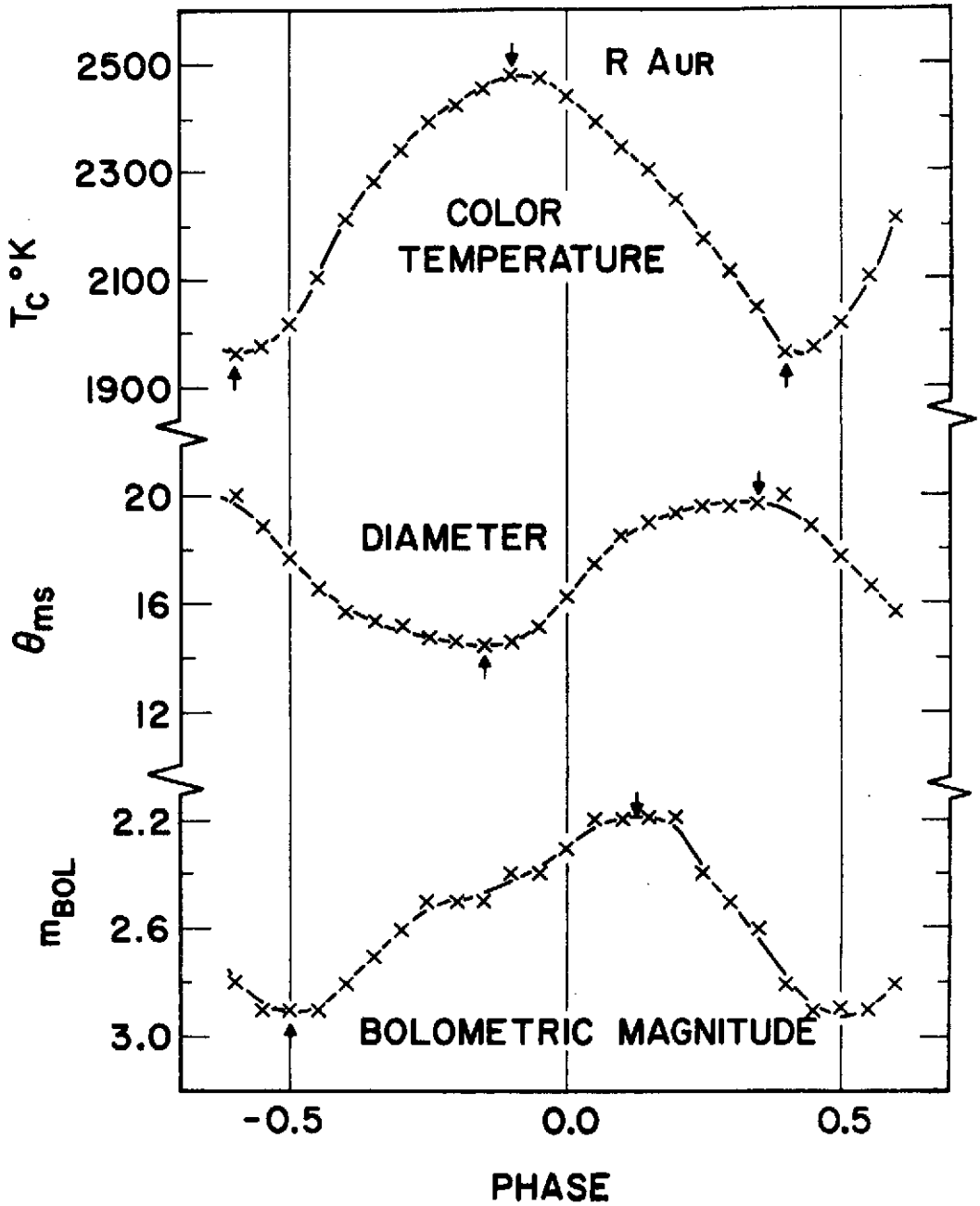

Figure 12b. Similar to figure 12a but for R Aur.

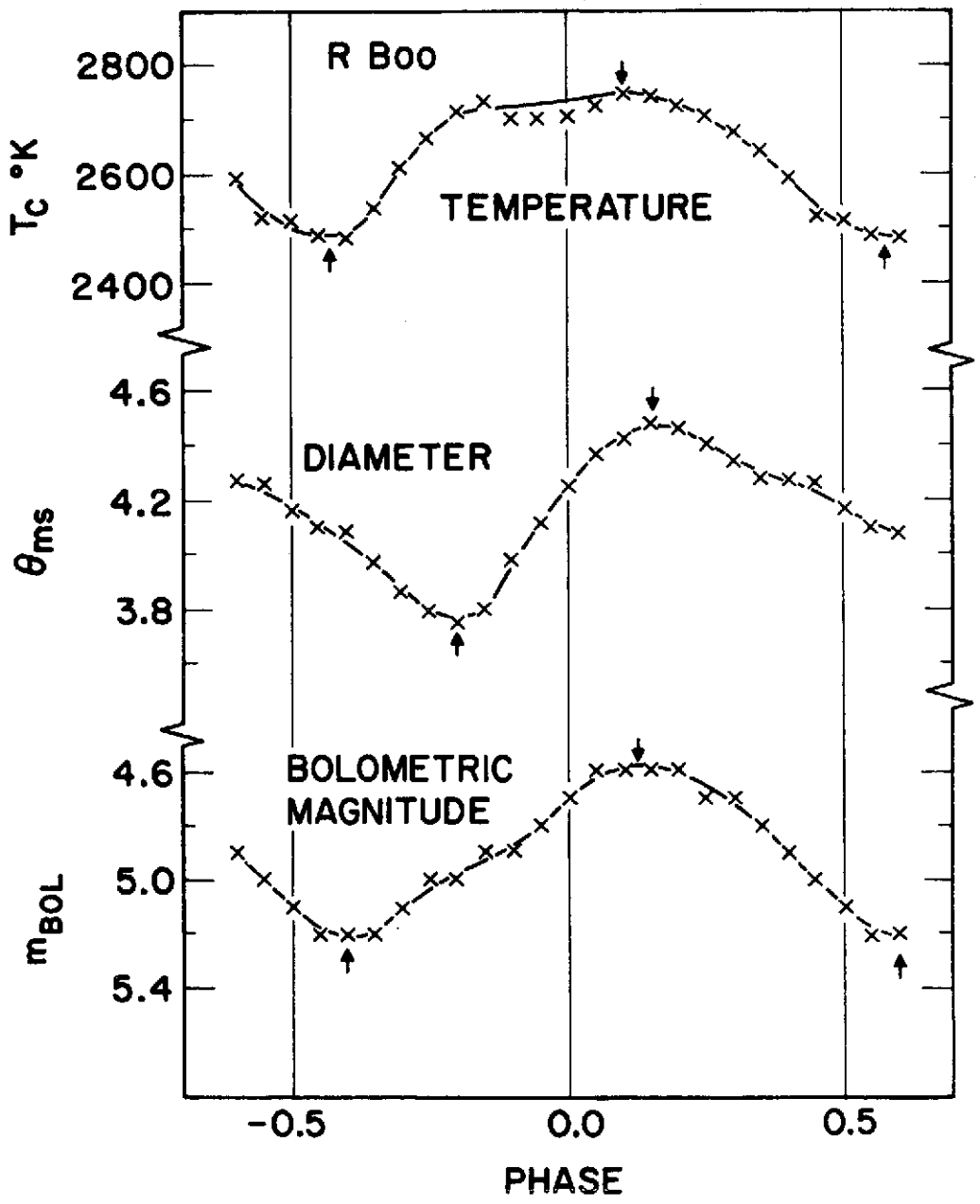

Figure 12c.Similar to figure 12a but for R Boo.

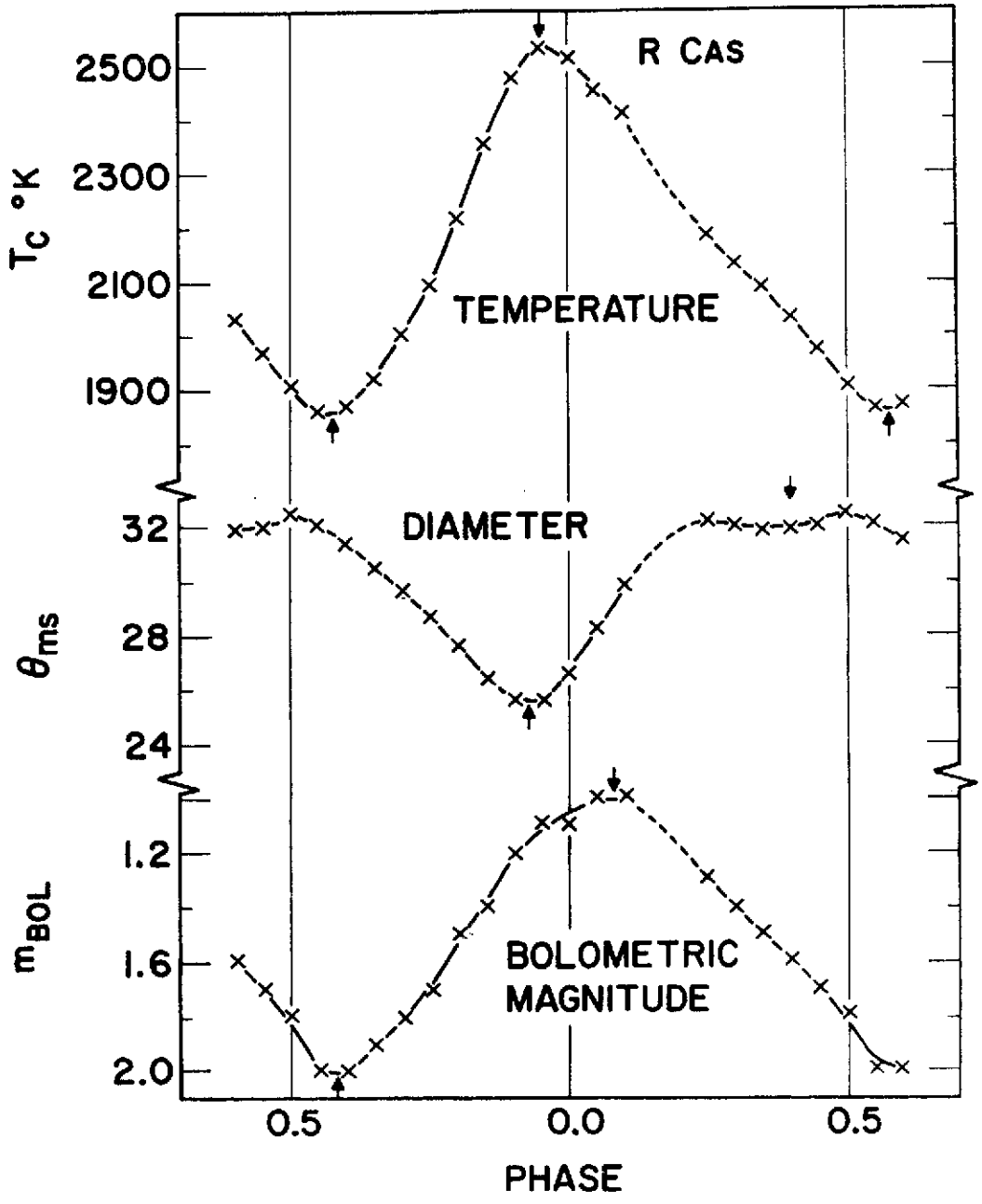

Figure 12d. Similar to figure 12a but for R Cas.

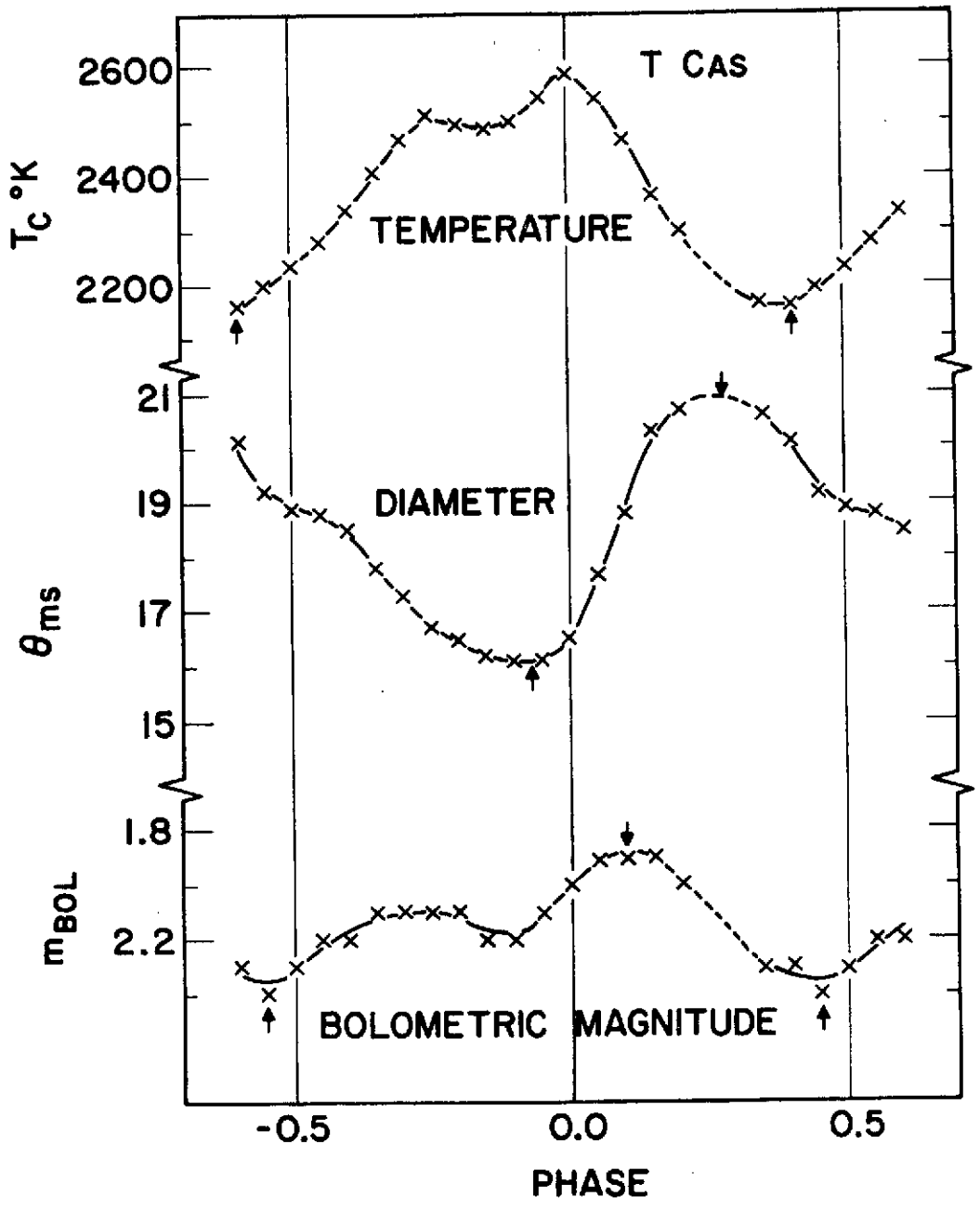

Figure 12e.Similar to figure 12a but for T Cas.

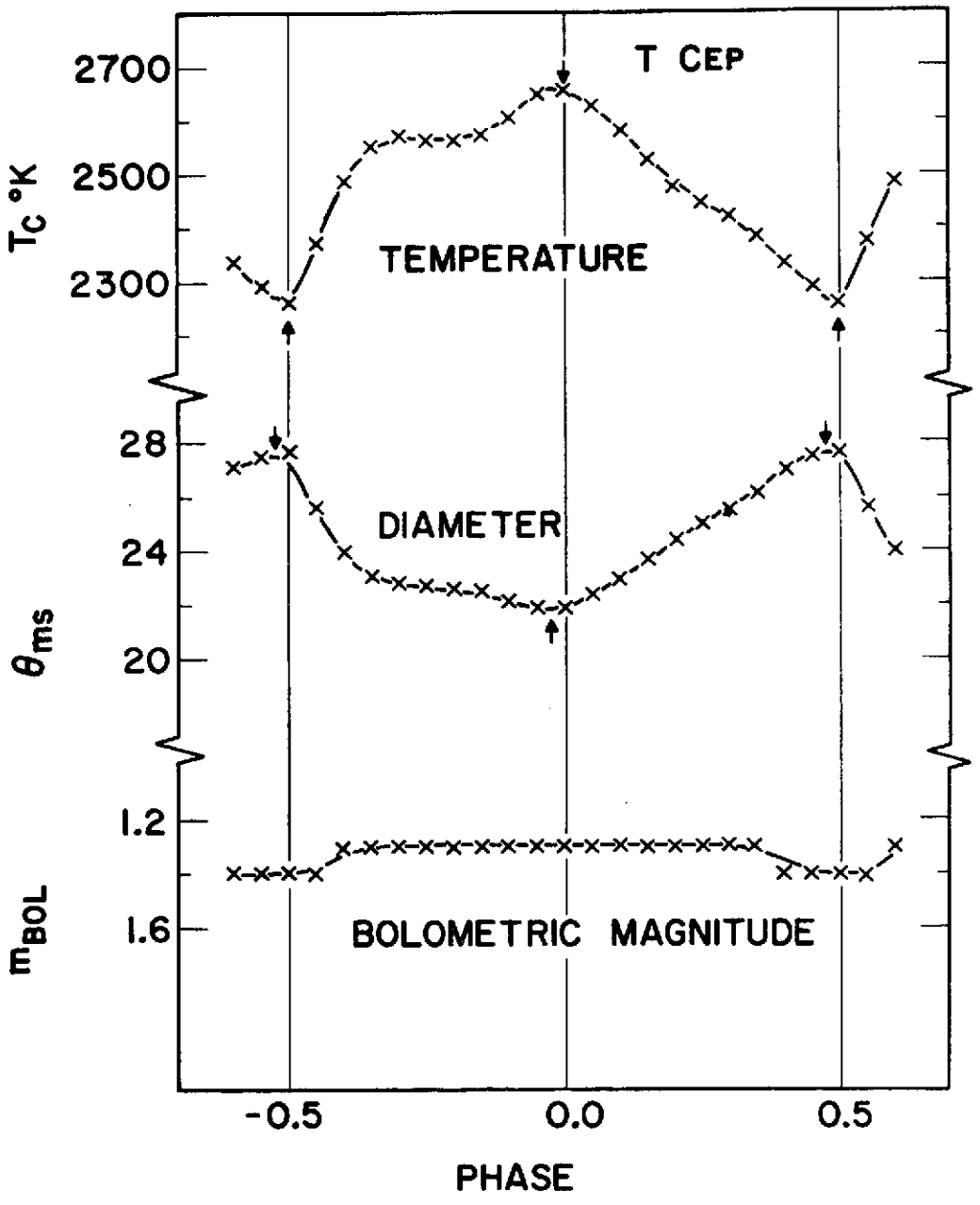

Figure 12f.Similar to figure 12a but for T Cep.

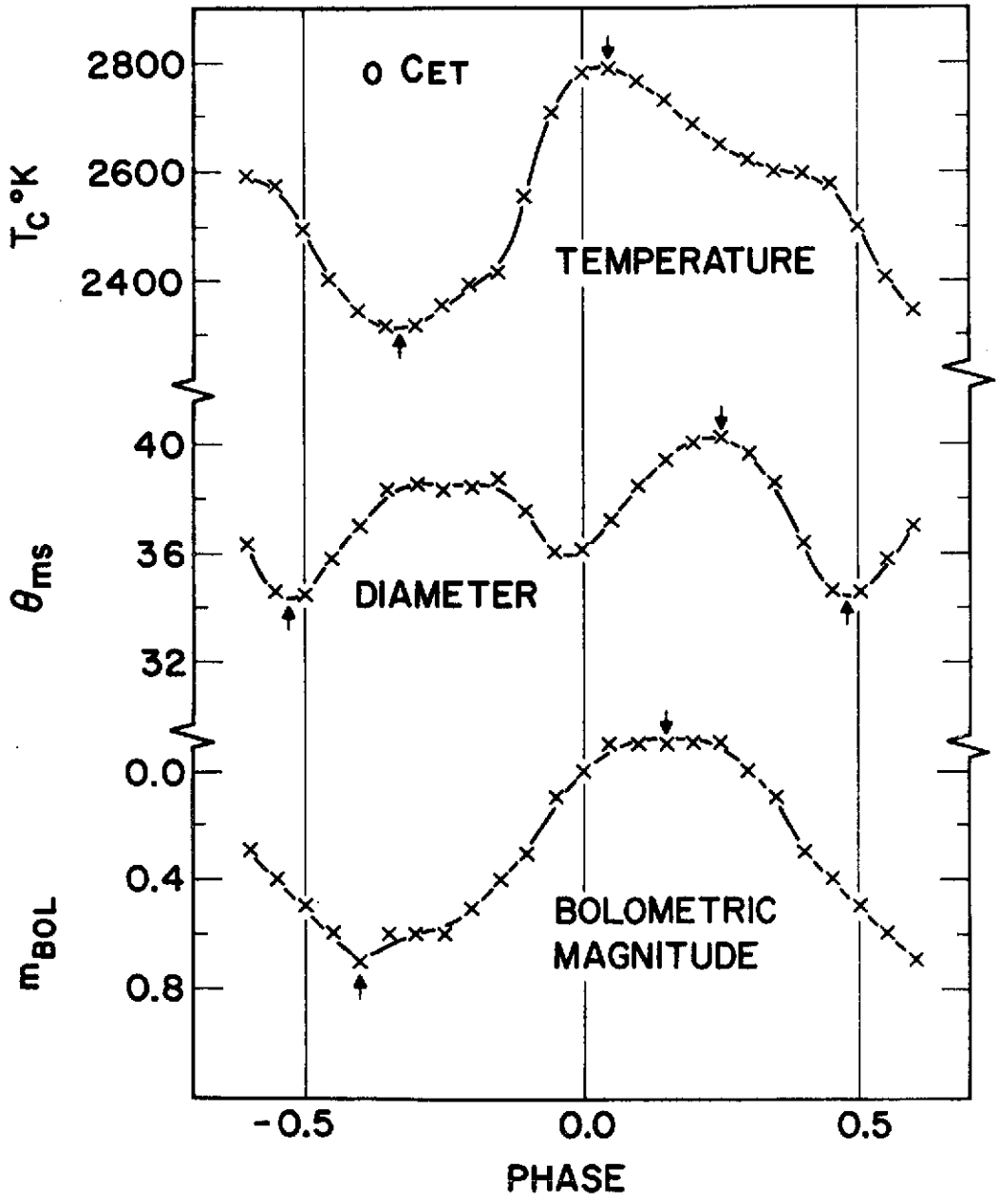

Figure 12g. Similar to figure 12a but for o Cet.

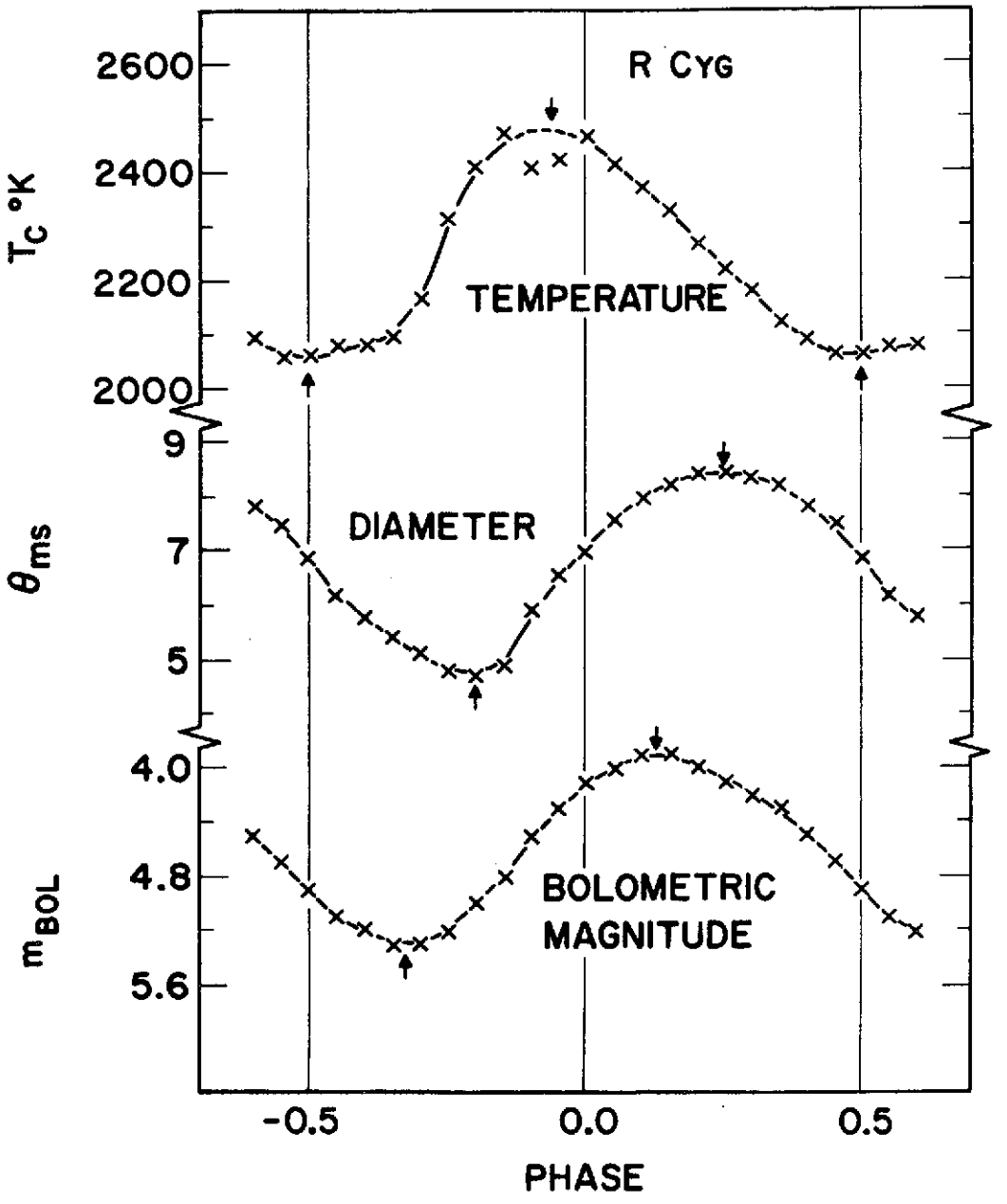

Figure 12h. Similar to figure 12a but for R Cyg.

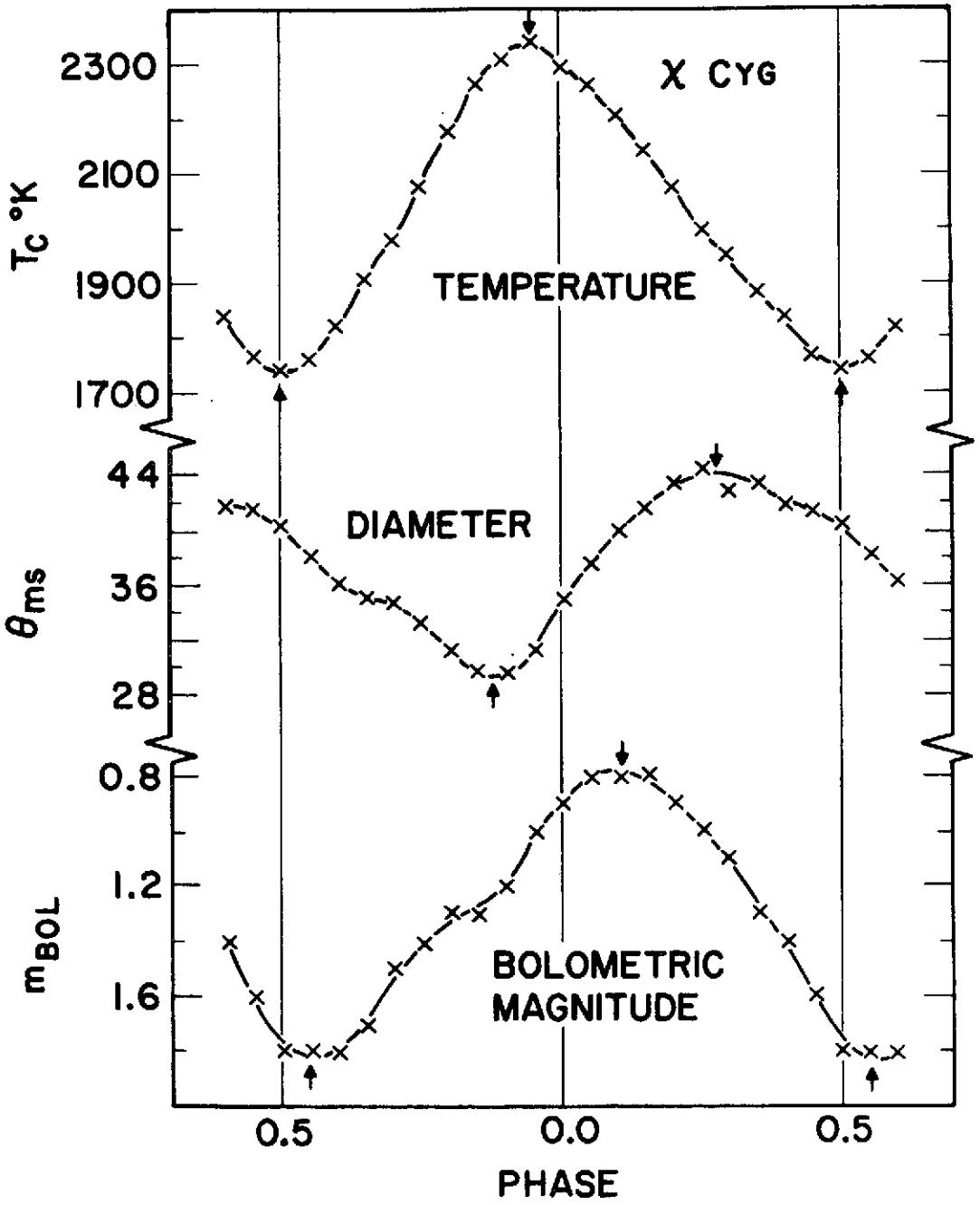

Figure 12i. Similar to figure 12a but for χ Cyg.

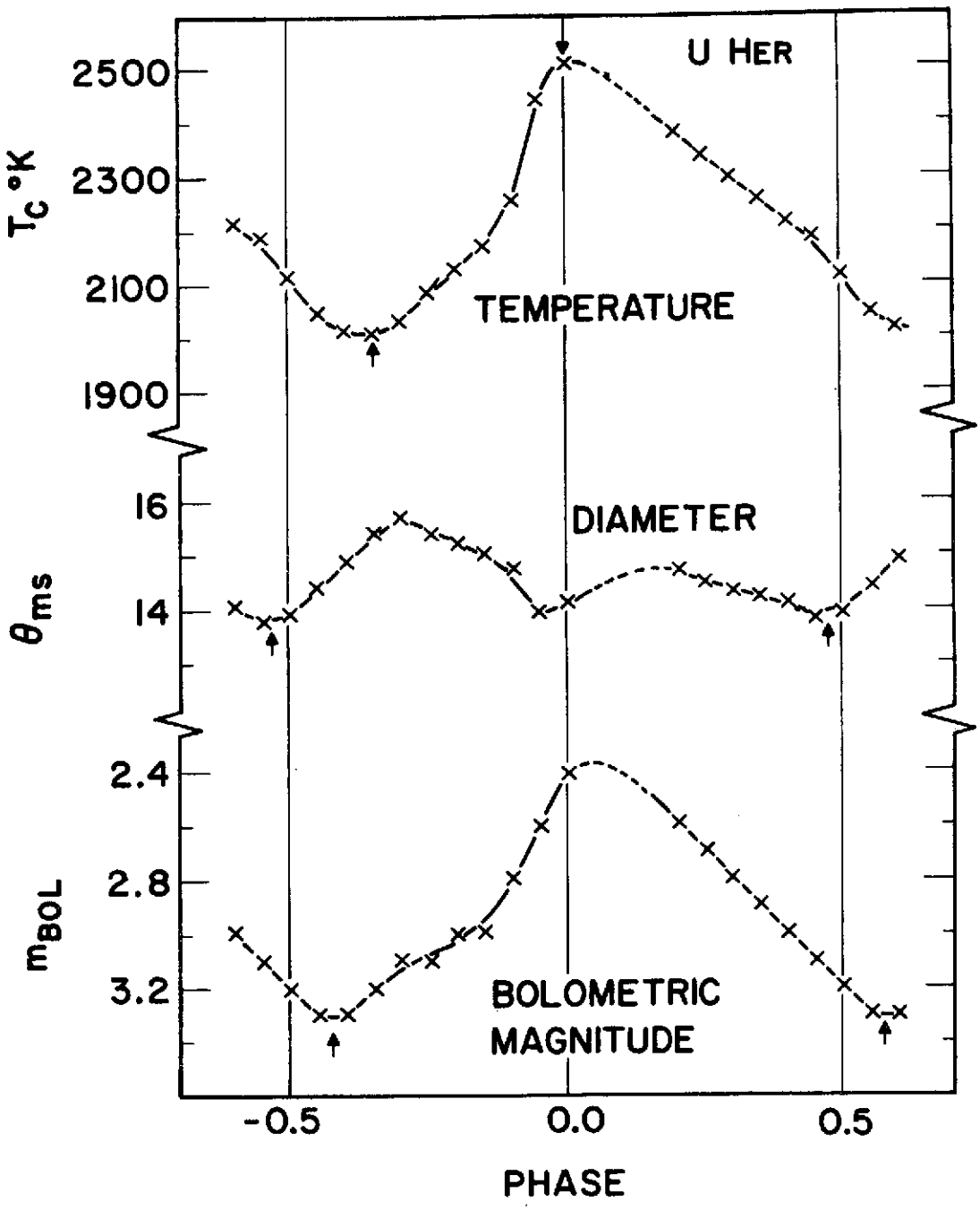

Figure 12j. Similar to figure 12a but for U Her.

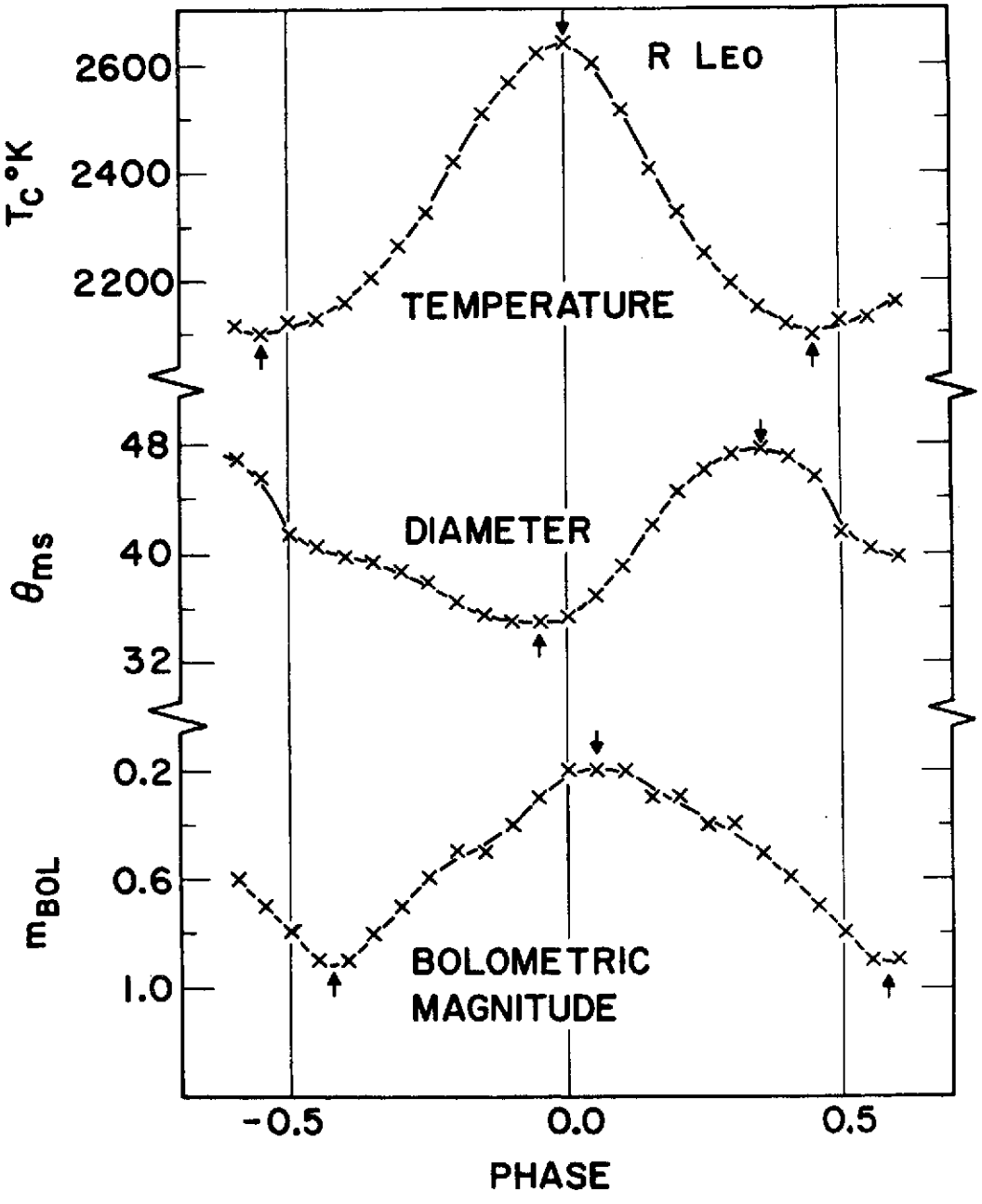

Figure 12k. Similar to figure 12a but for R Leo.

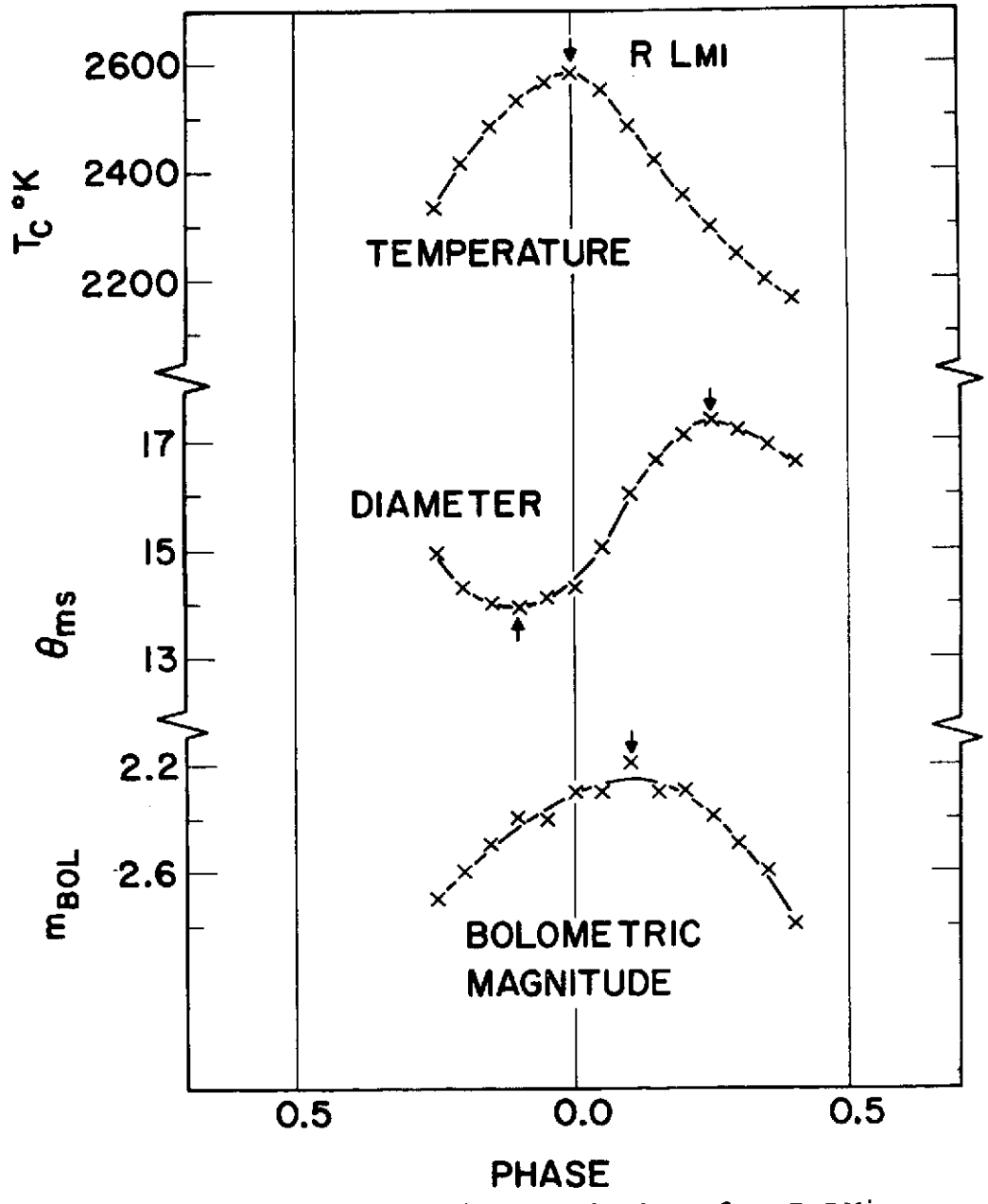

Figure 121. Similar to figure 12a but for R LMi.

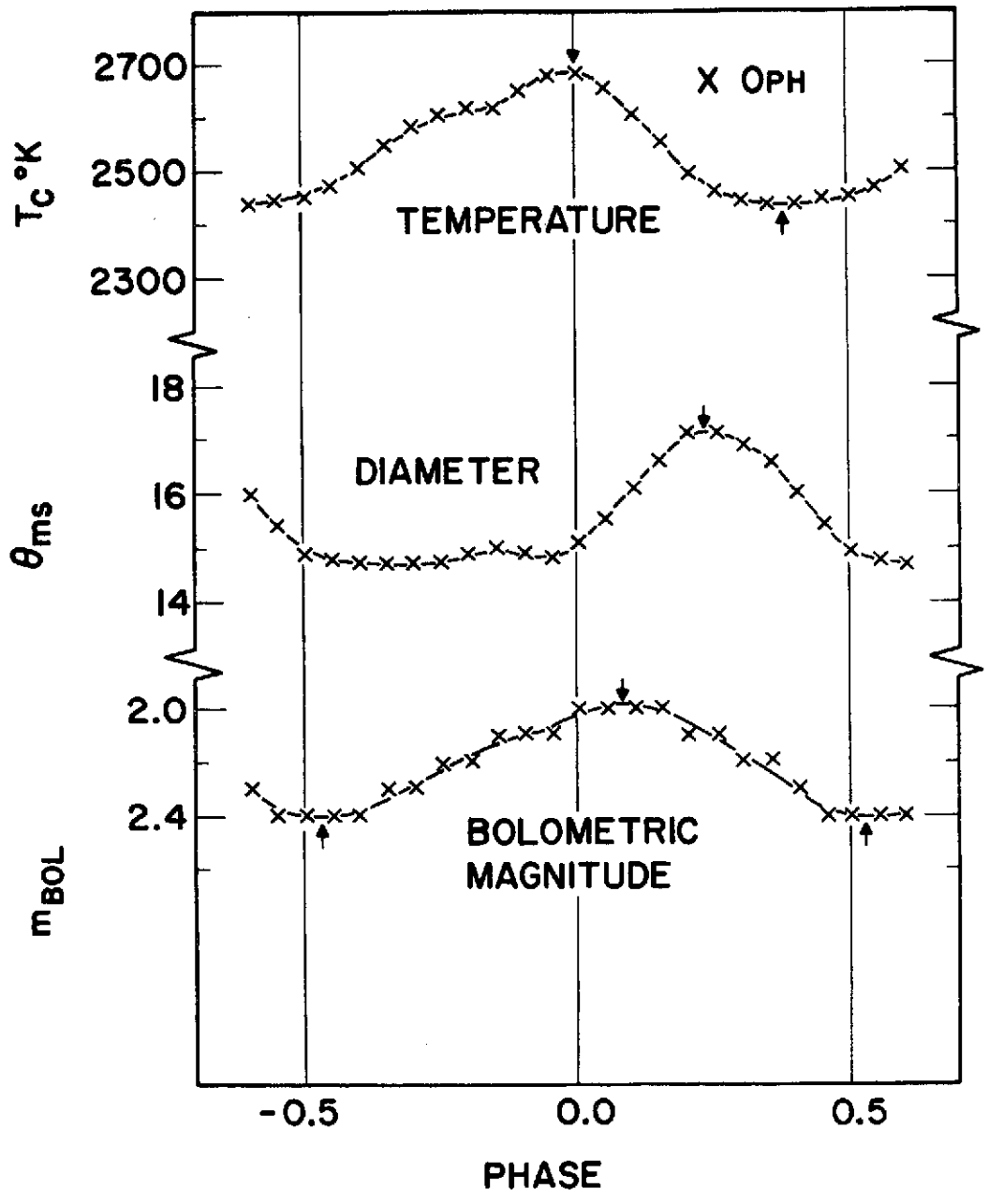

Figure 12m. Similar to figure 12a but for X Oph.

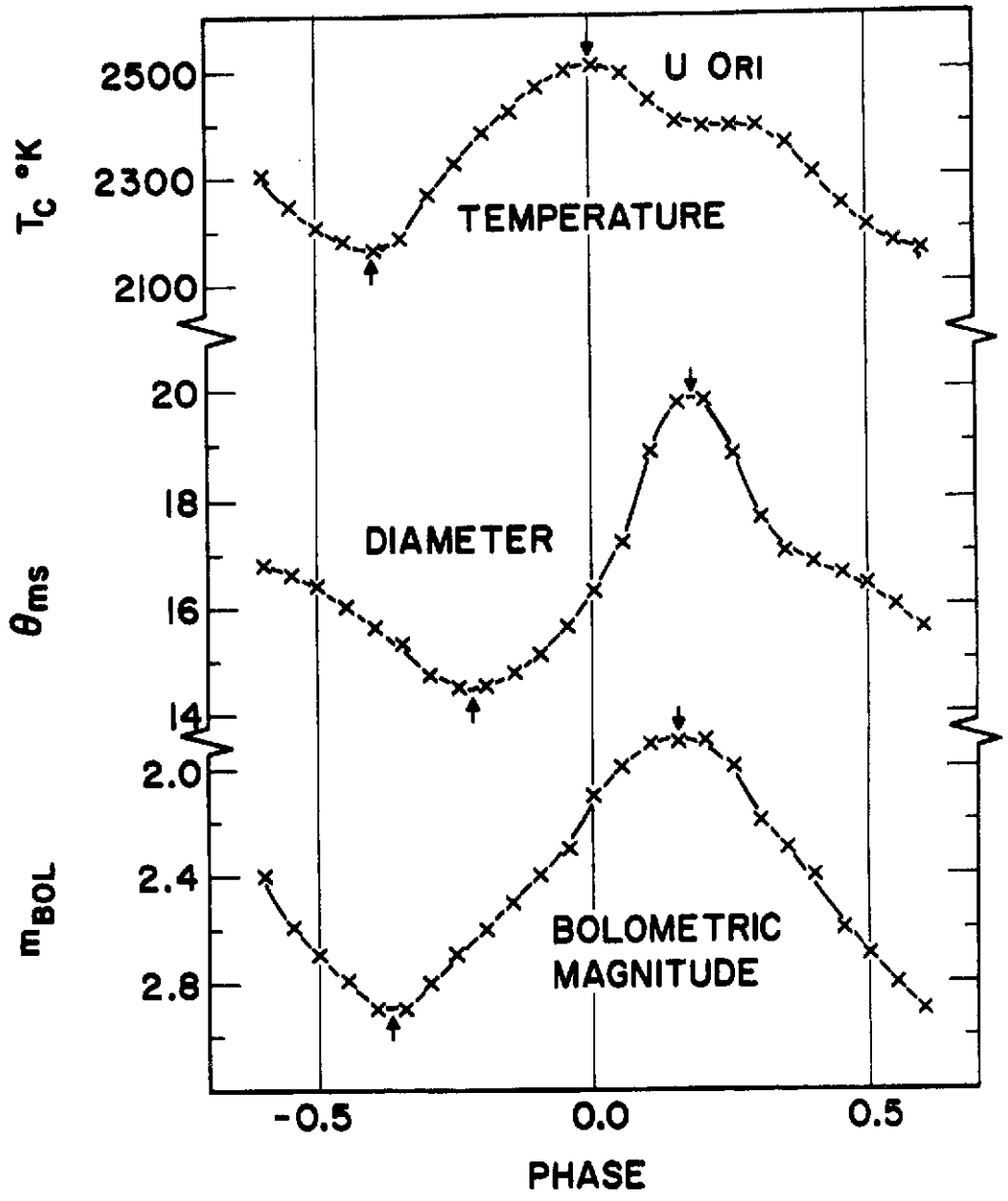

Figure 12n. Similar to figure 12a but for U Ori.

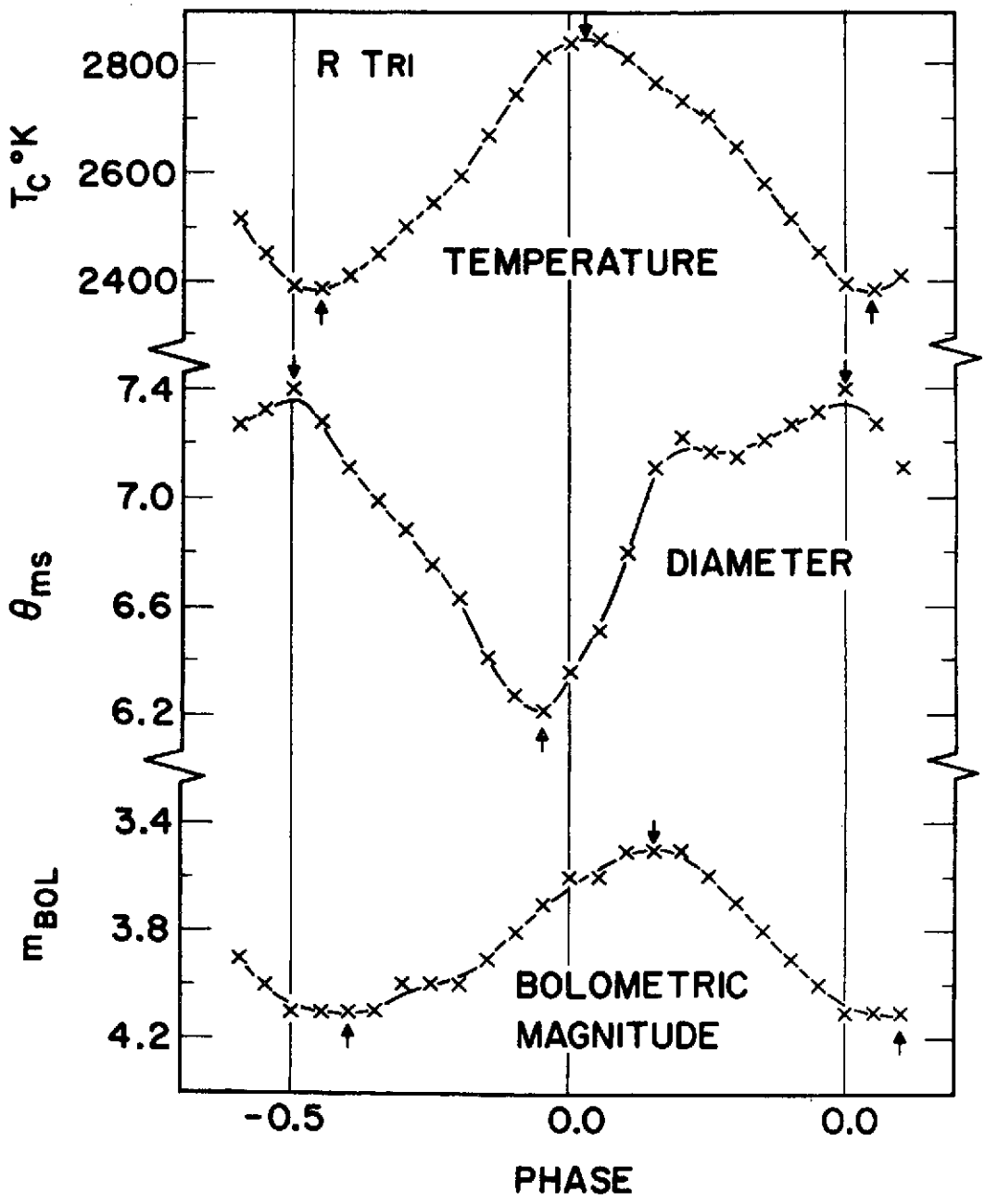

Figure 12o. Similar to figure 12a but for R Tri.

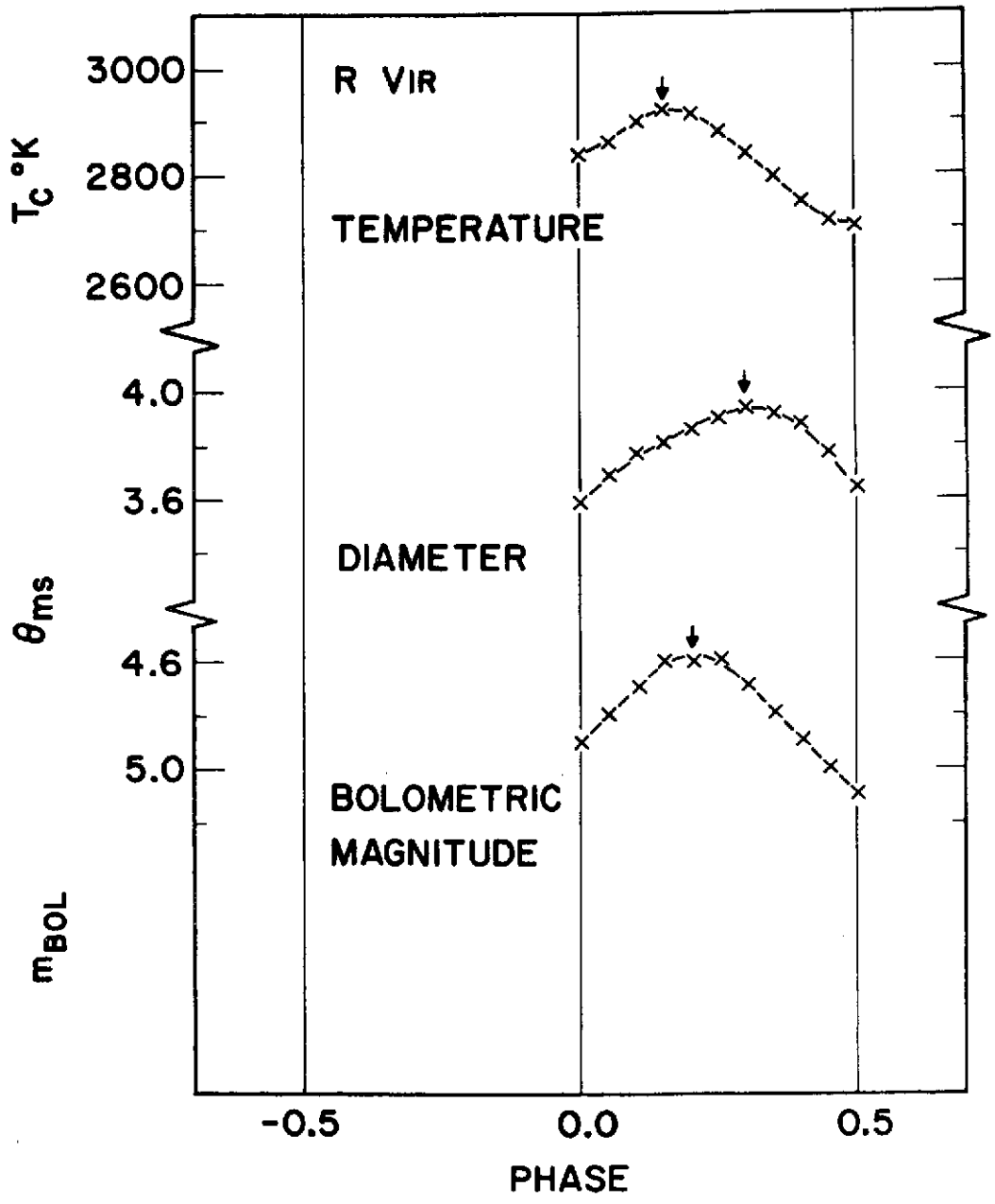

Figure 12p. Similar to figure 12a but for R Vir.

course, the carbon rich stars are not plotted because no 1.04μ data are available.

There exists one point which should again be stressed at this time. The 1.04μ and 3.5μ magnitudes, from which the color indices were formed, represent an average behavior of the stellar variability. The color indices were formed from smoothed curves. During phases where either one or both of the magnitudes are rapidly changing, the color index is more likely to be in error. This error may be propagated through the computations and result in departures from a smooth curve for the temperatures or radii.

It is extremely difficult to estimate the absolute accuracy of the results quoted in appendix IV, because the calculations are based on previously averaged data. As can be seen from prior figures (e.g. 4), the instantaneous brightness of a certain star does deviate from the adopted mean curves by up to $\pm$ 20%. The mean adopted magnitudes hopefully represent the true average behavior of the star.

The absolute accuracy of the color temperatures and angular diameters depends on a multitude of assumed values for various parameters. For example, if the assumption of a 10,000 °K color temperature for α Lyra is seriously in error, the color temperatures will be wrong. Other errors may be implicit: the absolute

calibration flux for zero magnitude at 3.5μ, the 3.5μ effective wavelength itself, the uniform disk approximation, as well as others.

On a positive note, however, the relative uncertainties in the calculated parameters should be smaller than the absolute errors. One of the chief sources of uncertainty lies in the assumption that the 1.04μ and 3.5μ magnitudes represent the same optical depth in the stellar photosphere and are unchanged throughout the cycle. A second source of misgiving results from the averaging process used to determine the mean 1.04μ and 3.5μ magnitudes as functions of phase.

Due to the above reasons, no error bars are plotted on the curves of figure 12. A conservative guess on the relative uncertainties of individual points is estimated to be about $\pm$ 20%.

Some of the individual stars of appendix IV and figure 12 merit further comment (other than the obvious ones):

T Cep: Although the shapes of the temperature and angular diameter curves are in fair agreement with other stars, the luminosity remains constant in direct contrast to the other variables.

o Cet: Mira itself unfortunately does not possess the best quality 3.5μ data. Its results should be viewed

with a more skeptical eye than most of the others.

R Cyg and χ Cyg: S type stars. Temperatures near minimum may be influenced by unknown bands affecting the 1.04μ magnitudes (Lockwood, 1972). These temperatures must be referred to as equivalent temperatures.

A few general comments are suggested by figure 12. The color temperature reaches a maximum near zero phase (maximum visual brightness) and attains a minimum value near phase 0.5, or approximately minimum visual magnitude. The angular diameters are largest near phase 0.3 and smallest near phase -0.1. The total luminosity maximum occurs near phase 0.1 and minimum near phase -0.4. All of the above phases of extrema are in excellent agreement with Pettit and Nicholson (1933), which appears to be the only other source of information for these quantities. A capsule description of Mira variables is that they are hottest when smallest and coolest when largest.

Table XIV summarizes the average spectral type as well as the calculated quantities of temperature, angular diameter and luminosity extrema. The average spectral types are taken from table IV. Also included in table XIV are the average temperature and angular diameter, their absolute and percentage change, and

Table XIV

Summary of Calculated Parameters of the Miras

Star	Average Spectral Type max	min	Color Temperatures $T_{c_{max}}$ °K	$T_{c_{min}}$ °K	ΔT °K	$\overline{T}$ °K	$\frac{\Delta T}{\overline{T}}$	Angular Diameter θ_{max} ms	θ_{min} ms	$\Delta\theta$ ms	$\overline{\theta}$ ms	$\frac{\Delta\theta}{\overline{\theta}}$	Luminosity m_{Bol} max	m_{Bol} min	Δm_{Bol}
R Tri	M4e$^+$	M8.2	2850	2390	460	2620	.18	7.2	6.2	1.0	6.7	.15	$3^m.5$	$4^m.1$	$0^m.6$
R Boo	M4.5e	M8.0	2750	2480	270	2615	.10	4.5	3.7	0.8	4.1	.20	4.6	5.2	0.6
R Vir	M4.5e	-	2920	-	-	-	-	3.9	-	-	-	-	4.6	-	-
o Cet	M5.5e	M9.0	2790	2320	470	2555	.18	40.2	36.0	4.2	38.1	.11	-0.1	0.7	0.8
R Aql	M6.5e	M8.5	2770	2280	490	2525	.19	17.1	14.0	3.1	15.6	.20	2.0	2.6	0.6
R Aur	M6.5e	M9.0	2480	1960	520	2220	.23	20.0	14.5	5.5	17.3	.32	2.2	2.9	0.7
R Cnc	M6.5e	-	2650	-	-	-	-	-	-	-	-	-	2.2	-	-
T Cep	M6.5e	M8.5	2660	2260	400	2460	.16	27.5	21.9	5.6	24.7	.23	1.3	1.4	0.1
U Her	M6.5e	M9.0	2510	2010	500	2260	.22	15.7	13.8	1.9	14.8	.13	(2.4)	3.3	0.9
X Oph	M6.5e	M8.5	2680	2440	240	2560	.09	17.1	14.7	2.4	15.9	.15	2.0	2.4	0.4
U Ori	M6.5e	M9.0	2510	2170	340	2340	.15	19.8	14.5	5.3	17.2	.31	1.9	2.9	1.0
R Ser	M6.5e	-	-	2220	-	-	-	-	-	-	-	-	-	3.8	-
R Cas	M7e	M10	2530	1860	670	2195	.31	32.5	25.6	6.9	29.0	.24	1.0	2.0	1.0
R Leo	M7e	M9.0	2640	2100	540	2370	.23	47.6	34.9	12.7	41.2	.31	0.2	0.9	0.7
R LMi	M7e	M8.8	2590	-	-	-	-	17.4	13.9	3.5	15.7	.22	2.2	(2.8)	(0.6)

Table XIV (continued)

Star	Average Spectral Type max	min	Color Temperatures $T_{c_{max}}$ °K	$T_{c_{min}}$ °K	ΔT °K	$\bar{T}$ °K	$\frac{\Delta T}{\bar{T}}$	Angular Diameter θ_{max} ms	θ_{min} ms	$\Delta\theta$ ms	$\bar{\theta}$ ms	$\frac{\Delta\theta}{\bar{\theta}}$	Luminosity $m_{Bol_{max}}$	$m_{Bol_{min}}$	Δm_{Bol}
T Cas	M7.5e	M8.5	2590	2160	430	2375	.18	20.7	16.1	4.6	18.4	.25	1.9	2.2	0.3
R Cyg	S3,9e	-	2460	2060	400	2260	.18	8.5	4.7	3.8	6.6	.57	3.9	5.3	1.4
χ Cyg	S4,7e	M9.0	2340	1740	600	2040	.29	44.4	29.6	14.8	37.0	.40	0.8	1.8	1.0

the range in total luminosity. The temperature(ΔT_c), diameter ($\Delta\theta$) and luminosity (Δm_{Bol}) ranges are simply the differences between maximum and minimum, whereas the average temperature ($\overline{T}_c$) and average angular diameter ($\overline{\theta}$) represent the arithmetic average of the extrema.

Table XV lists the phases at which the color temperature, angular diameter, and luminosity reach their extreme values, as determined from figure 12. Also included in the last line are the mean values, the standard deviation of the mean and the number of stars used to compute the mean.

Because some stars were radically different in the phases of the extrema of some of the parameters, they were omitted from the averages. U Her was not included in the angular diameter averages, o Cet was omitted at minimum θ, and, of course, T Cep was deleted from the bolometric magnitude phases because it appears to be constant over the entire cycle.

From the results listed in table XIV, it comes possible to extend the color temperature-spectral type relation of table XII to lower temperatures and later spectral types. It must be emphasized, however, that the temperature versus spectral type function (as determined by non-variable or mildly variable M giants) may be inherently different from that found by

Table XV

Phases at which Color Temperature, Angular Diameter, and Bolometric Magnitude Attain Extrema

Star	T_c max	T_c min	θ max	θ min	m_{Bol} max	m_{Bol} min
R Aql	0.00	-0.48	0.25	-0.10	0.07	0.48
R Aur	-0.10	0.40	0.35	-0.15	0.12	0.50
R Boo	0.10	-0.42	0.15	-0.20	0.12	-0.40
R Cnc	-0.05	--	$\geq$0.25	$\leq$0.15	0.05	--
R Cas	-0.05	-0.42	0.40	-0.07	0.10	0.42
T Cas	0.00	0.40	0.27	-0.07	0.10	0.45
T Cep	0.00	0.50	0.47	-0.02	Constant	
o Cet	0.05	-0.33	0.25	0.47 (-0.02)	0.15	-0.40
R Cyg	-0.07	0.50	0.25	-0.20	0.12	-0.32
χ Cyg	-0.05	0.50	0.27	-0.12	0.10	-0.45
U Her	0.00	-0.35	-0.30	0.47 (-0.03)	>0.00	-0.42
R Leo	0.00	0.45	0.35	-0.05	0.05	-0.42
R LMi	0.00	--	0.25	-0.10	0.10	--
X Oph	0.00	0.38	0.22	--	0.07	-0.47
U Ori	0.00	-0.40	0.17	-0.22	0.15	-0.37
R Ser	--	-0.45	$\leq$0.25	--	--	-0.45
R Tri	0.02	-0.45	0.50	-0.05	0.15	-0.40
R Vir	0.15	--	0.30	--	-.20	--
Mean	0.00	-0.48	0.30	-0.11	0.11	-0.43
	$\pm$0.01	$\pm$0.02	$\pm$ .03	$\pm$ .02	$\pm$ .01	$\pm$ .02
	N=17	N=15	N=15	N=12	N=15	N=14

studying the Mira type variables. Table XVI lists the spectral type, color temperature and color index as deduced from the Miras in table XIV. The color temperatures for the Miras are a weighted average of the stars of each spectral type. Temperatures for spectral types M4 - M7.5 were determined from the average spectral type at maximum, while the temperatures for M8.0 - M10 were deduced from the average spectral type at minimum.

The [1.04μ]-[3.5μ] color index versus T_c^{-1} of figure 13 is an extension and duplication of figure 11. The solid line is the assumed color index as a function of temperature for a 10,000 °K reference color temperature which was defined to have zero index. The spectral types labeled to the left of the line represent the color index as determined from the normal M giant stars of table XII; the spectral types plotted to the right of the line are inferred from table XIV for the Miras.

As is evident from figure 13, the temperature or color index agreement is best near spectral type M8 and poorest for earlier types. As previously stated, interstellar extinction has been ignored. This reddening may affect the calculated temperatures but probably not enough to account for the observed discrepancy.

Table XVI

Color Temperature and Color Index

Versus Spectral Type for the Mira Variables

Spectral Type	Color Temperature	Color Index
M4-M4.5	2840 °K	$2^{m}.08$
M5.5	2790	2.13
M6.5	2610	2.36
M7	2590	2.40
M7.5	2590	2.40
M8.0	2480	2.56
M8.2	2390	2.70
M8.5	2290	2.90
M8.8	-	-
M9.0	2110	3.24
M10	1860	3.87

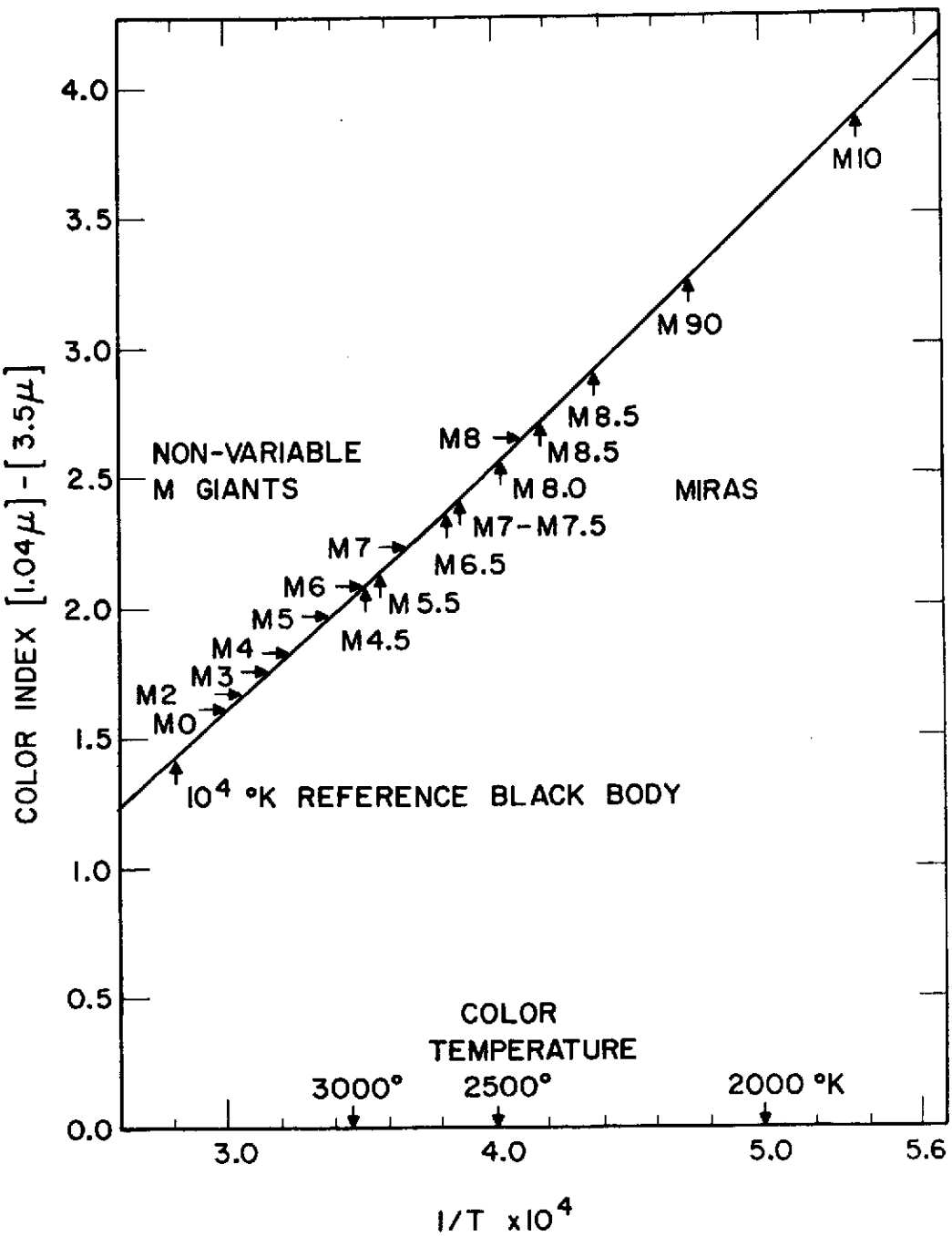

Figure 13. A comparison of the color index-spectral type relation versus color temperature as determined for the non-variable or mildly variable M giants and for the Miras.

A comparison between the effective temperatures for M giants, as listed in table XII, and the color temperatures for Miras (table XVI), shows that the temperatures of Lee (1970), Johnson (1966) and Smak (1964) bracket those of the present study. Jones (1968) produced a color temperature-spectral type relation for M giant stars from narrow band photometry in the 4700-11200 Å region. When his color temperatures are compared to those deduced from the non-variable and variable stars of this study, the agreement is fair. The two extremely different wavelength regions do not yield discordant color temperatures.

VIII

VISUAL MAGNITUDES AND BLANKETING

In addition to the previous calculations of color temperature, angular diameter, and bolometric magnitude, a comparison between the calculated and the observed visual magnitudes allows a determination of visual absorption which is caused by lines or molecular bands.

The first step in this procedure is to deduce the visual blanketing for the non-variable or mildly variable M giant standard stars of table XI. From the adopted color index-color temperature relation, temperatures dependent on spectral type may be calculated in a manner similar to that previously described. The earliest spectral types possess color indices less than $2^{m}.0$. For these color indices, the linear approximation between color index and T_c^{-1} is no longer valid and it was not used. The color temperatures for these "early" sources were calculated by interpolation of table XIII. Once the color temperature is known, the solid angle subtended by the source, the uniform disk angular diameter, and the visual magnitude are computable. Of course, the implicit assumption in these calculations is that the stellar photosphere is radiating as a black body which

may be characterized by one temperature. This unique temperature is assumed to be applicable to all three (0.55, 1.04 and 3.5μ) wavelengths.

Table XVII again lists the standard M giants, their spectral type, color index (C.I.), color temperature (T_c), angular diameter (θ), calculated and observed visual magnitudes ($m_{v\ calc}$, $m_{v\ obs}$) and the difference (Δ) between them.

As is evident from table XVII, MO stars appear brighter than their calculated visual magnitude by about $0^m.3$. This difference decreases, changes sign about M3 and then grows larger as the spectral type advances.

This apparent excess of MO-M2 stars can be attributed to a variety of causes. One source of discrepancy may be in the adopted 3.5μ effective wavelength and its absolute calibration. However, for the purposes of the discussion which follows, the disagreement between the observed and calculated visual magnitudes near spectral types MO and M1 is considered remarkably small and will not alter the ensuing results. The main point to be stressed is that as the temperature decreases, the amount of blanketing at visual wavelengths increases.

The next step in the visual calculations is to determine the blanketing in the same manner for the

Table XVII

Calculated Parameters for M Giant Standard Stars

Star	Spectral Type	Color Index	T_c °K	θ ms	m_v Calc	m_v Obs	Δ
β And	MO III	$1^m.64$	3289	16.6	$2^m.41$	$2^m.05$	$-0^m.36$
μ UMa	MO III	1.60	3333	10.2	3.37	3.04	-0.33
75 Leo	MO IIIb	1.60	3333	3.7	5.57	5.18	-0.39
α Vul	MO III	1.58	3356	5.3	4.74	4.45	-0.29
γ Eri	M1 III	1.51	3390	9.9	3.28	2.95	-0.33
χ Peg	M2 III	1.57	3367	5.0	4.83	4.80	-0.03
α Cet	M2 III	1.63	3300	15.0	2.61	2.53	-0.08
π Leo	M2 III	1.78	3125	6.2	5.02	4.71	-0.31
83 UMa	M2 IIIab	1.66	3257	5.8	4.77	4.73	-0.04
β Peg	M2 IIb-IIIa	1.80	3106	21.0	2.41	2.53	0.12
55 Peg	M2 III	1.59	3344	5.2	4.79	4.50	-0.29
μ Gem	M3 IIIa	1.76	3155	17.3	2.69	2.85	0.16
ρ Per	M4 IIIa	1.84	3067	18.6	2.79	3.39	0.60

Table XVII (continued)

Star	Spectral Type	Color Index	T_c °K	θ ms	m_v Calc	m_v Obs	Δ
ω Vir	M4-4.5 III	1.79	3125	7.9	4.48	5.28R	0.80
HR 5299	M4-4.5 III	1.87	3040	8.9	4.47	5.28	0.81
VY Leo	M5 III	1.96	2941	11.3	4.28	5.78	1.50
RR UMi	M5 III	1.76	3155	10.8	3.71	4.59	0.88
τ^4 Ser	M5 IIb-IIIa	2.23	2717	13.8	4.63	-	-
OP Her	M5 IIb-IIIa	1.93	2976	7.3	5.10	6.32	1.22
R Lyr	M5 III	1.96	2941	20.6	2.98	4.0H	1.02
W Cyg	M4e-M6	2.17	2762	16.7	4.06	5.1H	1.04
RZ Ari	M6 III	2.02	2890	12.9	4.16	5.93	1.77
RS Cnc	M6 IIIa	2.16	2770	18.8	3.77	5.95	2.18
X Her	M6e	2.07	2841	15.9	3.88	-	-
g Her	M6 III	2.07	2841	21.2	3.25	5.05	1.80
CH Cyg	M6	2.48	2532	15.0	5.22	-	-
SW Vir	M7 III	2.23	2717	19.5	3.89	-	-
RX Boo	M8:	2.64	2433	24.9	4.58	-	-

Mira variables. Appendix IV lists the calculated and observed visual magnitudes as a function of phase (or alternatively, of temperature) for the Miras. As stated previously, the observed brightness is the mean visual magnitude as determined by Campbell (1955) from the AAVSO observations. The effective wavelength for this data (based on the human eye) may be somewhat different than the 0.55μ used in the calculations. This difference may introduce uncertainties into the absolute amount of visual absorption. However, with the lack of simultaneous UBV photometry or mean photometric light curves for the entire cycle, there is no alternative.

In order to compare similar points in the stellar cycle, the times or phases of maximum and minimum temperature were chosen as reference marks. These times were then assumed to represent earliest and latest spectral types. The differences between the observed and calculated visual magnitudes were tabulated for these reference points.

As an alternative method of computation, the reference marks were selected to be the phases of visual observed extrema (e.g., zero phase for maximum visual magnitude and near phase $\pm$ 0.50 for minimum). The difference in visual magnitude was also tabulated for these points.

Table XVIII summarizes the results of these two different methods. Column 1 lists the spectral type, column 2 names the star whose average spectral type at maximum or minimum fulfills column 1, column 3 lists the phase of the temperature extrema (maximum T_c for spectral types M4 - M7.5; minimum T_c for later spectral types), column 4 tabulates the difference between observed and calculated visual magnitudes. Column 5 lists the phase of visual observed extrema and column 6 tabulates the magnitude difference for this alternative method. Due to the visual influence of its companion, X Oph was omitted at minimum from the calculations.

As evidenced by table XVIII, there is really very little difference in these two alternative methods of computation. For this reason, both results were used to determine a mean visual absorption as a function of spectral type for the Miras.

Smak (1964) attempted to ascertain the amount of visual blanketing by TiO bands as a function of spectral type or effective temperature for M giants. His results for blanketing and his effective temperatures are listed in table XIX. Included in table XIX, and as determined by this study, are the blanketing and color temperature (table XVII) for the non-variable standard stars. These same quantities for the Miras,

Table XVIII

Visual Blanketing Summary for Miras

Spectral Type	Star	Phase of T_c extrema	Δ	Phase of Visual Extrema	Δ
M4	R Tri	0.02	$0^m.7$	0.00	$0^m.5$
M4.5	R Boo	0.10	0.8	0.00	0.1
	R Vir	0.15	0.9	0.00	0.0
M5.5	o Cet	0.05	1.6	0.00	1.4
M6.5	R Aql	0.00	1.9	0.00	1.9
	R Aur	-0.10	3.8	0.00	2.2
	R Cnc	-0.05	2.2	0.00	1.9
	T Cep	0.00	2.0	0.00	2.0
	U Her	0.00	2.2	0.00	2.2
	X Oph	0.00	2.3	0.00	2.3
	U Ori	0.00	1.5	0.00	1.5
M7	R Cas	-0.05	2.7	0.00	2.4
	R Leo	0.00	3.0	0.00	3.0
	R LMi	0.00	2.1	0.00	2.1
M7.5	T Cas	0.00	3.0	0.00	3.0
M8	R Boo	-0.42	4.0	0.50	4.2
M8.2	R Tri	-0.45	4.0	-0.47	4.0
M8.5	R Aql	-0.42	5.3	-0.45	5.2
	T Cep	0.50	5.1	0.47	5.1
	T Cas	0.40	5.4	0.45	5.6

Table XVIII (continued)

Spectral Type	Star	Phase of T_c extrema	Δ	Phase of Visual Extrema	Δ
M9.0	R Aur	0.40	6.0	0.50	6.7
	o Cet	-0.32	4.9	-0.37	4.9
	U Her	-0.35	3.9	-0.40	4.3
	R Leo	+0.45	4.3	-0.42	4.7
	U Ori	-0.40	4.8	-0.37	4.8
M10	R Cas	-0.42	4.4	-0.40	4.5

Table XIX

Visual Blanketing as a Function of Spectral Type

Spectra Type	Smak (1964)		THIS STUDY			
			Non-Variables		Miras	
	T_e	$\delta T_i O$	T_c	Δ	T_c	Δ
MO	3340	$0^m.00$	3320	$-0^m.34$		
M1	3200	0.22	3440	-0.33		
M2	3090	0.45	3240	-0.10		
M3	2980	0.77	3150	0.16		
M4	2850	1.13	3070	0.74	2850	$0^m.6$
M4.5					2840	0.4
M5	2710	1.59	2940	1.15		
M5.5					2790	1.5
M6	2500	2.27	2840	1.92		
M6.5					2610	2.1
M7	2250	3.23	2710	-	2590	2.6
M7.5					2590	3.0
M8	2000	4.33	2430	-	2480	4.1
M8.2					2390	4.0
M8.5					2290	5.3
M9					2110	4.9
M10					1860	4.5

as summarized in tables XVI and XVIII, are also listed.

As may be deduced from table XIX, this color index-color temperature method agrees quite well with Smak's (1964) values. The difference in δTiO near spectral type MO cannot be simply resolved by an additive constant but is deeply embedded in the absolute fluxes, color temperatures and other assumptions previously quoted and cannot be further resolved at this time. However, to obtain agreement between the two summaries, the addition of about 0.3 to 0.4 magnitudes to column 5 or, as an alternative, the subtraction of that same amount from column 3, would bring the results into excellent agreement. It deserves to be mentioned that Smak defined his δTiO correction to be zero at spectral type MO.

In addition to the δTiO absorption at temperature or visual magnitude extrema, the visual blanketing as a function of phase, or probably more significantly as a function of color temperature, may be computed throughout the entire cycle of variation. Figure 14 depicts the δTiO absorption ($\Delta=m_{v\ calc}-m_{v\ obs}$) versus color temperature for the M type Miras which possess complete cycle parameters. The data for figure 14 was taken from appendix IV. The binary, X Oph, is omitted.

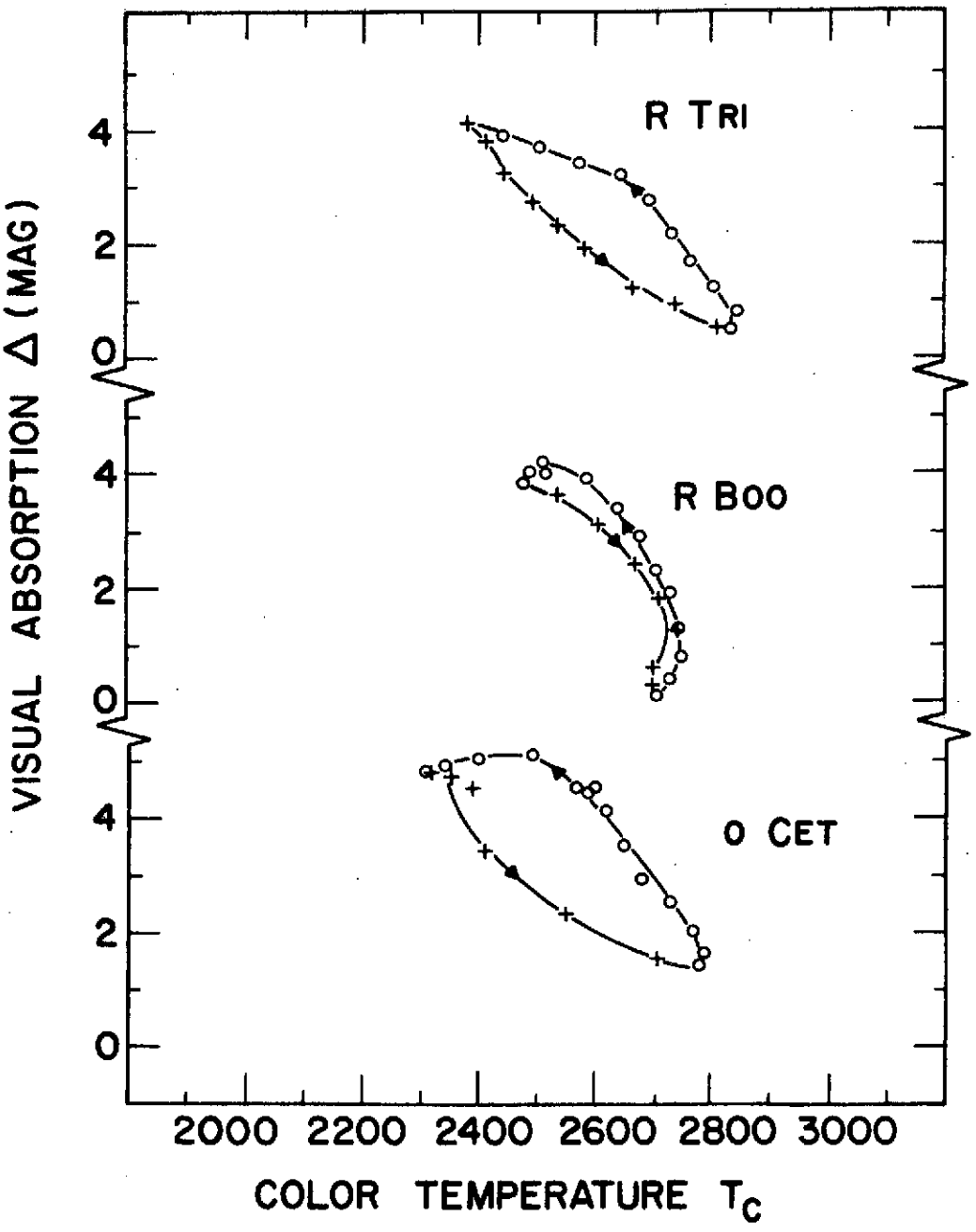

Figure 14a. Visual absorption in magnitudes versus color temperature throughout the full cycle of variability for the earliest M stars of this study.

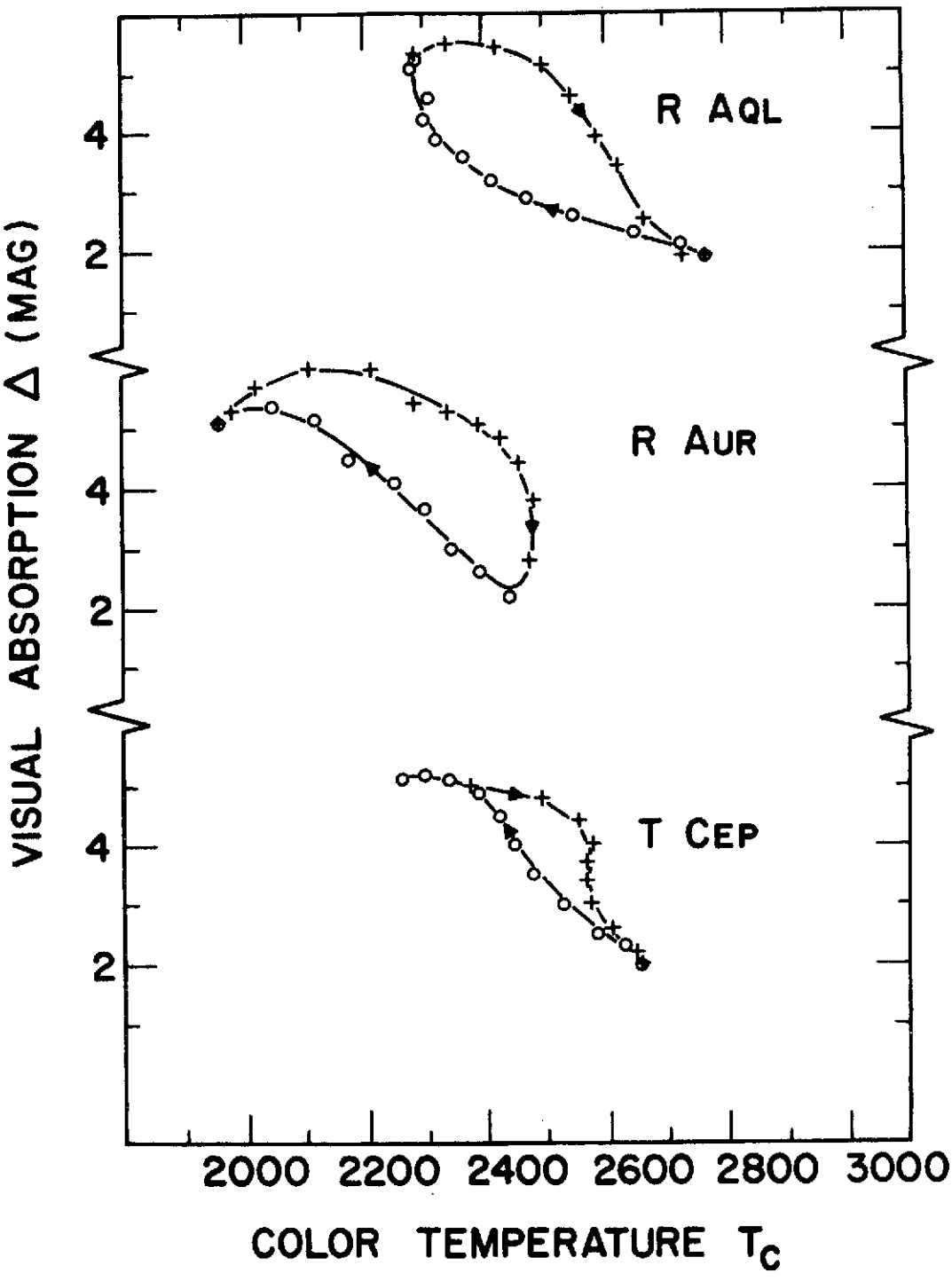

Figure 14b. Similar to figure 14a but for M stars of later spectral type.

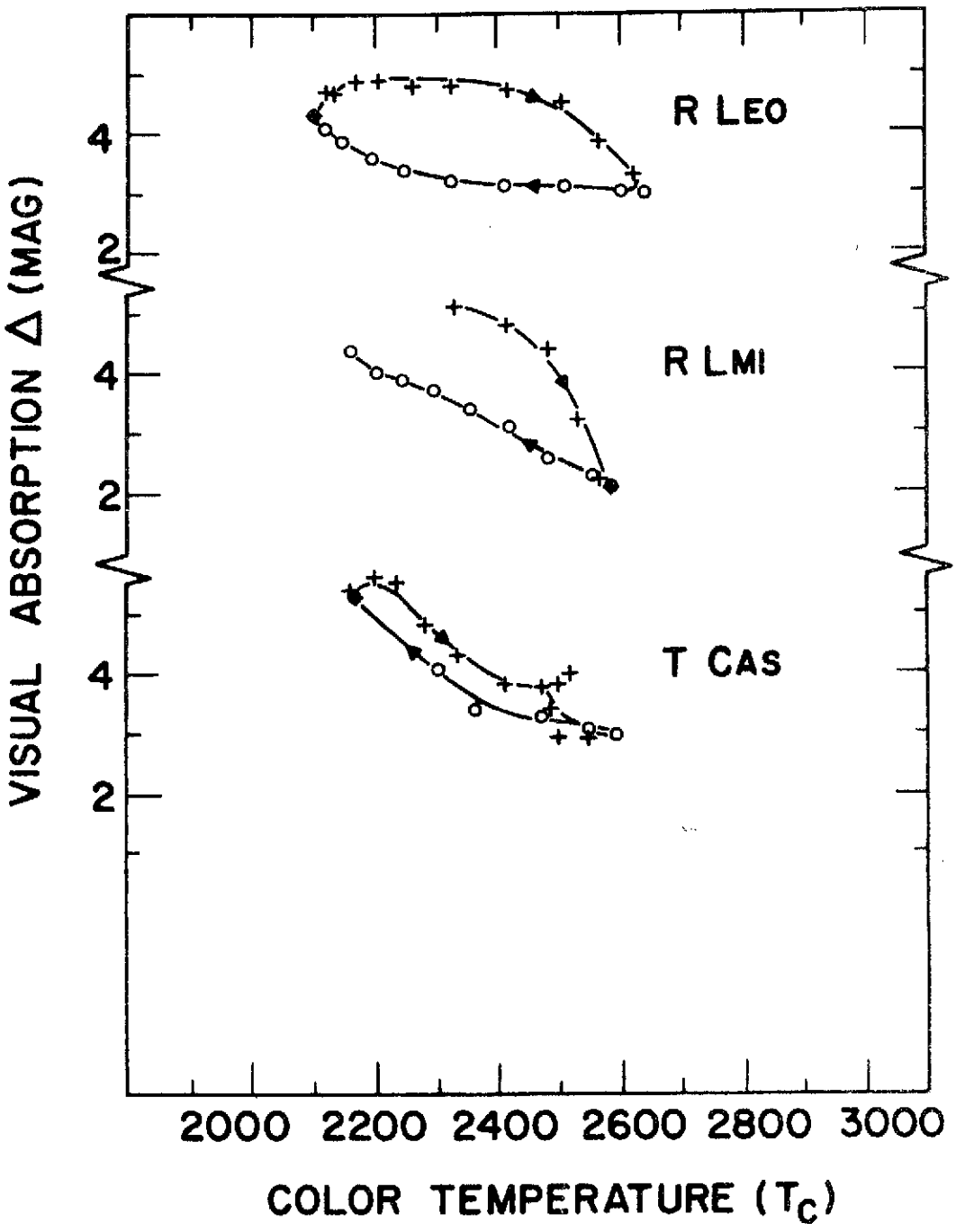

Figure 14c.Similar to figure 14b.

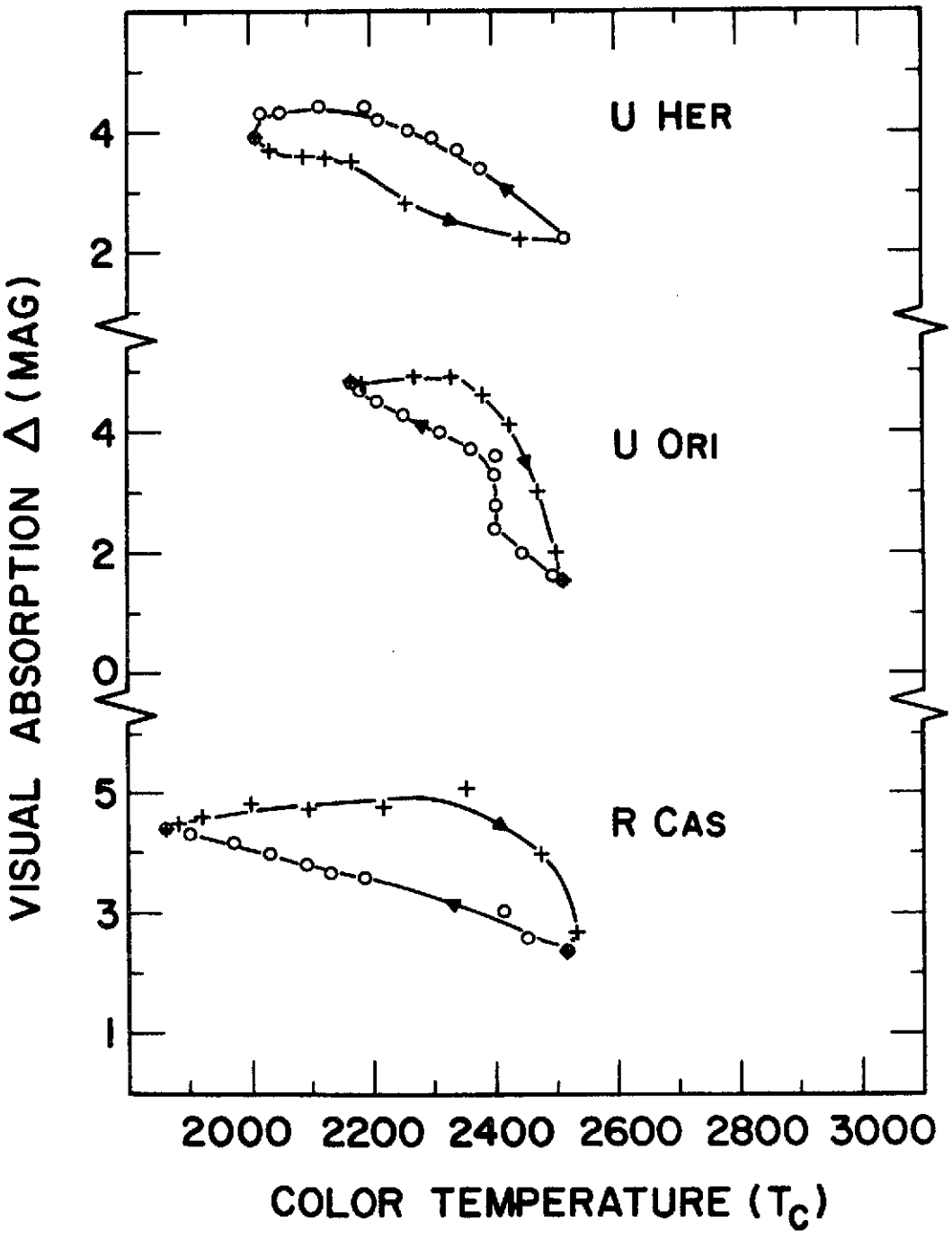

Figure 14d. Similar to figure 14b.

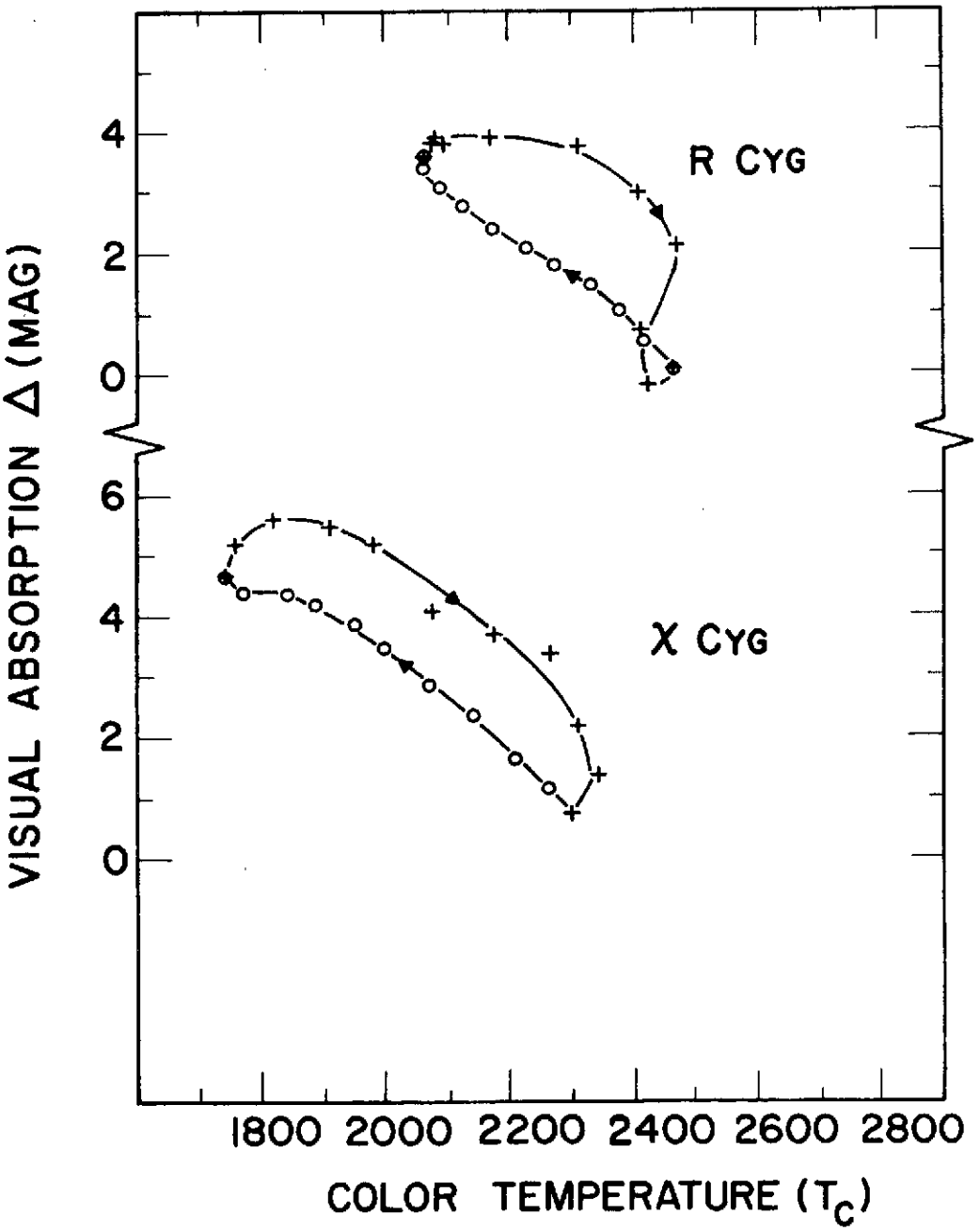

Figure 14e. Similar to figure 14a but for the S stars R Cyg and χ Cyg.

Two S stars, χ Cyg and R Cyg, have been included in figure 14 for comparative purposes. As previously mentioned, near minimum light, the 1.04μ magnitudes are influenced by unidentified absorption bands. The color temperatures, as deduced from the color indices, may then be cooler than appropriate for the photosphere. Other quantities calculated from this temperature would also be in error.

Lockwood and Wing (1971) give no equivalent M spectral types for R Cyg but cite equivalent types M2-M9.0 for the mild S star, χ Cyg. For χ Cyg, the very early spectral type is consistent with the rather small amount ($\sim 3^{m}\!/4$) of visual absorption at zero phase. The $4^{m}\!.7$ of absorption at minimum temperature is also in agreement with the M9.0 spectral type. The visual blanketing-color temperature relation throughout the complete cycle appears similar to that of the M stars.

As is evidenced by figure 14, the visual blanketing is not a unique function of color temperature. There appear to be two distinct values of absorption for a given temperature, depending on whether the star is on the ascending or descending branch of the light curve. The amount of blanketing executes loops in the blanketing-temperature diagram akin to a hysteresis curve. This behavior has been previously noticed by Spinrad

and Wing (1969) in their plots of molecular band strength versus temperature.

In figure 14, not all of these loops circle in the same sense. The clockwise loops imply increasing absorption as the color temperature decreases on the descending portion of the light curve. As the color temperature reaches a minimum value and begins to rise, the blanketing does not recover as quickly, possibly implying a further formation of, or increase in, the amount of TiO. This amount of TiO is then not a unique function of temperature, but depends on the stellar history.

To the contrary of these clockwise loops, a few stars cycle in the opposite sense. It is perhaps significant that these exceptions tend to be of earlier spectral type. Spinrad and Wing (1969) noticed these opposite loops also.

The exact processes contributing to these loops, as well as the significance of the clockwise or counter-clockwise behavior, are beyond the scope of this present work.

IX

RADIAL VELOCITIES

Another quantity which may be computed in order to compare with observational data is the radial velocity of the stellar photosphere. Scott (1942) assumed that the bright hydrogen emission lines of Mira variables originated at about the same level as the photosphere. His calculations, based on this assumption, provided an acceptable explanation for the luminosity variation of Mira.

Unfortunately, the emission lines are present only for about one-half cycle centered on maximum light, and, therefore, cannot be used to trace the photospheric radial velocity throughout the entire cycle. Merrill and Burwell (1930) published radial velocity curves of emission lines for selected Miras. The stars which are in common with this project are: T Cas, R Ser, U Ori, R Leo, χ Cyg, R Cyg, and R Cas. T Cas, in contrast to most other stars, had either a constant velocity or a smaller range. The trait of the velocity curve in common among the Miras appears to be a relatively broad region of maximum velocity of approach, sometime after zero phase. This expansion velocity seems to maximize somewhere near phase 0.15. Joy (1926)

produced a mean curve for the emission line velocity for Mira itself in which the expansion velocity maximizes near phase one-quarter, minimizes near 0.5 phase and has secondary minima and maxima near phase 0.9 and 0.75, respectively.

If the assumption of emission lines originating near the photosphere is valid, the radial velocities, as calculated from the angular diameters in appendix IV, should approximate the emission line velocities where comparisons can be made. Due to their apparent brightness and data coverage, three representative stars (R Leo, R Aql, and T Cas) were selected for comparison purposes. The radial velocities were computed from equation 16 to represent the shape of the velocity curve, not its absolute scale.

$$\dot{\theta}(\phi) = \theta(\phi+0.05)-\theta(\phi)+[\theta(\phi)-\theta(\phi-0.05)]$$

$$= \theta(\phi+0.05)-\theta(\phi-0.05) \qquad (16)$$

where $\dot{\theta}$ represents the radial velocity in arbitrary units and ϕ is the phase. This equation was utilized in an attempt to average or smooth out the fluctuations and errors in computation of temperature and angular diameters. Figure 15 graphs this radial velocity as a function of phase for R Leo, R Aql, and T Cas.

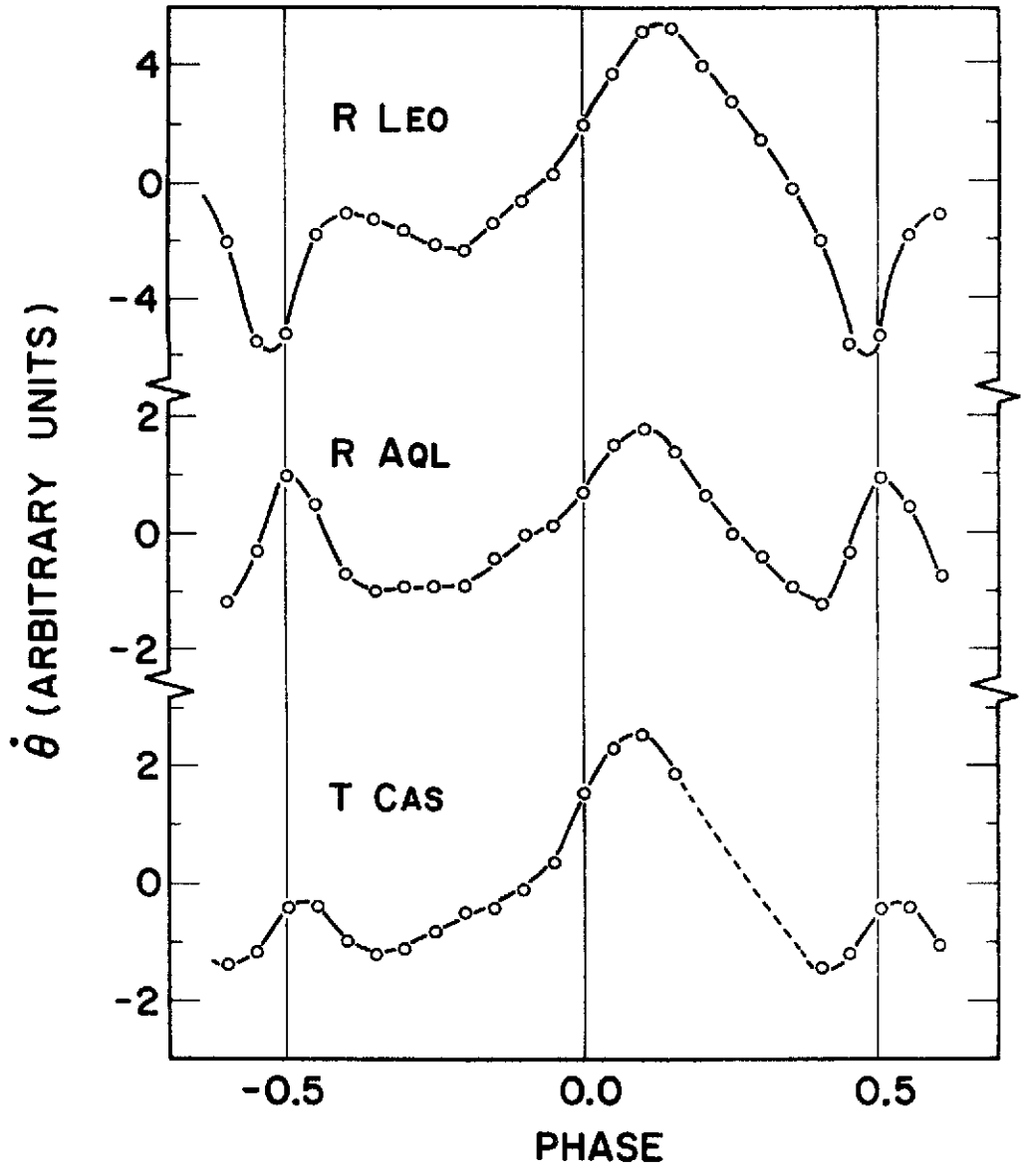

Figure 15. Computed radial velocity versus phase for three representative stars R Leo, R Aql, and T Cas.

A positive $\dot{\theta}$ implies expansion.

The general shape of the radial velocity curves is emphasized, not the detailed structure. The angular size absolute error estimates are already quite large, although the relative errors should be smaller. From figure 15, it is apparent that the outward velocity reaches maximum near phase +0.1, while the inward velocity attains a minimum near phase +0.45. Secondary velocity extrema occur near phase -0.4 and -0.3, respectively. The maximum diameter takes place near phase 0.3 where the outward velocity reaches zero, while the minimum diameter occurs near phase -0.1. Both these results are in agreement with table XV -- as they should be. They are also in reasonable agreement with Merrill and Burwell (1930).

It is unfortunate that the 3.5μ data for o Cet are not more complete or trustworthy so that a better radial velocity comparison may be made on the same star. The general shape of the radial velocity curve of R Leo does appear similar to the hydrogen emission line velocity curve of Mira as determined by Joy (1926). A shift of R Leo's velocities by about 0.1 cycle toward larger phase would bring the two curves into excellent agreement. The two curves show the primary maximum of outward velocity, the primary

minimum, and suggestions for the secondary extrema.

The reason for the apparent displacement of the computed radial velocities of figure 15, with respect to the observational velocities, is not clear at this time. The calculated results are not in good agreement with Joy's (1926) emission lines, nor Scott's (1942) corrected values. The deduced velocities of figure 15 do not mirror the behavior of the absorption lines.

On the plus side, the velocity curves of figure are in good agreement with that deduced for Mira by Pettit and Nicholson (1933). From their graphs, the maximum expansion velocity happens near phase +0.1 and has a broad minimum centered near phase -0.4.

X

CARBON-RICH MIRAS

Although the Mira type and semi-regular variables of the C spectral designation have not been included in any of the previous computations, the characteristic behavior deserves to be mentioned at this time.

The carbon stars observed as part of this project are listed in table II, but are enumerated again as: T Cnc, WZ Cas, S Cep, V CrB, U Cyg, RS Cyg, RY Dra, R Lep, W Ori, and SS Vir. Their period, spectral type, visual magnitude and 3.5μ range were also summarized in table II.

Unfortunately, the 3.5μ data are either incomplete or indecisive for T Cnc, RY Dra, R Lep, W Ori and SS Vir. T Cnc, RY Dra and W Ori are semi-regular variables of relatively small visual amplitude. Their 3.5μ observations could be adequately described in each case by a constant magnitude ($+0^{m}.26$, $-0^{m}.51$, $-0^{m}.89$, respectively) with about a 10% uncertainty. The 3.5μ data are insufficient on R Lep to allow any statement. Visual data were available for SS Vir, although the 3.5μ points are of limited phase span.

Another semi-regular variable, RS Cyg, had visual observations available. However, even though the 3.5μ coverage is well distributed over the entire cycle, it demonstrated no alterations beyond the observational uncertainties and its 3.5μ magnitude is adopted as $+0^{m}.94 \pm 0^{m}.1$. To the contrary, another small amplitude semi-regular variable, WZ Cas, showed significant 3.5μ changes, but no visual data for phase computation were available from the AAVSO.

On a more positive note, three carbon stars, namely S Cep, V CrB and U Cyg, possess good 3.5μ data coverage as well as AAVSO visual curves. Their 3.5μ measurements were plotted in figure 6 and the adopted mean curves were listed in table V.

In contrast to the M stars, no 1.04μ measurements throughout the variability cycle exist for carbon stars; therefore, no color temperatures, angular sizes nor luminosities may be similarly computed. These parameters must wait until observations which represent a true photospheric continuum level become available.

Mendoza and Johnson (1965) have published UBVRIJKLM observations of carbon stars and concluded that the observed energy distributions "differ relatively little from those of ordinary K and M giants for wavelengths longer than that of the V

filter (0.55μ) but that they differ greatly for the shorter wavelengths". They imply the effective temperatures of carbon stars are similar to the M giants.

Gordon (1968) developed a spectral classification method for carbon stars and Richer (1971) deduced their color temperatures on the basis of the (I-L) index of Johnson (1966). Fujita et al., (1965) published color temperatures for carbon stars and graphed a conversion from C to M spectral type. Table XX lists their conversion from C to M type, their color temperature, the color temperature of Richer (1971) and the color temperatures for M stars deduced from this study. As may be seen from the table, the agreement among the various methods of color temperature determination seems fair to good. If the conversion from C to M classification of Fujita, et al., (1965) is valid, table XX supports Mendoza and Johnson's (1965) contention that the temperatures of carbon stars are similar to M stars.

Other quantities existing at the present are the visual and 3.5μ data which then may be compared for M, S, and C stars to ascertain similarities or differences. From the 3.5μ phase curves of figure 6, there seems to be an indication that carbon stars may reach their 3.5μ maximum somewhat nearer to zero phase

Table XX

Intercomparison of Carbon Stars and M Stars

Spectral Type	Color Temperature °K :	M Equivalent Spectral Type *	Color Temperature °K This Study	
			non-variables	Miras
CO	4400			
C1	(3800)			
C2	~3250	(3200)	~MO	3320	---
C3	3050	2700	M2	3240	---
C4	2900	2600	M3.5	~3100	---
C5	2750	2450	M5	2940	~2820
C6	2600	2300	M6	2840	~2700
C7	2500	2200	M7	2710	2590
C8	2350	2000	M8	2430	2480
C9	2200	1800	M9	---	2110

* Fujita, et al., 1965.

: Richer (1971).

than do the M and S stars. The C type stars appear to minimize about the same phase as M stars but earlier than the S stars. Eight M stars exist for which a mean 3.5μ range may be computed. For this group, the mean visual range is $5^{m}.3 \pm 0^{m}.2$ (standard deviation of the mean) whereas the observed mean 3.5μ range is $0^{m}.5 \pm 0^{m}.1$. For the four S stars, the mean visual range is $7^{m}.1 \pm 0^{m}.4$ and at 3.5μ it is $0^{m}.9 \pm 0^{m}.2$. For the carbon stars, excluding the constant RS Cyg, the mean visual range is $3^{m}.2 \pm 0^{m}.3$ while the 3.5μ range is $0^{m}.8 \pm 0^{m}.1$. Thus, the mean range of 3.5μ variability appears very similar, although C and S type stars may have a somewhat larger range than do the M stars. The smaller visual range of the carbon stars is probably reflected in the excess TiO absorption of the M and S stars and is not likely due to inherently different temperatures.

From the available data of this study, in agreement with Mendoza and Johnson (1965), the carbon stars do not differ significantly from the M and S type variables. However, there is a suggestion, supported by only a few stars, that the carbon stars possess a somewhat greater range in 3.5μ magnitude and tend to reach 3.5μ maximum nearer zero phase than do the M type stars.

XI

COMPARISONS WITH OTHER OBSERVATIONAL RESULTS

Theoretical studies of long period variable stars are not only sadly lacking in number, but the predictions which do exist do not lend themselves to a comparison of observable parameters. Therefore, this section will compare the computations of this present study with other observational results. Comparison of color temperature, effective temperature, visual absorption and radial velocity have been previously mentioned.

The number of cool giants whose angular diameters have been measured is sparse. For the non-variable standards of table XVII, only β And, α Cet and β Peg have angular diameters determined by various interferometric methods (Pease, 1931; Brown, 1968; Gezari, Labeyrie and Stachnik, 1972). Table XXI summarizes these observations as well as the uniform disk diameters calculated in this project and taken from table XVII.

Table XXI

Summary of Angular Diameter Measurements

Star	Angular Diameter (ms) This study	previous work
β And	16.6	10.8*
α Cet	15.0	9.4 - 11.5*
β Peg	21.0	21:, 16 ≠

* Brown (1968) (as extracted from the Carnegie Yearbooks).

: Pease (1931).

≠ Gezari, et al., 1972.

As table XXI indicates, the agreement is satisfactory only for β Peg, although the more recent measurements by speckle interferometry (Gezari et al., 1972) have reduced its size.

For the Mira variables, only o Cet itself has been measured with the 20-foot Michelson interferometer. Its angular diameter was 47 ms (Pease, 1931), as compared to 36 - 40 ms computed by this study. Mira has also been measured by the speckle interferometry methods of Bonneau and Labeyrie (1973). They reported, at visual phase 0.09, an angular diameter of 51 $\pm$ 5 ms at a wavelength of 7500 Å with the diameter increasing toward bluer wavelengths.

At 1.04μ, they set an upper limit of 50 ms. At visual phase 0.38, they also reported a 55 ± 5 ms diameter at 7500 Å. The diameters inferred by this project at phases 0.09 and 0.38 are 38 and 37 ms, respectively. The angular size of R Leo has been measured at infrared wavelengths by lunar occultation (Becklin, 1972). Its reported extent of 50 ms compares well with the 35-47 ms range of this study.

As previously stated, the absolute errors of the computed angular diameters of this study are probably quite large (~30%), although the relative errors should be smaller. Even though the agreement is far from excellent, it seems that the angular diameters deduced from the [1.04μ] - [3.5μ] color index and the 3.5μ absolute calibration are not inconsistent with the diameters measured by other means. There is an indication (Bonneau and Labeyrie, 1973) that the diameters decrease at longer wavelengths. This reduction would bring the results for the Miras into better agreement but would compound the differences for the standards of table XXI.

In a project similar to the present research, one of the earliest and, yet, most often quoted studies of LPV stars is the work of Pettit and Nicholson (1933). Working with a thermocouple at the Newtonian focus of the Mt. Wilson 100-inch telescope from 1921-1927,

they measured 11 long period variables. From their observations of radiometric magnitudes and water cell absorption, they determined temperatures, angular diameters and luminosities as functions of visual phase.

Comparison can be made of 9 stars (R Aql, R Cnc, o Cet, R Cyg, χ Cyg, R Leo, R LMi, X Oph, R Tri) which the two projects held in common. Table XXII summarizes the computed temperature, diameter and radiometric magnitude range of Pettit and Nicholson (1933) and the similar quantities from this work. As is evident from the table, there exists some discrepancy as to the temperature and diameter extrema, although, in some cases the agreement is excellent. Differences in absolute calibration, but, particularly differences in methods of temperature determination could account for the disagreement.

Despite some of the individual star discrepancies which exist between this present study and the earlier work of Pettit and Nicholson (1933), several corroborating generalizations concerning the average behavior of Mira variables can be deduced. Table XXIII tabulates the mean characteristics as determined by the two projects. The errors listed represent the standard deviation of the mean. Some of Pettit and Nicholson's results are quoted without

Table XXII

The Measurements of Pettit and Nicholson

Compared to the Present Study

	Pettit and Nicholson			This Study		
Star	Temperature Range °K	Angular Diameter$_{ms}$	Radiometric Magnitude	Color Temperature	θ_{ms}	m_{bol}
R Aql	2320-1920	19-28	1.8-2.7	2770-2280	14-17	2.0-2.6
R Cnc	2320-(1700)	16-(31)	1.9-2.9	2650-		2.2-
o Cet	2640-1920	38-55	-0.3+0.8	2790-2380	36-40	-0.1-0.7
R Cyg	2790-(2010)	5.4-(9.7)	3.6-5.0	2460-2060	4.7-8.5	3.9-5.3
χ Cyg	2240-1640	34-57	0.4-1.6	2340-1740	30-44	0.8-1.8
R Leo	2170-1800	50-63	0.1-1.0	2640-2100	35-48	0.2-0.9
R LMi	2270-(1780)	18-24	2.0-3.1	2590-	14-17	2.2-
X Oph	2390-1890	19-28	1.6-2.3	2680-2440	15-17	2.0-2.4
R Tri	3270-2460	4.3-7.8	3.4-4.3	2850-2390	6.2-7.2	3.5-4.1

Table XXIII

Mean Variable Characteristics

Quantity	This Study	Pettit and Nicholson
Visual Range	$5^m.4 \pm 0^m.3$	$5^m.9$
Luminosity Range	$0^m.7 \pm 0.1$	$0^m.9$
$\Delta T/\overline{T}$	0.19 ± 0.02	0.26
$\Delta\theta/\overline{\theta}$	0.25 ± 0.03	0.37
Phase of Temperature		
Maximum	0.00 ± 0.01	-0.01 ± 0.01
Minimum	-0.48 ± 0.02	0.49 ± 0.02
Phase of Angular Diameter		
Maximum	0.30 ± 0.03	0.28 ± 0.02
Minimum	-0.11 ± 0.02	-0.03 ± 0.01
Phase of Luminosity		
Maximum	0.11 ± 0.01	0.14
Minimum	-0.43 ± 0.02	-0.45

error estimates because no uncertainty was published. Due to the smaller number of objects, the errors are probably at least as large as those calculated from this study. The Pettit and Nicholson data for the temperatures and diameters of 6 stars were taken from their table III, graphed, and statistically treated in a manner similar to the results of the present work.

As is evident by table XXIII, the agreement between the two projects is astonishingly excellent. Although slight differences exist, the present study, with its improved infrared equipment, confirms the results of 50 years ago.

Again, as evidenced by table XXIII, the maximum luminosity occurs near phase +0.1 and lags the maximum compression by about one-quarter cycle. The number of stars is not sufficient to ascertain this phase lag of luminosity with respect to minimum radius as a function of composition, spectral type or visual range.

The physical explanation for the lag of luminosity behind visual brightness can be explained as follows: the visual energy output is dependent on blanketing but is a very strongly dependent function of temperature (e.g., exponential), whereas the luminosity is

dependent on the fourth power of the temperature. As the phase increases from zero, the temperature declines but the photosphere expands; and, for a short period of time (~0.1 cycle), the solid angle is increasing more rapidly than T^4 is declining. This phase lag is also apparent at the 3.5μ wavelength where the observed energy output is approximately proportional to R^2T.

XII

MODELS FOR RED GIANTS

Unfortunately, there has been a scarcity of theoretical models which attempt to explain the physical properties or the basis for the rather extensive observational data. Admittedly, the observations which have been gathered on Long Period Variable Stars are of a descriptive or catalog nature. Some models have emerged, but the predicted quantities may not be directly observable, and confirmation is difficult or non-existent.

The dynamical models for LPV stars require static models of stellar structure for non-variable red giants as a springboard from which pulsation theory may be applied. Only in recent years have reasonable model atmospheres been constructed which take into account all of the recent infrared observations of these cool giants. The photospheric temperatures typically range from 2000 to 3500 °K and imply a Planckian energy distribution peaking near 1μ. Only since the early 1960's have methods become available which allow the detailed structure of the cool stellar atmosphere to be explored.

Various authors have provided important contributions to the theory of model atmospheres for red giants. Review articles by Munch (1960) on

stellar atmospheres; Keenan (1960) on physical properties; Merrill (1960) on spectra; Weymann (1963) on mass loss; Smak (1966) on general traits; Johnson (1966) on infrared measurements, temperatures and bolometric corrections; Spinrad and Wing (1969) on infrared spectra; Vardya (1970) on late type atmospheres; and Neugebauer, Becklin and Hyland (1971) on sources of infrared radiation, together provide the most recent information and theory regarding red giant characteristics. The interior structure of red giants has been calculated by Harm and Schwarzschild (1966), while Iben (1967) has studied their evolutionary status. This preceding list is by no means complete and exhaustive, but it is included only as a starting point (or perhaps a terminating point) for the study of red giants.

The physical state of a one solar mass red giant's interior may be described as an inert, hydrogen deficient, isothermal core at a temperature of about 50 million degrees, a pressure of about 10^{21} dynes/cm^2, a radius of about 10^{-3} of the stellar radius and a mass of about one-fourth of the stellar mass (Harm and Schwarzschild, 1966). The energy generation arises from hydrogen burning in a very narrow shell surrounding the inert core. The energy transport is by radiation until convection

sets in at about 1/50 of the stellar radius. At the photosphere of this one solar mass red giant, typical values are: radius ~200 $R_{\odot}$, temperature ~3000 °K, pressure ~20 dynes/cm^2, density ~10^{-10} gms/cm^3, and surface gravity ~0.3 cm/sec^2 (Keeley, 1970a).

Because this present work deals primarily with stellar variability, the red giant models have only been briefly discussed in order to provide background information as to their physical nature.

XIII

MODELS FOR LONG PERIOD VARIABLE STARS

It is now generally accepted that radial pulsations are the cause of the observed variations in many types of intrinsically variable stars. Model atmospheres have been calculated for stars earlier than the M spectral type. Dynamic computations require these static models as a basis from which to proceed. Radial pulsation theory has attempted, and succeeded quite admirably, to explain the observed variability of the hotter stars, especially the Cepheids. The literature is quite extensive on subjects such as period, stability of the pulsation, cause, amplitude and phase dependence of radius, temperature and luminosity.

Ritter (1879) was the first to suggest that radial oscillations, with their associated surface temperature alterations, could provide the explanation necessary to describe the more regular periodic variables. Since that time, with a few roadblocks and detours along the way, and primarily due to the early work of Eddington (1917, 1918 a,b) and the later work of Zhevakin (1959, 1960) and Christy (1964), the pulsation hypothesis has steadily become acceptable. Rosseland's (1949) book and recent

review articles by Zhevakin (1963) and Christy (1966) have summarized the pulsation theory of stellar variability.

The earliest pulsational models assumed that the oscillation amplitude occurred throughout the entire stellar volume. The period was then proportional to $\bar{\rho}^{-1/2}$ or $R^{3/2} M^{-1/2}$. Fernie (1964) demonstrated that the period could be described by being proportional to $R^2 M^{-1/2}$. This latter functional dependence could be explained by having the stellar atmosphere, and not the entire volume, participate in the oscillations. For the giant stars, the stellar core is inert. The pulsation amplitudes are damped and approach zero at the core-atmosphere boundary. In the Cepheids and Miras, although the partially degenerate core makes the extended atmosphere possible, the physical processes contributing to the variability occur in the stellar atmosphere.

Many of the early models made approximations which, although allowing computational results, were not totally justified. It is now believed that the radial oscillations of the stellar atmosphere are non-adiabatic and non-linear and may be solved only by modern computer methods.

Christy (1964, 1968, 1969) attempted to solve the Cepheid variability problem with advanced

computers and techniques. His work, which was based on the contributions of many previous authors, appears to have been successful in explaining the cause, maintenance, and description of the pulsations. Christy's model treated non-adiabatic, non-linear motions of the stellar atmosphere which surrounds the stationary stellar core that supplies the energy generation. The observed temperature, radial velocity, luminosity and phase lag problems of Cepheid variables are adequately predicted by his results.

As previously stated, theoretical model atmospheres for red giant stars have only recently been constructed. Without these static models for a basis, dynamical calculations have been almost non-existent. One of the first LPV models to include the ionization zones of HI and HeII and the dissociation of H_2 was constructed by Kamijo (1962). His attempt to fabricate a red giant stellar model to explain Mira, itself, used linear, adiabatic pulsations and met with some success.

Most recently, Keeley (1970a, 1970b) tried to improve upon the static and dynamic models by using non-linear, non-adiabatic equations, which were solved with the aid of a computer. He also made an approximate attempt to explain o Cet and was reasonably

successful. His model for Mira assumed a mass of one solar mass, an inert core comprising 54% of the total mass, a luminosity of 10^{37} ergs/second, a mean effective temperature of 2600 °K and a 300 day period.

To summarize Kelley's results: The radial velocity of the outer mass zone shells is characterized by an asymmetric curve which has a rise time from maximum inward to maximum outward velocity of about 40% of a cycle; the maximum rate or expansion occurs about 0.2 cycle after minimum radius; the maximum luminosity happens about 0.3 cycle after maximum compression, while minimum output occurs about 0.1 cycle before minimum radius; the luminosity curve has a steeper rise to maximum than decline to minimum and its range in bolometric magnitude is about $1^{m}.6$. Unfortunately, Keeley was able to conclude little about the visual light curves or about the effective temperature and its changes. He stated that the phase relation of the luminosity to the radius is similar to that found for Cepheids.

In order to compare quantities, table XXIV summarizes the results of Pettit and Nicholson (1933), the results of this study, and the predictions of Keeley (1970b).

Table XXIV

Intercomparison of Observational and Theoretical Results

Quantity	Pettit and Nicholson	This Study	Keeley
Phase lag of maximum luminosity to minimum radius	0.15	0.22 ± 0.03	0.3
Phase lag of minimum radius to minimum luminosity	0.42	0.32 ± 0.04	0.1
$\Delta R/\overline{R}$	0.37	0.25 ± 0.03	0.45
Δm_{bol}	$0^m.9$	$0^m.7\pm0.01$	$1^m.6$

As evidenced by table XXIV, the agreement is quite good. No error estimations are listed in the table. Keeley's results were read from his figures.

The radial velocity curves computed by Keeley appear similar to those of figure 15, although the agreement is far from excellent. In his models, shock waves were produced in the outer zones of the atmosphere. Shock waves have been observed in LPV stars (Deutsch and Merrill, 1959; Odgers and Kushwaha, 1960) and there is reason to believe that these shocks contribute to, or are the cause of, the high mass loss rates of about $2 \times 10^{-6} M_{\odot}$/year, as calculated by Gehrz and Woolf (1971).

Both Keeley (1970b) and Christy (1968) give excellent descriptions of the physical processes which maintain the pulsations and produce the observed phase lags. It must be emphasized that, although the agreement is certainly not perfect, there appears to exist no major difficulty between observation and theory. The processes which result in variability seem to be similar for both the Cepheids and the long period variables.

XIV

SUMMARY

Infrared observations at an effective wavelength of 3.5μ of a selected group of Long Period Variable (LPV) stars have been amassed throughout the full cycle of variability. Contrary to some beliefs of ten years ago, stars do vary in the infrared. Some of the LPV's of this program altered their 3.5μ flux by a factor of three.

Although the radiation from Mira type variables did not repeat exactly in amplitude nor time of occurrence, the stars were sufficiently regular such that mean infrared light curves were produced. These mean curves were inter-compared for stars of spectral classification, M, S, and C.

The 1.04μ narrow band photometry of Lockwood (1972) and Lockwood and Wing (1971) was utilized to form a color index [1.04μ]-[3.5μ] as a function of phase for stars which the two programs held in common. A color temperature scale was deduced from this color index on the assumption that α Lyra radiates as a 10,000 °K black body at these two respective wavelengths. The color temperature derived in this manner also assumed that the opacities of the two wavelengths were the same and that the cool star radiated as a black body.

From this color temperature through the Planck formula and from the 3.5μ magnitudes converted to absolute fluxes, the angular size of the source was calculated. With these two parameters, apparent visual and bolometric magnitudes as functions of phase were then calculated for the Mira variables. These quantities, as well as the computed radial velocities, were compared to observational quantities whenever possible. A color temperature-spectral type relation was also determined for the LPV stars and agreed adequately with the same relation as deduced for the non-variable or mildly variable M giants. The visual blanketing attributed to titanium oxide was also calculated as a function of spectral type and color temperature.

The results for the Miras were as follows: The color temperature reached maximum simultaneously with maximum visual light (defined to be zero phase), while minimum temperature was attained almost exactly one-half cycle later; the maximum compression (minimum radius) occurred about one-tenth cycle before maximum temperature, whereas maximum radius was about four-tenths of a cycle after minimum radius; maximum luminosity happened about one-tenth cycle after maximum temperature while the minimum energy output took place nearly one-half cycle later. The fractional change of

temperature was typically 20% while that of the diameter was somewhat greater and the luminosity altered by about a factor of two.

These results are in excellent agreement with the thermocouple results of Pettit and Nicholson (1933). The phase relation of maximum luminosity to minimum radius is similar to that observed for the extensively studied Cepheid type variables and possibly suggests that the physical mechanism producing the alterations might be similar. The cause of the variability, which must act like a Diesel engine absorbing heat upon compression and releasing heat upon expansion, appears to be Eddington's opacity valve. According to the models of Keeley (1970a, b), this valve is the region of H^- and neutral hydrogen.

Due to the general scarcity of models concerning long period variables, unfortunately little may be stated to support or denounce particular assumptions. It is hoped that this project will inspire more completely developed theoretical models which will explain the variations of these bloated stars.

XV

SUGGESTIONS FOR FUTURE WORK

By and large, the results presented here confirm those of Pettit and Nicholson's (1933) work on diameters and luminosities of long period variable stars. This present work was able to modify only a few of their results.

The standard plea is for more observational data of all types throughout the entire cycle of variation. An improved method of temperature determination would, of course, be of the most practical use. A temperature scale must be developed for C and S stars so that physical parameters and variations may be compared to similar quantities for M stars. Spectra capable of radial velocity measurements are needed near minimum light where the available data are most scarce.

There exists another experiment which could serve as a direct check on the validity of the assumptions which resulted in the computed angular diameters. A fifty foot interferometer should be able to resolve many of the objects listed. o Cet, R Cas, R Leo and χ Cyg have diameters exceeding 25 milliseconds of arc. The interferometer could follow these variables throughout their respective cycles and could hopefully

confirm at least the shape of, if not the absolute calibration of, the angular size versus phase curves.

REFERENCES

1. Ahnert, P., 1964, Mitt. Verh. Sterne (Sonneberg), 2, p. 66.

2. Ahnert, P., 1965, ibid, 3, p. 6.

3. Allen, C. W., 1963, Astrophysical Quantities, 2nd Ed., Athlone Press, London.

4. Becklin, E. E., 1972, Santa Cruz Meeting of the Astr. Soc. of the Pacific.

5. Bonneau, D. and Labeyrie, A., 1973, Ap. J. (Letters), 181, L1.

6. Brown, R. H., 1966, Ann. Rev. of Ast. and Astrophysics, vol. 6, p. 13, ed. L. Goldberg, Palo Alto.

7. Cameron, D. and Nassau, J. J., 1956, Ap. J. 124, p. 346.

8. Campbell, L., 1955, Studies of Long Period Variables, AAVSO, Cambridge.

9. Campbell, L. and Jacchia, L., 1941, The Story of Variable Stars, Blakiston Co., Philadelphia.

10. Christy, R. F., 1964, Rev. Mod. Phys., 36, p. 555.

11. Christy, R. F., 1966, Ann. Rev. of Ast. and Astrophysics, vol. 4, p. 353, ed. L. Goldberg, Palo Alto.

12. Christy, R. F., 1968, Quar. JRAS, 9, p. 13.

13. Christy, R. F., 1969, JRASC, 63, p. 299.

14. Clayton, M. L. and Feast, M. W., 1969, MNRAS, 146, p. 411.

15. Deutsch, A. J. and Merrill, P. W., 1959, Ap. J., 130, p. 570.

16. Dyck, H. M., Forrest, W. J., Gillett, F. C., Stein, W. A., Gehrz, R. D., Woolf, N. J. and Shawl, S. J., 1971, Ap. J., 165, p. 57.

17. Eddington, A. S., 1917, Observatory, 40, p. 290.

18. Eddington, A. S., 1918, MNRAS, 79, p. 2.

19. Eddington, A. S., 1918, MNRAS, 79, p. 177.

20. Eggen, O. J., 1955, A. J., 60, p. 21.

21. Eggen, O. J., 1972, Ap. J., 174, p. 45.

22. Fernie, J. D., 1959, Ap. J., 130, p. 611.

23. Fernie, J. D. and Brooker, A. A., 1961, Ap. J., 133, p. 1088.

24. Fernie, J. D., 1964, Ap. J., 140, p. 1482.

25. Forrest, W. J., 1973, Private communication.

26. Fujita, Y., Yamashita, Y., Kamijo, F., Tsuji, T., and Utsumi, K., 1965, Publ. Dom. Ast. Obs. Victoria 12, p. 293.

27. Gehrz, R. D., 1971, Unpublished Ph.D. Thesis, University of Minnesota, Minneapolis.

28. Gehrz, R. D., and Woolf, N. J., 1971, Ap. J., 165, p. 285.

29. Gezari, D. Y., Labeyrie, A. and Stachnik, R. V., 1972, Ap. J. (Letters), 173, L1.

30. Gillett, F. C., Merrill, K. M. and Stein, W. A., 1971, Ap. J., 164, p. 83.

31. Glasby, J. S., 1969, Variable Stars, Harvard University Press, Cambridge.

32. Gordon, C., 1968, PASP, 80, p. 597.

33. Harm, R. and Schwarzschild, M., 1966, Ap. J., 145, p. 496.

34. Harrington, J. P., 1965, A. J., 70, p. 569.

35. Hetzler, C., 1936, Ap. J., 83, p. 372.

36. Hoffleit, D., 1964, Catalogue of Bright Stars, 3rd ed., New Haven.

37. Iben, I., Jr., 1967, Ap. J. 147, p. 624.

38. Johnson, H. L., 1964, Bol. Obs. Ton. y Tac., 3, p. 305.

39. Johnson, H. L., 1965, Comm. of the LPL, 3, #53, p. 73.

40. Johnson, H. L., 1966, Ann. Rev. of Ast. and Astrophysics, Vol. 4, p. 193, ed. L. Goldberg, Palo Alto.

41. Johnson, H. L., Mitchell, R. I., Iriarte, B. and Wisniewski, W. Z., 1966, Comm. of the LPL, vol. 4, no. 63, p. 99.

42. Jones, D. H. P., 1968, MNRAS, 139, p. 189.

43. Joy, A. H., 1926, Ap. J., 63, p. 298.

44. Kamijo, F., 1962, PASJ, 14, p. 271.

45. Keeley, D. A., 1970, Ap. J., 161, p. 643.

46. Keeley, D. A., 1970, Ap. J., 161, p. 657.

47. Keenan, P. C., 1960, Stars and Stellar Systems, vol. 6, Chap. 14, ed. J. L. Greenstein, Univ. of Chicago Press, Chicago.

48. Keenan, P. C., 1966, Ap. J. (Supplement) 13, no. 118, p. 333.

49. Kukarkin, B. V., Parengo, P. O., Efremov, Yu. I., and Golopov, P. N., 1958, General Catalog of Variable Stars, Moscow.

50. Lee, T. A., 1970, Ap. J., 162, p. 217.

51. Lockwood, G. W. and Wing, R. F., 1971, Ap. J., 169, p. 63.

52. Lockwood, G. W., 1972, Ap. J. (Supplement), Vol. 24, no. 209, p. 375.

53. Mayall, M. W., 1972, AAVSO.

54. Mendoza, E. E., V and Johnson, H. L., 1965, Ap. J., 141, p. 161.

55. Merrill, P. W. and Burwell, C. G., 1930, Ap. J., 71, p. 285.

56. Merrill, P. W., 1938, The Nature of Variable Stars, Macmillan Co., New York.

57. Merrill, P. W., 1960, Ap. J., 131, p. 385.

58. Merrill, P. W., 1960, Stars and Stellar Systems, Vol. 6, Chap. 13, ed. J. L. Greenstein, University of Chicago Press, Chicago.

59. Munch, G., 1960, Stars and Stellar Systems, Vol. 6, Chap. 1, ed. J. L. Greenstein, University of Chicago Press, Chicago.

60. Murdock, T. L., 1972, Unpublished Ph.D. Thesis, University of Minnesota, Minneapolis.

61. Neugebauer, G. and Leighton, R. B., 1969, Two Micron Sky Survey, NASA, Washington, D. C.

62. Neugebauer, G., Becklin, E., and Hyland, A.R., 1971, Ann. Rev. of Ast. and Astrophysics, Vol. 9, p. 67, ed. L. Goldberg, Palo Alto.

63. Odgers, G. J. and Kushwaha, R. S., 1960, Pub. Dom. Astr. Obs. Vic., 11, p. 253.

64. Payne-Gaposchkin, C., 1954, Variable Stars and Galactic Structure, Univ. of London, Athlone Press, London.

65. Pease, F. G., 1931, Ergebn. Exacten Naturwiss, 10, p. 84.

66. Pettit, E. and Nicholson, S. B., 1933, Ap. J., 78, p. 320.

67. Richer, H. B., 1971, Ap. J., 167, p. 521.

68. Ritter, A., 1879, Wiedemanns Annalen, 8, p. 172.

69. Rosseland, S., 1949, The Pulsation Theory of Variable Stars, Clarendon Press, Oxford.

70. Schneller, H., 1965, Mitt. Verh. Sterne (Sonneberg), 3, p. 86.

71. Schwartz, P. R. and Barrett, A. H., 1970, Proc. Conference on Late Type Stars, ed. M. Dyck and W. Lockwood, Kitt Peak Contribution no. 554.

72. Scott, R. M., 1942, Ap. J., 95, p. 58.

73. Smak, J., 1964, Ap. J. (Supplement), Vol. 9,p. 141.

74. Smak, J. I., 1966, Chapter in Ann. Rev. of Astr. and Astrophysics, Vol. 4, p. 19, ed. L. Goldberg, Palo Alto.

75. Spinrad, H. and Newburn, R. L., Jr., 1965, Ap. J., 141, p. 965.

76. Spinrad, H. and Wing, R. F., 1969, Ann. Rev. of Ast. and Astrophysics, vol. 7, p. 249, ed. L. Goldberg, Palo Alto.

77. Takayanagi, W., 1960, PASJ, 12, p. 314.

78. Taylor, J. H. and Jates, H. W., 1957, J. Opt. Soc. America, 47, p. 223.

79. Terrell, C. L., 1969, A. J. 74, p. 413.

80. Vardya, M. W., 1970, Ann. Rev. of Ast. and Astrophysics, Vol. 8, p. 87, ed. L. Goldberg, Palo Alto.

81. Weymann, R., 1963, Ann. Rev. of Ast. and Astrophysics, Vol. 1, p. 97, ed. L. Goldberg, Palo Alto.

82. Wilson, W. J. and Barrett, A. H., 1970, Proc. Conference on Late Type Stars, ed. M. Dyck and W. Lockwood, Kitt Peak Contribution no. 554.

83. Woolf, N. J. and Ney, E. P., 1969, Ap. J., (Letters), 155, L181.

84. Wyckoff, S., 1970, Ap. J., 162, p. 203.

85. Zhevakin, S. A., 1959, Sov. Astr., 3, p. 389.

86. Zhevakin, S. A., 1960, Sov. Astr., 4, p. 422.

87. Zhevakin, S. A., 1963, Ann. Rev. of Ast. and Astrophysics, Vol. 1, p. 367, ed. L. Goldberg, Palo Alto.